Comprehensive analysis of nanodiamond evidence reported to support the Younger Dryas Impact Hypothesis

Tyrone L. Daulton[1,2]*, Sachiko Amari[1], Andrew C. Scott[3], Mark Hardiman[4], Nicholas Pinter[5], R. Scott Anderson[6]

[1]Washington University in St. Louis, Department of Physics and Laboratory for Space Sciences, St. Louis, Missouri 63130, U.S.A.
[2]Washington University in St. Louis, Institute for Materials Science and Engineering, St. Louis, Missouri 63130, U.S.A.
[3]Department of Earth Sciences, Royal Holloway University of London, Egham, Surrey, TW20 0EX, U.K.
[4]Department of Geography, University of Portsmouth, Portsmouth, PO1 3HE, U.K.
[5]Department of Earth and Planetary Sciences, University of California Davis, Davis California 95616, U.S.A.
[6]School of Earth Sciences and Environmental Sustainability, Northern Arizona University, Flagstaff, Arizona 86011, U.S.A.

*correspondence: T. L. Daulton, e-mail: tdaulton@physics.wustl.edu

submitted to *Journal of Quaternary Science*
June 25, 2015
Modified February 8, 2016

ABSTRACT: During the end of the last glacial period in the Northern Hemisphere near 12.9k cal a BP, deglacial warming of the Bølling-Ållerod interstadial ceased abruptly and the climate returned to glacial conditions for a ≈ 1,300 year interval known as the Younger Dryas stadial. The Younger Dryas Impact Hypothesis proposes that the onset of the Younger Dryas climate reversal, Pleistocene megafaunal extinctions, and disappearance of the Clovis paleoindian lithic technology were coeval and caused by continent-wide catastrophic effects of impact/bolide events in North America. While there are no known impact structures dated to the Younger Dryas onset, physical evidence of the impact/bolide events is argued to be present in sediments spanning several continents at stratigraphic levels inferred to date to the Bølling-Ållerod / Younger Dryas boundary (YDB). Reports of nanometer to submicron-sized diamonds in YDB sediments, in particular the rare 2H hexagonal polytype of diamond, lonsdaleite, have been presented as strong evidence for shock processing of crustal materials. We review the available data on diamonds in sediments and provide new data. We find no evidence for lonsdaleite in YDB sediments and find no evidence of a spike in nanodiamond concentration at the YDB layer to support the impact hypothesis.

KEYWORDS: Nanodiamonds; cubic diamond; hexagonal diamond; lonsdaleite; Younger Dryas Impact Hypothesis

Introduction

The Younger Dryas (YD) Impact Hypothesis attempts to explain the rapid and dramatic changes that occurred at the end of the Pleistocene as arising from catastrophic extraterrestrial mechanisms. The earliest versions of the YD Impact Hypothesis speculated that North America was impacted by intense cosmic rays from a supernova (Brakenridge, 1981, 2011; Firestone and Topping, 2001, 2002; Firestone *et al.*, 2006), mineral debris that condensed in the supernova outflow (Firestone and Topping, 2001, 2002; Firestone *et al.*, 2006), and a comet (Melton and Schriever, 1933; Sass, 1944) whose orbit was perturbed into the inner solar system by the supernova shockwave (Firestone *et al.*, 2006). Multiple comet fragments have also been hypothesized to have struck the oceans across the globe (Kristan-Tollmann and Tollmann, 1992, 1994; Tollmann, 2001). A planet-sized fragment of a supernova has even been speculated to have entered the solar system, modified planetary orbits, and caused terrestrial impacts (Allan and Belair, 1994, 1997). A body ejected from a supernova has also been suggested to have struck North America (Firestone, 2009). Other early versions speculated that, during the Late Pleistocene, the Earth was irradiated by a burst of cosmic rays from the galactic core (LaViolette, 1987, 2005) and/or impacted by large solar flares in addition to coronal mass ejections from the sun (LaViolette, 2005, 2011), where the solar eruptions were induced by a supernova shockwave (Firestone *et al.*, 2006). The YD Impact Hypothesis has since evolved into several highly-controversial versions, most proposing that the abrupt YD climate reversal, Pleistocene megafaunal extinctions, and disappearance of the Clovis paleoindian lithic technology were coeval and caused by continent-wide catastrophic effects of one or more impact/bolide events in North America 12.9k cal a BP (e.g., Firestone *et al.*, 2007).

The coeval timing of the above events, a requirement for a singular causal mechanism, has not been firmly established (see van Hoesel *et al.*, 2014) and is a point of controversy. The onset of the YD stadial either spanned, or is dated to within, a couple hundred years of 12.9k cal a BP, depending on the applied chronometer (see, Meltzer and Holliday, 2010; Fiedel, 2011; van Hoesel *et al.*, 2014; Meltzer *et al.*, 2014). However, the chronologies of the Pleistocene megafaunal extinctions (timing and rate of population decline) are not well constrained and are debated. During the Pleistocene, at least 33 (or > 70%) of North American

megafaunal genera disappeared (Barnosky *et al.*, 2004) and, of these, the extinction of 16 genera (e.g., mammoths, mastodons, giant short-faced bears, saber-tooth tigers) are constrained between 12,000 and 10,000 ^{14}C a BP (~13,800 - 11,400 cal a BP) (Grayson, 2007; Faith and Surovell, 2009; Woodman and Athfield, 2009). Additionally, a recent study that compared ancient DNA and radiocarbon data over the last 56k a concluded that the megafauna extinction events are correlated with the multiple Dansgaard-Oeschger interstadial warming events (Copper *et al.*, 2015), suggesting the YD stadial is not unique. Furthermore, Pleistocene megafaunal extinctions were not limited to North America and also occurred at different times in South America, the Caribbean, Africa, Eurasia, and Australia. For discussions on the climatic changes that define the YD stadial see e.g., Berger (1990) and Carlson (2013), and on the dynamics of the paleoindian populations during this period see Collard *et al.* (2010).

There are no recognized impact structures in North America that date to the onset of the YD stadial. Several geomorphic features have been suggested as possible YD craters: oriented shallow depressions in Alaskan, Canadian, and Siberian permafrost (Allan and Belair, 1994, 1997), the Carolina Bays (Melton and Schriever, 1933; Allan and Belair, 1994, 1997; Firestone and Topping, 2001; Firestone *et al.*, 2007, 2010a; Firestone, 2009; Kinzie *et al.*, 2014, Kenneth *et al.,* 2015a), small playa basins of the High Plains (Firestone *et al.*, 2006), and deep depressions in four of the Great Lakes (Firestone *et al.*, 2007, 2010a; Firestone, 2009); however, there is no evidence to support their impact origin (see Holliday *et al.*, 2014). The 4 km-diameter, circular Corossol structure in the Gulf of St. Lawrence has also been suggested as a possible YD-age crater based on the discovery of a single 4 cm long breccia clast suggesting impact metamorphism (Higgins *et al.*, 2011). However, the breccia clast could have been deposited by glacial activity from one of many distal impact structures in Quebec (Reimold *et al.*, 2014). More importantly, the age of the Corossol structure is poorly constrained between the Mid-Ordovician to just prior to the Quaternary glaciations (Lajeunesse *et al.*, 2013).

To account for a non-crater-forming YD impact event, the inferred YD impactor has been variously interpreted as a porous, loosely-bound, low-density impactor (Firestone *et al.*, 2006); as highly fragmented multiple impactors (Kristan-Tollmann and Tollmann, 1992, 1994; Firestone *et al.*, 2007; Firestone, 2009; Kennett *et al.*, 2009a,b; Bunch *et al.*, 2012; Wittke *et al.*, 2013; Napier *et al.*, 2013; Petaev *et al.*,

2013a,b); as oblique-trajectory impactors into the Laurentide ice sheet (Firestone *et al.*, 2007); or as a bolide airburst similar to the Tunguska event, but orders of magnitude larger (Firestone, 2009; Israde-Alcántara *et al.*, 2012a). However, bolide/impact scenarios that produce catastrophic environmental effects on an intercontinental scale and disperse shock-transformation products globally – while not forming a crater – have been argued to be improbable and inconsistent with geologic evidence and physical models (Deutsch *et al.*, 1994; Melosh, 2009; French and Koeberl, 2010; Boslough 2012; Boslough *et al.*, 2012, 2013; Boslough, 2013a; Holliday *et al.*, 2014). It has further been suggested that the YD impact crater remains undiscovered (Kristan-Tollmann and Tollmann, 1994; Firestone *et al.*, 2010a; Kinzie *et al.*, 2014), despite suggestions that such a large and geologically young crater should be easily recognized.

While there are no known impact structures in North America that date to the YD onset, YD impact proponents nonetheless argue that physical evidence of the impact/bolide event is present in sediments, at multiple sites in North America, South America, Europe, and the Middle East that are claimed to be chronologically synchronous with the Bølling-Ållerod / YD boundary (YDB) layer (see, Kennett *et al.*, 2015a,b). Elevated concentrations of a range of minerals interpreted as products of impact/bolide processes and geochemical indicators of the impactor/bolide are reported in these inferred YDB layers. Multifarious criticisms have been raised regarding the identification, analysis, and interpretation of these materials as impact markers (Deutsch *et al.*, 1994; Southon and Taylor, 2002; Pinter and Ishman, 2008; Marlon *et al.*, 2009; Surovell *et al.*, 2009; Gill *et al.*, 2009; Paquay *et al.*, 2009, 2010; Haynes *et al.*, 2010a,b; Scott *et al.*, 2010; Daulton *et al.*, 2010; Daulton, 2012; Pinter *et al.*, 2011; Pigati *et al.*, 2012; Hardiman *et al.*, 2012; Boslough, 2013a,b; van Hosesel, 2014; van Hoesel *et al.*, 2014; 2015; Holliday *et al.*, 2014; Thy *et al.*, 2015; Scott *et al.*, 2015) as well as regarding the dating of their host sediment horizons (e.g., see Blaauw *et al.*, 2012; van Hoesel *et al.*, 2013, 2014; van Hosesel, 2014; Ives and Froese, 2013; Meltzer *et al.*, 2014; Holliday *et al.*, 2014, Boslough *et al.*, 2015; Holliday *et al.*, 2015). Accurate dating of stratigraphy at high resolution (required for proper evaluation of the YD Impact Hypothesis) is difficult because sites frequently have complex depositional/erosional histories and, except for lakebeds or ice sheets, rarely preserve a continuous record of sedimentation. Consequently, measurements that can provide sufficient chronological control are often poorly constrained or

nonexistent. Meltzer *et al.* (2014) performed a critical analysis of the chronologies at 29 sites (including the Greenland ice sheet) in which the YDB layer has been studied in detail. The nature of the site, luminescence and radiocarbon ages, and age-depth models were examined. Meltzer *et al.* (2014) concluded that sediments at only three sites (Daisy Cave, San Miguel Island, California; Sheriden Cave, Ohio; and Big Eddy, Missouri) could be dated with any confidence to the YD onset.

Materials that have been reported in YDB layer sediments and interpreted as markers of supernova/impact/bolide processes include: tektites including one embedded in a YD-dated tree trunk (Kristan-Tollmann and Tollmann, 1994); paleoindian chert artifacts with high-velocity particle tracks, with embedded chondritic micrometeorites, and with isotopic anomalies in K, U, and Pu (Firestone and Topping, 2001; Firestone *et al.*, 2006, 2010a; Firestone, 2009); millimeter-scale magnetic particles embedded in mammoth tusks and other Pleistocene megafaunal remains (Firestone *et al.*, 2006); iron micrometeorites and mammoth tusks with rusty pits (Baker *et al.*, 2008); radioactive sediment; radioactive mammoth bones and teeth (Firestone *et al.*, 2006, 2007, 2010a,b); magnetic grains and elevated Ir concentrations inside an extinct horse skull (West *et al.*, 2007; Firestone *et al.,* 2010a); magnetic grains (Darrah *et al.*, 2007) and fullerenes with isotopically anomalous helium (Darrah *et al.*, 2007; Firestone *et al.*, 2007); high abundance of unoxidized Fe-Ni, Cu-Ni, Fe-Sn-Ni, and Pt minerals (Darrah *et al.*, 2007), anomalously high concentrations of elements including U, Th, Ir, Pt, Ni, Cr, and Cu (see Firestone *et al.*, 2007; Bunch *et al.*, 2010; Petaev *et al.*, 2013a,b; Andronikov *et al.*, 2014); chondritic iron oxide framboids (Fayek *et al.*, 2012); pyrite framboids (Israde-Alcántara *et al.*, 2012a); shocked quartz with planar deformation features (Mahaney *et al.*, 2010); siliceous "scoria-like objects"; and lechatelierite (amorphous SiO_2) (Bunch *et al.*, 2012; Wittke *et al.*, 2013a,b,c). While all the proposed impact markers discussed up to this point are reported in one or several YDB sediments, the following markers are reported in many to most YDB sediments studied: magnetic minerals ("grains", "microspherules"); carbonaceous combustion products (charcoal/soot, "glass-like carbon," "carbon elongates," and "carbon spherules") (e.g., see Firestone *et al.*, 2007; Kennett *et al.*, 2008); nanometer to submicron-sized diamonds (loosely termed "nanodiamonds"); as well as controversial phases "n-diamond" and "i-carbon" (e.g., see Kennett *et al.*, 2009a,b; Kinzie *et al.*, 2014). Further, excess ^{14}C (defined by the difference between radiocarbon dates and actual dates) is reported in terrestrial YDB

sediments, including tree remains, carbon spherules, glass-like carbon, and charcoal contained within those sediments, as well in Icelandic YDB marine sediments (see Kristan-Tollmann and Tollmann, 1994; Firestone and Topper 2001; Firestone *et al.*, 2006; Firestone, 2009; LaViolette, 2011). A number of these reported markers are no longer considered credible, some are currently considered credible by only a few YD impact proponents, and others continue to be widely debated (for reviews see Pinter *et al.*, 2011; Boslough *et al.*, 2012; van Hosesel, 2014; van Hoesel *et al.*, 2014; Holliday *et al.*, 2014; Taylor and Bar-Yosef, 2014).

Reports of nanodiamonds, in particular the rare 2H hexagonal polytype of diamond, lonsdaleite, in YDB sediments; carbonaceous forms in these sediments (carbon elongates, carbon spherules, and glass-like carbon); and Greenland ice, all reportedly dating to the YDB, continue to be presented as strong evidence for multiple impact/bolide events. We review the available data on diamonds as well as associated carbonaceous minerals in sediments and provide additional data for evaluating the YD Impact Hypothesis.

Experimental Methods

Millimeter-scale carbonaceous spherules and/or their fragments were isolated from Arlington Canyon, Santa Rosa Island California sediments AC-003 (Kennett *et al.*, 2008; 2009b) and SRI 09-28A from Locality III (Scott *et al.*, 2010; 2016) that were dated to the YDB (12,800-13,100 cal a BP and 12,718-13,079 cal a BP, respectively). Full details describing the collection/acquisition of those sediments are provided in the accompanying paper, Scott *et al.* (2016). Three different specimen sets were separately crushed between sapphire discs: 1) five spherules/fragments from SRI 09-28A; 2) eight spherules/fragments from AC-003; and 3) 13 acid-washed spherules/fragments from AC-003. Each specimen set should contain at least one spherule containing nanodiamonds given that Kinzie *et al.* (2014) state, "For carbon spherules, 111 of 153 samples investigated (73%) contained no detectable NDs [nanodiamonds]" and "ND concentrations in carbon spherules is >35% at three sites."

The finely crushed material from each set was deposited directly on amorphous carbon-coated Cu transmission electron microscopy (TEM) grids (dry mount). Additional TEM grids were prepared by depositing several µL aliquots of ethanol- or nanopure water-suspended particles on the support film of the TEM grids (wet mount).

In addition, a sequence of sediment from Lommel Belgium that bracketed and included the presumed YDB-aged black mat that is reported to contain nanodiamonds (Tian *et al.*, 2011) was provided by Ph. Claeys. Black mat sediment (7.064g) was processed by acid dissolution. The sediment was first treated with 10M HF - 1M HCl followed by 6M HCl, and this alternating treatment was repeated eight additional times to remove silicates. This was followed by an alternating treatment of 6M HCl - 2M HF followed by 6M HCl - 0.6M H_3BO_3 and this was repeated four additional times to dissolve remaining silicates. The residue was divided into colloidal and non-colloidal fractions by colloidal separation using NaOH (pH = 10) following the procedure commonly used to concentrate nanodiamonds from primitive meteorites (see Lewis *et al.*, 1987). Due to the surface charge on the diamonds, they are expected to stay in suspension in basic solution (Lewis *et al.*, 1989). The colloidal fraction was then oxidized with $Cr_2O_7^{2-}$ for 20.5 hours at ~80°C, and the remaining residue was treated with $HClO_4$ for 2.0 hours at 204°C to further remove carbonaceous matter other than the diamond. Colloidal separation of the residue was again carried out in an attempt to further concentrate diamonds. Several µL aliquots of the final colloidal suspension were deposited on TEM grids.

Specimen nanostructure was characterized using a JEOL JEM-2100F field emission scanning transmission electron microscope. This instrument was equipped with a high-resolution pole piece and a Schottky field emission gun: 0.5 nA at 1 nm full width at half maximum probe diameter. This instrument was operated at 200kV and, at that energy, has a rated point resolution of 0.23 nm and a lattice resolution of 0.1 nm. The instrument was equipped with a Bruker Quantax 200-STEM energy dispersive X-ray spectroscopy (EDXS) system that consisted of an XFlash 60 mm^2 active-area silicon drifted detector (SDD) as well as drift correction and HyperMap software packages for spectral mapping. The instrument was also equipped with a Gatan Model 863 Tridiem electron energy-imaging filter (GIF) with spectrum imaging package (model 777 STEMPack) capable of electron energy loss spectroscopy (EELS), EELS spectral imaging, and electron energy-filtered imaging. The GIF utilized an Ultrascan 1000 FT 2048 x 2048 pixel, 16-bit, fiber optically coupled, peltier-cooled, charge-coupled device (CCD) camera as the main detector. For scanning (S)-TEM imaging, the instrument is equipped with Gatan Model 805 dark-field (DF) and bright-field (BF) STEM detectors as well as a Gatan Model 806 high angle annular (HAA)-DF STEM detector capable of *Z*-contrast imaging. For

conventional TEM imaging, the instrument has a retractable Gatan Orius SC1000B 2672 x 4008 pixels, 14 bit, fiber optically coupled, peltier-cooled CCD camera mounted on-axis directly above the GIF.

Elemental maps were acquired by STEM-EELS and STEM-EDXS spectral imaging in which EELS and EDXS spectra, respectively, were collected at each pixel position within a STEM region of interest. For STEM-EELS, a spectrometer 5 mm diameter entrance aperture, a collection angle of $2\beta = 22.66 \pm 0.06$ mrad, and an energy dispersion of 0.2 eV/channel were used to measure an energy loss region of 640 to 1050 eV. The EELS spectra were corrected for dark current and channel-to-channel gain variation of the CCD detector array and collected in the diffraction mode of the microscope (i.e., image coupling to the EELS spectrometer). Ratios of integrated EELS core-loss signal between elements were converted to their corresponding atomic ratios using partial cross-sections that were calculated from theoretical Hartree-Slater models. Unlike maps of EELS core-loss signal, maps of relative elemental compositions are, in principle, not influenced by variations in specimen thickness and electron diffraction. Ratios of integrated EDXS signal between elements were converted to their corresponding atomic ratios using standardless k-factors.

Experimental Results

Grain fragments of crushed carbonaceous spherules deposited on the TEM grids were systematically examined using a variety of techniques, including: selected area electron diffraction (SAED); bright-field, dark-field, and high-resolution imaging; and EDXS spot analysis. In total for all specimens, approximately 2000 grains were individually examined. The carbonaceous spherules primarily consisted of amorphous material (~95%) dominated by C and O, but also exhibiting a range of common elements that varied and included: Al, Ca, Fe, K, Mg, Na, P, S, Si, and/or Ti. A small fraction of these amorphous grains (~ several percent thereof) contained nanocrystals embedded within their matrix. In no case were any of these nanocrystals found to be carbonaceous, and no nanocrystals of diamond were observed. The remainder of the material (~5%) on the TEM grids from the crushed spherules consisted of submicron- (hundreds of nanometer-) sized monocrystalline non-carbonaceous minerals (e.g., aluminosilicates, pyrite), disordered graphite, and

polycrystalline aggregates of graphene/graphane/graphite (with some trace elements present). In comparison, spherules examined in Daulton *et al.* (2010) contained higher abundances of graphene/graphane/graphite aggregates than those examined here. No diamonds were observed.

The acid-dissolution residues of YDB Lommel sediments contained submicron crystals that were rich in O, Al, Si, Zr, and/or Ti. No diamonds were observed. The Lommel residue was subsequently subjected to harsher acid dissolution treatment to remove more of the non-diamond minerals. These further-processed residues still contained abundant non-carbonaceous submicron crystals that survived acid dissolution. Again no diamonds were observed, although an exhaustive search was not performed. It was our intention to perform mass balance measurements of the nanodiamond abundance in Lommel sediment horizons across the YDB. In the mass balance approach, abundance is estimated from the initial mass of the sediment and the mass of the resultant acid dissolution residue (assuming pure diamond isolates). For non-pure isolates, mass modal abundances of minerals present in the residues are required to estimate the initial diamond abundance. Due to the large amounts of surviving non-diamond minerals in the Lommel black mat acid residue, and as will be discussed latter, quantitative mass balance measurements are incapable of yielding any reliable abundance estimations for diamond. Therefore, it was not possible to determine if there was a peak in the diamond concentration at the Lommel YDB.

van Hoesel (2014) were similary unable to find nanodiamonds in their acid dissolution residues of "black mat" YDB sediment from Lommel or from Murray Springs, Arizona. As is the case for any mineral phase that was not observed, lack of observation of diamond does not demonstrate the total absence of said mineral in the samples examined; it can, at best, only constrain its possible abundance. For the specimens we examined, it was not possible to accurately constrain the possible abundance of nanodiamonds.

The Nanodiamond Evidence

One of the main lines of evidence presented to support the YD Impact Hypothesis has been the reports of cubic and hexagonal nanodiamonds within bulk terrestrial and lacustrine sediments; carbonaceous forms in these sediments (carbon elongates, carbon spherules, and glass-like carbon); and Greenland ice, all reportedly dating to

the YDB (Firestone *et al.*, 2007, 2010a; Kennett *et al.*, 2009a,b; Kurbatov *et al.*, 2010; Israde-Alcántara *et al.*, 2012a,b; Kinzie *et al.*, 2014). In a culmination of several connected studies, Kinzie *et al.* (2014) report a nanodiamond-containing YDB sediment horizon (with nanodiamonds completely absent above and below this horizon) that span several continents at 9 out of 22 YDB sites studied. If correct, this would suggest that a unique event occurred at the time this layer was deposited. In regard to the nature of this event, much emphasis has been placed on the reported discovery of lonsdaleite in YDB sediments (Kennett *et al.*, 2009b; Redmond and Tankersley, 2011; Israde-Alcántara *et al.*, 2012a; Kinzie *et al.*, 2014).

Lonsdaleite

Lonsdaleite is the 2H hexagonal polytype of diamond (space group 194, $P6_3/mmc$: a = 2.508 Å, c = 4.183 Å: Yoshiasa *et al.*, 2003) that differs structurally from the 3C cubic polytype of diamond (space group 227, $Fd\bar{3}m$: a = 3.567 Å) in the stacking sequence of tetrahedral close packed planes. In cubic diamond, the stacking sequence is $(A^b)(B^c)(C^a)\ldots$, whereas in lonsdaleite it is $(A^b)(B^a)\ldots$ (Fig. 1). Lonsdaleite was first discovered in laboratory experiments to synthesize diamond. Bundy and Kasper (1967) after discovering lonsdaleite in transformation products of their high-static-pressure compression experiments, became aware of a Netherlands patent (1965) reporting the formation of hexagonal diamond by shock compression. They subsequently identified lonsdaleite in the Canyon Diablo iron meteorite and attributed it to shock formation (Bundy and Kasper, 1967). Additional reports of lonsdaleite soon followed in meteorites (Hanneman *et al.*, 1967; Frondel and Marvin, 1967; Clarke Jr. *et al.*, 1981; Daulton *et al.*, 1996); interplanetary dust (Rietmeijer and Mackinnon, 1987); material from Ries, Popigai, Sudbury, and Obolon impact structures (Hough *et al.*, 1995; Koeberl *et al.*, 1997; Goryainov *et al.*, 2014; Shumilova *et al.*, 2014; Masaitis *et al.*, 1999; Gurov *et al.*, 2009); and peat from the Tunguska bolide epicenter (Kvasnitsa *et al.*, 1979; Kvasnytsya *et al.*, 2013). This has led to the perception that natural lonsdaleite was exclusively associated with shock metamorphism. Although in the case of interplanetary dust, Rietmeijer and Mackinnon (1987) argued against shock formation of the lonsdaleite they observed.

By contrast, the broader literature contains reports of natural lonsdaleite with no directly connected association with shock processes. The Russian literature reports

lonsdaleite within titanium placers of the Ukrainian Shield (Sokhor *et al.*, 1973); eclogites in Sal'niye Tundra, Kola Peninsula and the Urals (Golovnya *et al.*, 1977); metamorphosed and metasomatically modified rocks of the Kumdykol diamond deposit in North Kazakhstan (Shumilova *et al.*, 2011); and metamorphic rocks of the Kokchetav Massif in North Kazakhstan (Dubinchuk *et al.*, 2010). Additionally, lonsdaleite is reported in polycrystalline diamonds from the Udachnaya kimberlite pipe, Yakutiya (Gorshkov *et al.*, 1999; Titkov *et al.*, 2001) and in similar polycrystalline diamond from placers in Yakutiya (Kaminsky *et al.*, 1985; Petrovsky *et al.*, 2013). The situation is complicated further in that some published data identifying natural lonsdaleite, whether at impact structures or not, is not rigorously convincing, with identifications sometimes based on several diffuse X-ray lines or a few transmission electron microscopy (TEM) electron diffraction patterns. In some studies (Koeberl *et al.*, 1997; Masaitis *et al.*, 1999; Titkov *et al.*, 2001), no data are presented to support the lonsdaleite identification.

Microanalysis of lonsdaleite is difficult because it is always reported intergrown with cubic diamond and sometimes graphite on the nanometer to submicron scale. These phases often have high defect densities (e.g. dislocations, stacking faults, twin planes, and disordered grain boundaries). Consequently, the interpretation of structural measurements performed at a spatial scale greater than the grain size of these polycrystalline diamonds (such as with X-ray diffraction and TEM SAED) is not straightforward (see Daulton *et al.*, 2003). Németh *et al.* (2014) go so far as to speculate that lonsdaleite does not exist and is an illusion created by lattice faults in polycrystalline cubic diamond having nanometer grain size. Earlier, Cayron *et al.* (2008) had shown that many reports of hexagonal-diamond Si had misinterpreted micro/nanotwins in cubic-diamond Si; note that these Si phases are isostructural to carbon's lonsdaleite and cubic diamond, respectively. A stacking fault of tetrahedral close-packed planes in cubic diamond, …$(A^b)[(B^a)(A^b)(B^c)](C^a)$… where a (C^b) *plane* is missing and the preceding (B^c) plane is altered to (B^a), necessarily forms a unit cell and a half wide lamellae of lonsdaleite. While such lamellae should not be considered a 2H hexagonal phase, there is sufficient evidence that well ordered …$(A^b)(B^a)$… stacking of tetrahedral planes (Fig. 1, 2) occurs at scales up to, at least, tens of nanometers for C (e.g., see Chen *et al.*, 1996; Daulton *et al.*, 1996; Lifshitz *et al.*, 2001; Kulnitskiy *et al.*, 2013), Si (Dahmen *et al.*, 1989; Cerva, 1991; Algra *et al.*,

2011; Hauge *et al.*, 2015), Ge (Xiao and Pirouz, 1992; Vincent *et al.*, 2014), and SiC (Daulton *et al.*, 2003). Therefore, lonsdaleite, as well as other 2H hexagonal-diamond isostructural phases, do exist on at least this spatial scale. Nevertheless, some previous diffraction studies of heavily disordered cubic diamond minerals may have overestimated or misidentified the presence of lonsdaleite.

While the literature on lonsdaleite can be murky, it is clear that shock metamorphism has not been established as the exclusive mechanism by which lonsdaleite is formed in terrestrial deposits. Recall that lonsdaleite has been reported to form under high-static pressure (Bundy and Kasper, 1967). With the exception of lonsdaleite, none of the studies of YDB sediments report identification of any of the generally accepted and recognized shock minerals found at known impact structures (c.f., French and Koeberl, 2010; van Hosesel, 2014; van Hoesel *et al.*, 2014). Therefore, in the absence of other shocked minerals, the presence of lonsdaleite in sediments can only provide tenuous evidence for an association with shock processing. While it can be debated under what circumstances lonsdaleite can be used as an impact marker, it is premature to consider this question further in assessing the YD impact hypothesis as the reports of lonsdaleite in YDB sediments are not well supported.

Daulton *et al.* (2010) demonstrated that Kennett *et al.* (2009b) misidentified polycrystalline aggregates of graphene and graphane present in various carbonaceous forms within the sediments as lonsdaleite. Independent studies have confirmed this conclusion (Madden *et al.*, 2012; van Hoesel *et al.*, 2012; van Hosesel, 2014; Bement *et al.*, 2014) and have failed to observe lonsdaleite in YDB sediments (Tian *et al.*, 2011). Graphene is a two-dimensional, single-atom-thick planar molecule with sp^2 bonded carbon (1.42 ± 0.1 Å bond length) in a hexagonal arrangement of 2.46 ± 0.02 Å edge length (Geim and Novoselov, 2007; Elias *et al.*, 2009). Graphene was first observed as randomly oriented and uncorrelated sheets (i.e., a polycrystalline aggregate) within the cores of many circumstellar graphite spherules isolated from chondritic meteorites (Bernatowicz *et al.*, 1996). When graphene sheets are periodically stacked normal to their plane (e.g., *AB*, *AA*, or *ABC* stacking), they form various graphite polytype structures or turbostratic graphite if the stacking is disordered. Graphane is a hydrogenated form of graphene, with H bonded on the surface resulting in a out-of-plane puckering of C bonds and an effective contraction of the hexagonal edge length to between ≈ 2.34 - 2.46 Å (Elias *et al.*, 2009).

Kuratov *et al.* (2010) and Israde-Alcántara *et al.* (2012a), in which Kennett is a coauthor, also misidentified lonsdaleite. For example, the high-resolution (HR)-TEM lattice image of a nanocrystal from residues of Greenland ice shown in Figure 6 of Kuratov *et al.* (2010) and identified as lonsdaleite is inconsistent with the crystal structure of lonsdaleite. No crystallographic zone axis of lonsdaleite exists that can display two differently oriented sets of 2.06 Å spaced {002} planes because there is only one such set of planes in the structure (Fig. 3). The HR-TEM lattice image of a nanocrystal from Lake Cuitzeo identified as twinned lonsdaleite and shown in Figure 11B of Israde-Alcántara *et al.* (2012a) is inconsistent with the crystal structure of lonsdaleite. Using as spatial calibration the annotated 1.93 Å {101} spacing and scale marker of their figure, we measure a spacing of 1.75 ± 0.05 Å for the nearly vertical atomic planes (whose plane normal is perpendicular to the direction of the arrows in the figure) with cross plane angle of 67.4 ± 0.4°. Lonsdaleite lacks 1.75 Å spaced planes (see Table 1). If the plane spacings were both 1.93 Å (i.e., closest lonsdaleite spacing to our measured 1.75 Å spacing, see Table 1), the cross plane angle is restricted to 52.41° for <011>, 55.81° for <110>, or 80.15° for <121>, and all are inconsistent with the HR-TEM image. Furthermore, the most common twin configuration in diamond is twinning across the tetrahedral basal plane (e.g., $\{111\}_{3C}$ and $\{002\}_{2H}$) with twin angle of 70.53° (Σ=3) (see, Daulton *et al.*, 2003), and this twin configuration will not alter the 2H lonsdaleite structure (i.e., stacking sequence). Although stacking faults in lonsdaleite are frequently reported, twining in lonsdaleite is yet to be reported, with the exception of Israde-Alcántara *et al.* (2012a).

The recent study by Kinzie *et al.* (2014) reports no new or convincing evidence for lonsdaleite. Contrary to earlier publications (Kennett *et al.*, 2009b; Kuratov *et al.*, 2010; Israde-Alcántara *et al.*, 2012a), the term *"lonsdaleite-like"* is now used to describe these grains in Kinzie *et al.* (2014); note that all of these publications share at least one coauthor. Curiously, Kinzie *et al.* (2014) also state that "lonsdaleite has never been observed in any deposits of any age in Europe or North America, where YDB lonsdaleite-like crystals are currently found." The reason the term lonsdaleite-like is now used is simple; these grains are not consistent with lonsdaleite. Kinzie *et al.* (2014) argue that the grain shown in their Fig. 15, which is the same grain as shown in Figures 2a-c and S2 of Kennett *et al.* (2009b), is a lonsdaleite-like grain. The original identification of this grain by Kennett *et al.* (2009b) as lonsdaleite was

questioned by Daulton *et al.* (2010). Kinzie *et al.* (2014) wrote in response, "He [Daulton *et al.* (2010)] questioned figure 2A-2C of Kennett *et al.* (2009b). Although the analyses were insufficient to conclusively identify the nanocrystal shown as lonsdaleite, we find no evidence to eliminate it as a possibility." Despite their inability to conclusively identify the grain, Kennett *et al.* (2009b) categorically identified it as lonsdaleite, and Kinzie *et al.* (2014) identified it as lonsdaleite-like.

The grain in question displayed an azimuthally asymmetric polycrystalline diffraction pattern with partial rings (forming doubled rings, see Fig. 4), and this is indicative of heterogeneity either in the form of texturing or a multiphase mixture. Texturing (defined as a distribution of crystallographic orientations of polycrystalline grains, in which all possible orientations do not occur with equal probability) can produce asymmetric ring intensity. However, texturing can be ruled out because this diffraction pattern completely lacks intensity from many lonsdaleite reflections (see Fig. 4) including (101) and (102) (see Table 1; Bundy and Kasper, 1967; Frondel and Marvin, 1967) even for a wide range of specimen orientations achieved by tilting the TEM goniometer. The diffraction pattern is thus inconsistent with the lonsdaleite structure; however it is consistent with a two-phase aggregate of polycrystalline graphene/graphane, a mineral assemblage (Fig. 5) observed ubiquitously in the sediments (Daulton *et al.*, 2010; van Hoesel *et al.*, 2012; Bement *et al.*, 2014).

The identification by Kinzie *et al.* (2014) of other reported lonsdaleite-like grains is based on the same analysis used by Israde-Alcántara *et al.* (2012a) to identify lonsdaleite. Both use single, off-zone-axis HR-TEM lattice images and their fast Fourier transformations (FFTs) that can easily yield misleading results (e.g., see Kohno *et al.*, 2003; Cayron *et al.*, 2008; den Hertog *et al.*, 2012) and cannot provide a conclusive mineral identification. In particular, Kohno *et al.* (2003) demonstrated that HR-TEM images of twinned nanocrystals of cubic-diamond Si can be confused with hexagonal-diamond Si. The structural information contained in an individual HR-TEM image and its associated diffraction pattern is incomplete because they are two-dimensional projections of three-dimensional structures with potentially complex twin and stacking-fault configurations (see, Daulton *et al.*, 2003; den Hertog *et al.*, 2012). The analysis of a single HR-TEM image cannot conclusively determine the structure of a nanocrystal; instead, methods such as comparison of simulated phase-contrast lattice images to a through-focus series of HR-TEM images must be applied for a range of nanocrystal orientations (see also Billinge and Levin, 2007).

Kinzie *et al.* (2014) comment on an EELS analysis of a lonsdaleite-like grain, "Figure 17*B* is an HR-TEM image of a rounded 10-nm lonsdaleite-like crystal. The ED[X]S results were presented in Kurbatov *et al.* (2010), confirming that the crystal is carbon, and an EELS spectrum indicated high sp^3 bonding." However, the only EDXS and EELS results presented in Kurbatov *et al.* (2010) are found in their Figure 8 for a grain they claim is "n-diamond," not lonsdaleite. Further, the EELS C-K edge spectra and the associated low-loss plasmon peak at 22 eV reported by Kurbatov *et al.* (2010) are consistent with amorphous C (e.g., see Kincaid *et al.*, 1978; Fallon and Brown, 1993) from the ~ 70 nm thick TEM support film upon which the nanocrystals were mounted. The EELS spectra shown by Kinzie *et al.* (2014) for "n-diamond" is also consistent with amorphous C; as in the case of Kurbatov *et al.* (2010) and others, the spectra is likely dominated by contributions from the amorphous C TEM support film. Nevertheless, no C-K edge EELS spectrum of the lonsdaleite-like grain was published that can be evaluated here. Adding to the confusion, Kinzie *et al.* (2014) state in their Figure 17b caption, "*B*, HR-TEM image of a 10-nm lonsdaleite-like monocrystal from Lake Cuitzeo (YDB: 493 ppb at 280 cmbs)." However, Kurbatov *et al.* (2010) did not examine Lake Cuitzeo specimens.

Cubic Diamond

Nanometer-sized grains of the 3C cubic polytype of diamond in YDB sediments has also been interpreted as supporting the YD Impact Hypothesis. This interpretation is based on reports of cubic diamonds of nanometer to tens-of-micron size in Cretaceous/Tertiary boundary sediments (Carlisle and Braman, 1991; Hough *et al.*, 1997); of submicron to millimeter size at Ries, Popigai, Sudbury, Gardnos, and Obolon impact structures (Hough *et al.*, 1995; Koeberl *et al.*, 1997; Masaitis *et al.*, 1999; Gilmour *et al.*, 2003; Gurov *et al.*, 2009); and of submillimeter size in peat at the Tunguska bolide epicenter (Kvasnitsa *et al.*, 1979; Kvasnytsya *et al.*, 2013). Furthermore, ureilite and iron meteorites contain submicron- to millimeter-sized cubic diamond believed formed by shock (see Ksanda and Henderson, 1939; Nakamuta and Aoki, 2000) and primitive carbonaceous chondrites contain presolar cubic nanodiamonds (0.5-10 nm diameter, mean 2.6 nm) believed formed primarily by gas condensation (Lewis *et al.*, 1987; Daulton *et al.*, 1996). Submillimeter to centimeter polycrystalline aggregates of cubic diamond found in alluvial placers, known as

carbonados (from Mesoproterozoic deposits in Brazil and Central Africa) and yakutites/carbonados (from Yakutiya, Russia), have been attributed to formation by shock metamorphism (see Smith and Dawson, 1985; Kaminsky, 1994). However, Cartigny (2010) argued that a mantle origin for carbonados cannot be excluded. Formation mechanisms other than shock such as crystallization from a carbon-supersaturated fluid have been suggested (Ketcham and Koeberl, 2013), and the origins of carbonados remain poorly understood (Haggerty, 1999; 2014; Heaney, 2005; McCall, 2009; Cartigny, 2010). Yakutites have been described as differing from carbonados in several aspects (but see McCall, 2009), one being that they contain lonsdaleite (Kaminsky, 1994; Heaney *et al.*, 2005), which is traditionally associated with shock processing. However, yakutites have been reported in kimberlite pipes (Gorshkov *et al.*, 1999; Titkov *et al.*, 2001), which are volcanic in origin.

On the other hand, cubic diamonds of non-impact and non-shock origin occur widely in the crust. Centimeter-size down to tens-of-micron, or smaller, cubic diamonds (including polycrystalline aggregates variously known as framesite, boart, ballas, stewartite, diamondite, and sometimes carbonado/yakutite) occur as xenocrysts in volcanic rocks (e.g., kimberlites, lamproites, and ultramafic lamprohyres) of pipe structures formed during mantle eruptions through the crust (see Haggerty, 1999; Gorshkov *et al.*, 1999; Kurat and Dobosi, 2000; Titkov *et al.*, 2001; Nowicki *et al.*, 2007; Dobosi *et al.*, 2008; Shirey *et al.*, 2013). Micron- to tens-of-micron-sized cubic diamonds (microdiamonds) have been found worldwide as inclusions within or in association with metamorphosed crustal rocks of regional metamorphic terrains: Kokchetav Massif, Kazakhstan (Rozen *et al.*, 1972; Sobolev and Shatsky, 1990); Maksyutov Complex, Russia (Bostick *et al.*, 2003); Western Gneiss region, Norway (Dobrzhinetskaya *et al.*, 1995); Bohemian Massif, Germany (Stöckhert *et al.*, 2001); Lago di Cignana Western Alps, Italy (Frezzotti *et al.*, 2014); Rhodope Massif, Greece (Schmidt *et al.*, 2010); Dabie Shan, Su-Lu, and Qinling regions, China (Xu *et al.*, 1992, 2005; Yang *et al.*, 2003); and Akluilâk minette dike system, Canada (Cartigny *et al.*, 2004). Polycrystalline cubic microdiamonds have also been found in the ultrahigh-pressure metamorphic terrain of Erzgebirge, Germany (Dobrzhinetskaya *et al.*, 2013). The formation of metamorphic microdiamonds has been attributed to deep continental subduction of primary crustal rocks followed by rapid tectonic uplift of recrystalized material to the crust (see Ogasawara, 2005; Dobrzhinetskaya *et al.*,

2007; Dobrzhinetskaya, 2012). However, fluid-metasomatic formation of microdiamond in the crust has also been suggested (see Pechnikov and Kaminsky, 2008). Hawaiian mantle-derived, garnet pyroxenite xenoliths have been found to contain cubic nanodiamonds within melt inclusions (Wirth and Rocholl, 2003) and CO_2-H_2O-H_2S fluid inclusions (Frezzotti and Peccerillo, 2007). Cubic nanodiamonds also may be prevalent in metamorphic terrains; MicroRaman spectra of inclusions in garnets from the Maksyutov Massif (Bostick *et al.*, 2003) and the Rhodope Massif (Perraki *et al.*, 2006) suggest the presence of nanodiamonds or nanodiamond aggregates, although this has not been confirmed by other microanalytical techniques. All of these diamonds can be eroded from their source rocks, transported, and deposited into placer deposits, sediments (see de Wit, 2004), and sedimentary conglomerates (see Fleischer, 1998).

Cubic nanodiamonds have also been reported in sediments and in carbonaceous forms within sediments without clear association with impact structures and which do not date to the YDB. Nanometer to submicron-sized diamond were reported in carbon spherules, similar to those reported at the YDB, but from modern forest soils in Germany and Belgium (Yang *et al.*, 2008). Similar sized nanodiamonds were also reported in glass-like carbon from the Usselo horizon in Geldrop-Aalsterhut, The Netherlands; however that horizon postdates the YD onset by two centuries (van Hoesel *et al.*, 2012, 2013).

Diamond is chemically inert, highly resistant to weathering (e.g., decomposition and transformation), and will persist in the surface environment. Erosion of diamond-bearing source rocks and transport by wind or water could widely redistribute nanometer- to submicron-sized diamonds into distant alluvial deposits and sediments that bear little resemblance to the diamond source rocks. Similarly could be the case for micron-sized host grains containing nanodiamond inclusions, and those inclusions would be extracted from their host minerals during laboratory acid dissolution of the sediments. It is intriguing that nanodiamonds are present in the Pleistocene to Holocene sediments, and work is clearly needed to understand their origin. Similar to lonsdaleite, the literature on nanometer- to submicron-sized cubic diamonds in terrestrial deposits is complicated by the varying strength of the published data. Also, questions of laboratory contamination have been raised for some metamorphic rocks (see Chopin and Sobolev, 1995). Nevertheless, it is clear that the presence of these cubic diamonds in sediments cannot be used as an impact marker because shock

metamorphism does not appear to be the predominant formation mechanism of diamonds of that size found in the crust.

Nanocrystals of "n-diamond" and "i-carbon"

In addition to the two known polytypes of diamond, impact proponents also report nanometer-sized crystals of "n-diamond" and "i-carbon" in YDB sediments and Greenland ice (Kinzie *et al.*, 2014). While neither are polytypes of diamond, impact proponents often describe them as nanodiamonds. They also interpret these nanocrystals as evidence for a YD impact event. "N-diamond" is a hypothesized carbonaceous phase that displays diffraction lines strikingly similar to that of 3C diamond, with the notable exception that the Bragg reflections kinematically forbidden in 3C diamond are present. This has lead to the speculation that "n-diamond" is a modified form of 3C diamond polytype (Hirai and Kondo, 1991). Aggregates of nanocrystals that display "n-diamond" reflections sometimes exhibit additional reflections that are attributed to another hypothesized nanocrystalline carbon phase termed "C_8" or "i-carbon" (see, Matyushenko *et al.*, 1979; Hirai and Kondo, 1991). The atomic structure of "n-diamond" has yet to be determined and its identification as a modified form of 3C diamond remains controversial (e.g., see Wen *et al.*, 2007). Similary, "i-carbon" is controversial, and its atomic structure has not yet been determined.

In YDB sediments, "n-diamonds" are usually reported at much higher concentrations than cubic diamonds, and in many cases were "n-diamonds" are reported cubic diamonds are not observed. Table D2 of the supplementary materials of Kinzie *et al.* (2014) report "n-diamonds" present in 22 of 24 sites that date to the YDB, "i-carbon" in 20 of these sites, cubic diamonds were reported in only 8 of these sites, and hexagonal diamond in only 5. Israde-Alcántara *et al.* (2012a) report "n-diamonds" at Lake Cuitzeo, but write, ". . . we could not unequivocally identify the cubic allotrope. This may be due to masking by i-carbon and/or n-diamonds, which share some d-spacings with cubic NDs." Kinzie *et al.* (2014) write in regard to Lake Cuitzeo, "Using HRTEM and FFT, we identified . . . n-diamonds, i-carbon, and cubics [cubic diamond] have a ratio of 3:1:1."

The presence of "n-diamonds" in sediments cannot be used as an impact marker because they are also reported in sediments that do not date to the YDB and,

importantly, their formation by impact processes has not be demonstrated. Nanocrystals with diffraction patterns consistent with "n-diamond" were reported in surface forest soils in Germany and Belgium (Yang *et al.*, 2008). At Bull Creek, Oklahoma, cubic nanodiamonds were not found, but nanocrystals of "n-diamond" were reported in multiple horizons (Madden *et al.*, 2012) and in sediments dated <3000 ^{14}C a BP (Bement *et al.*, 2014). Firestone *et al.* (2007) reported nanodiamonds in glass-like carbon from the rims of Carolina Bays using nuclear magnetic resonance (NMR); while that identification was questioned (Kerr *et al.*, 2008), Kinzie *et al.* (2014) reported confirmation by TEM. Kinzie *et al.* (2014) wrote, "We used a focused ion beam to mill a piece of glass-like carbon extracted from the YDB layer at the M33 site, the rim of a Carolina Bay in Myrtle Beach, South Carolina (for site details, see Firestone *et al.*, 2007). The TEM analyses showed that diamonds were present only from the surface down to a depth of ≈0.75 μm and were not observed in the interior (fig. 14*A*)." The caption for Figure 14 of Kinzie *et al.* (2014) identifies these nanocrystals as "n-diamond". Firestone *et al.* (2010) earlier reported, "All of the Bay rims examined [15 in total] were found to have, throughout their entire 1.5-5-m sandy rims, a typical assemblage of YDB markers (magnetic grains, magnetic microspherules, iridium, charcoal, soot, glass-like carbon, *nanodiamonds* [emphasis added], carbon spherules, and fullerenes with helium-3)." However, Firestone *et al.* (2010a) did not disclose the methods and data by which the nanodiamonds were identified.

The Carolina Bays are thousands of shallow elliptical depressions with elevated rims scattered along the Atlantic Coastal Plain (see Brooks *et al.*, 2010), which formed asynchronously over a significant period of time with multiple periods of rim accretion with intervening periods of erosion (Grant *et al.*, 1998; Rodriguez *et al.*, 2012). Meltzer *et al.* (2014) write, "Firestone *et al.* (2) subsequently admitted that the ages of the Carolina Bays vary but then suggested that because sediment from 15 Carolina Bays contained supposed impact markers and because such impact markers occur only in the supposed YDB layer and were 'identical to those found elsewhere in the YDB layers that date to 12.9 ka,' the supposed YDB layer in the Carolina Bays must be the same age (ref. 2, p. 16019)." Rodriguez *et al.* (2012) studied Lake Mattamuskeet, one of four Carolina Bays on the Albemarle-Pamlico Peninsula of North Carolina that Firestone *et al.* (2007, 2010a) reported contain impact markers (including nanodiamonds) and concluded that rim accretion significantly postdated

the YD stadial. In fact, Firestone (2009) measured radiocarbon ages between 685-8455 ^{14}C a BP for glass-like carbon from several Carolina Bays including Myrtle that is reported to contain nanodiamonds (Firestone *et al.*, 2007; Kinzie *et al.*, 2014). Firestone (2009) suggests that the glass-like carbon from the Carolina Bays must be enriched in ^{14}C relative to their *assumed* YD age and offered the implausible scenario that the YD impactor was ejected from a near-Earth supernova to account for the enrichment. A more probable explanation is that the assumed YD age of those Carolina Bays is incorrect.

Nanodiamond Host Minerals

Nanometer-sized diamond, "n-diamond", and/or "i-carbon" have been reported within glass-like carbons (Firestone *et al.*, 2007, 2010a; Firestone, 2009; Israde-Alcántara *et al.,* 2012a supplemental materials; Kinzie *et al.*, 2014), carbon elongates (Kennett *et al.*, 2009b), and carbon spherules (Firestone, 2009, Firestone *et al.*, 2010a; Kennett *et al.*, 2009a; Israde-Alcántara *et al.,* 2012a supplemental materials; Kinzie *et al.*, 2014) from YDB sediments as well as acid dissolution residues of these sediments. Glass-like carbon was described by Firestone *et al.* (2007) as "Pieces up to several cm in diameter . . . associated with the YDB and [Carolina] Bays, and their glassy texture suggests melting during formation, with some fragments grading into charcoal." Firestone *et al.* (2007) also describe "Carbon spherules (0.15–2.5 mm) are black, highly vesicular, subspherical-to-spherical objects (Fig. 3). SEM analyses show them to have cracked and patterned surfaces, a thin rind, and honeycombed (spongy) interiors. SEM/energy dispersive spectrometer and microprobe analyses show that the spherules are dominantly carbon (75%)." Kennett *et al.* (2009b) describes, "Carbon elongates differ from the carbon spherules in having an irregular array of walls and voids, whereas carbon spherule interiors display a well-organized honeycomb (reticulated) pattern. Both types are composed entirely of glass-like amorphous carbon indicative of high-temperature formation. The general shape of elongates ranges from angular (hexagonal in cross-section) to subrounded." Kinzie *et al.* (2014), with Kennett as a coauthor, report carbon spherule abundances at Arlington Canyon that are equal to the sum of carbon spherule and carbon elongate concentrations reported by Kenneth *et al.* (2008, 2009b). No explanation was

provided by Kinzie *et al.* (2014) on why they reclassified the so-called carbon elongates as carbon spherules (see also Hardiman *et al.*, 2012).

While carbon spherules may have multiple origins, most carbon spherules studied in YDB sediments have external and internal morphologies indistinguishable from sclerotia (Fig. 6) of saprobic (e.g., *Sclerotium Athelia rolfsii*), phytopathogenic (e.g., *Rhizoctonia solani, Botryotinia cinerea*), and ectomycorrhizal (e.g., *Cenococcum geophilum*) fungi (Scott *et al.*, 2010), to name a few. Sclerotia are resting bodies (i.e., persistent propagules) of fungi, composed of closely packed (pseudoparenchymatous) hyphae, whih have a range of morphologies and form during periods of environmental stress (see Smith *et al.*, 2015). Typically, they usually consist of an outer rind of tightly packed hyphal tips that develop an impervious thick-walled and pigmented (melanized) layer surrounding a medulla of hyphae with extended vacuoles that store reserves of glyocgen, proteins, lipids, and polyphospates. Viable sclerotia can remain dormant for many years during adverse conditions and germinate in favorable conditions to produce mycelia. Sclerotia are ubiquitous in forest litter and soils, and even after death can persist for at least many thousands of years (see Trappe, 1969; Hormes *et al.*, 2004; Benedict, 2011; McLaren *et al.,* 2014). Further, fossil sclerotia (or similar structures) of *Palaeosclerotium pusillum* have been reported preserved in the matrix of coal dated to the Middle Pennsylvanian (≈ 310 Ma) (Rothwell, 1972; Dennis, 1976; Taylor *et al.*, 2015). Consequently, sclerotia are common at archaeological sites (e.g., see McWeeney, 1989; Shay and Kapinga, 1997; Deal, 2005), and the common association of sclerotia with wood-charcoal in sediments has lead to the suggestion that charring of sclerotia by wildfires may contribute to their long-term preservation (Benedict, 2011). Carbon spherules were extracted from YDB sediments by flotation (Firestone *et al.*, 2007; Kennett *et al.*, 2008, 2009b; Israde-Alcántara *et al.*, 2012a; Kinzie *et al.*, 2014), and this method will readily collect dead sclerotia, which float in water (see Trappe, 1969; Shay and Kapinga, 1997, Benedict, 2011). Scott *et al.* (2010) suggested that carbon elongates in YDB and other sediments include non-spherical sclerotia and/or arthropod fecal material.

Israde-Alcántara *et al.* (2012a) responded to Scott *et al.* (2010), asserting that ". . . charred and uncharred sclerotia have textured, filamentous, low-reflectivity interiors, whereas at Cuitzeo [their study site], SEM imaging demonstrates that CSp have smooth, glassy, highly reflective interiors with no evidence of filamentous structure observed in fungal sclerotia (or cellular structure found in charcoal) (SI Appendix,

Fig. 5)" (see also Israde-Alcántara *et al.*, 2012b). However, fungal sclerotia can be hollow (see, Ferdinandsen and Winge, 1925; Trappe, 1931) and have smooth interior surfaces (Fig. 7) (private communication M. Watanabe). In the image of a carbon spherule from Arlington Canyon shown in the supplemental materials of Kennett *et al.* (2009b) septal pores which allow movement of cytoplasm and organelles in fungi hyphae (see, Reichle and Alexander, 1965; van Peer *et al.*, 2009) are clearly evident (Fig. 8) and conclusively identify it as a fungal sclerotia at some undetermined stage of diagensis (private communication M. Watanabe). Septa pores are also clearly evident in the image of a carbon spherule from a Carolina Bay that is attributed to Allen West (see, Largent, 2008). We also observed septal pores in carbon spherules from the YDB layer at Arlington Canyon provided to us by J. West and J. J. Johnson (e.g., see Fig. S5D of the supplemental materials of Scott *et al.*, 2010). Further, our measured elemental composition of an Arlington Canyon carbon spherule is similar to that of fossil sclerotia. The amorphous matrix of the spherules had an elemental composition, as determined by EDXS, of 82.49 at.% C, 13.40 at.% O, and 0.35 at.% Si, consistent with that reported for YDB carbon spherules (Firestone *et al.*, 2010a; Israde-Alcántara *et al.*, 2012a). In comparison, fossilized sclerotia from sediments of Lake Biwa, Japan contained 83 at.% C, 15 at.% O, and 2 at.% Si (Itoh *et al.*, 2013). Sclerotia undergo diagenetic changes in composition and structure while in sediments. Itoh *et al.* (2012) demonstrated that the high O/C≈ 0.5 in initally viable *C. geophilum* sclerotia within soils decreased to 0.3 to 0.1 with increased diagensis.

Israde-Alcántara *et al.* (2012a) also responded that "CSp also contain numerous noncarbon particles, including aluminosilicates, indicating that these cannot be primary biological entities, such as sclerotia." Their reasoning is inconsistent with their own observation that "CSp are dominantly carbon (>87%) with minor particulates, such as Si, Al, and Fe, concentrated in the rind," suggesting that the aluminosilicates are embedded in or present on the surface of the carbon spherules. Furthermore, Israde-Alcántara *et al.* (2012a) neglect studies such as Watanabe *et al.* (2001, 2004a) that found the exteriors and interiors of sclerotia contained inorganic components such as Al_2O_3, SiO_2, and Fe_2O_2. Inorganic nanocrystals (e.g., boehmite) were also reported in *C. geophilum* sclerotia and were thought to have formed by Al dissolution-precipitation reactions (Watanabe *et al.*, 2004b).

Kinzie *et al.* (2014) claimed that, "There is no credible mechanism by which fungi can create NDs in sclerotia," and "There is no plausible process by which sclerotia

could extract NDs from surrounding sediment." Within crushed spherule fragments that we studied (from Arlington Canyon, AC-003), TEM revealed the presence of amorphous-carbonaceous grains with numerous rounded nanocrystals embedded with their matrix (Fig. 9) that were strikingly similar to nanodiamond containing fragments reported by Kennett *et al.* (2009b), Bement *et al.* (2014), and Kinzie *et al.* (2014). Electron diffraction from the embedded nanocrystals is nearly identical to that reported for "n-diamond" in YD boundary sediments (Fig. 10). Kinzie *et al.* (2014) report that "n-diamond" is far less resistant to oxidation by perchloric acid during acid dissolution than cubic diamond, and state, "This was an advantage when analyzing cubic NDs but a major disadvantage for the other allotropes, which were no longer present [in the acid residues]."

To further characterize the nanocrystals embedded in the Arlington Canyon carbon spherule fragments, EDXS and EELS spectral image maps were collected, and representative elemental maps are shown in Fig. 11. These maps revealed that the nanocrystals were Cu (see also Daulton *et al.*, 2010). Native Cu (space group 225, *Fm-3m*: a = 3.6149 Å) has the same diffraction lines as "n-diamond" that differ by ≈ 1% in plane spacing (Table 2). The Cu nanoparticles may be stabilized from oxidation by the amorphous carbon that surrounds them, by adsorbed surface groups, or by a protective oxide surface layer. The primary oxidation product of copper, Cu_2O, is also present in the spherules (Daulton *et al.*, 2010). Cuprite, Cu_2O (Space Group 224, *Pn-3m*: a = 4.2696 Å), has essentially the same diffraction lines as the controversial "i-carbon", with planar spacings differing by ≈ 1% (Table 2). The crushed spherules also contained nanocrystals that were not embedded in any matrix (Fig. 12). Elemental mapping demonstrated these nanocrystals were copper sulfides (e.g., covellite, chalcocite, digenite, geerite, anilite, djurleite and/or roxbyite). All the amorphous carbon fragments with embedded nanocrystals that we examined contained Cu nanocrystals. We found no nanocrystals (embedded within amorphous C or not) that were consistent with diamond, "n-diamond", or "i-carbon". While our observations cannot prove that diamond, "n-diamond," and "i-carbon" are not present in the carbon spherules (and sediments), they clearly demonstrate that native Cu nanocrystals occur at far higher concentrations than "n-diamond" – should that modified form of 3C diamond exist and be present in the YDB. Since Cu nanocrystals were not reported in previous studies of YDB nanodiamonds, they were undoubtedly misidentified as "n-diamond" in the previous studies. Similarly, Cu_2O

nanocrystals were not reported and were likely misidentified as "i-carbon" in those studies.

Interestingly, common wetlands plants (undoubtedly present in "black mat" forming environments) have been shown to form nanocrystals of Cu near roots with the possible assistance by endomycorrhizal fungi (Manceau *et al.*, 2008), and such fungi include species known to form sclerotia (Münzenberger *et al.*, 2009). The filamentous fungi *Hypocrea lixii* (Salvadori *et al.*, 2013) and *Trichoderma koningiopsis* (Salvadori *et al.,* 2014*)* have been shown to synthesize spherical nanocrystals of Cu from mine waste waters. *Hypocrea lixii* is the telomorph (i.e., sexual reproductive stage) of *Trichoderma harzianum*, a widely distributed fast growing soil fungal species (Chaverri and Samuels, 2002). Mycoparasitic species of *Hypocrea/Trichoderma* can grow on sclerotia surfaces and penetrate the rind (Elad *et al.*, 1984; Benhamou and Chet, 1996). Sclerotia in forest soils have been shown to contain *H. lixii* (Asmaya *et al.*, 2015). Further, the sclerotia colonizing fungus *Fusarium oxysporum* (Xu *et al.*, 2008) has been shown to form nanoparticles of copper sulfide (chalcocite) (Hosseini *et al.*, 2012). Biomineralization mechanisms (see Pantidos and Horsfall, 2014) could account for the nanocrystalline Cu and Cu compounds observed in the carbon spherules.

Furthermore, nanocrystals (e.g., aluminosilicates and other minerals including diamond, if present) associated with the carbon spherules could be located on surfaces or within the often-reported fissures and cracks that exist now (e.g., Fig. 10), or existed previously but were closed by organic carbon accumulation and/or by low-intensity burning/annealing in sporadic wildfires. Furthermore, nanometer-sized minerals including diamond can readily enter biological systems, and this has opened the possibility of their use for drug delivery and raised concerns over their toxicity in the environment (e.g., Zhang *et al.*, 2012; Perevedentseva *et al.*, 2013). For example, nanodiamonds labeled with tritium were shown to absorb on the surface of roots and penetrate into wheat shoots (Myasnikov *et al.*, 2014).

Nanodiamond Abundances

Whether or not a unique event – but not necessarily an impact – occurred at the onset of the YD stadial depends on if nanodiamonds occur in YDB sediments at concentrations significantly elevated with respect to underlying and overlaying

sediments. Kinzie *et al.* (2014) reported nanodiamond concentrations of several hundred *parts per billion* (ppb) at the YDB layer and 0 ppb for multiple horizons at depths of tens to hundreds of centimeters above and below the YDB layer for 9 sites worldwide. However, it is technologically impossible with present instrumentation and techniques to accurately estimate concentrations of nanometer-sized minerals in sediments at and below ~tens to hundreds of *parts per million* (ppm) concentrations.

The problems associated with representative sampling and dating of fluvial sediment samples are discussed in Scott *et al.* (2016); therefore we focus on the methodology used by Kinzie *et al.* (2014) to measure nanodiamond concentrations. Similar methodologies were employed by several coauthors of Kinzie *et al.* (2014) (e.g., Kennett *et al.*, 2009a,b; Kurbatov *et al.*, 2010; Israde-Alcántara *et al.*, 2012a), as well as by (Bement *et al.*, 2014). Remarkably, Kinzie *et al.* (2014) tested their nanodiamond isolation and measurement methodology using a control sediment specimen loaded with a relatively large (0.01%) concentration of synthetic nanodiamonds, in contrast to the three to four orders-of-magnitude lower abundances (11-494 ppb) they reported for the YDB bulk sediments they processed by acid dissolution. Acid dissolution is the technique by which nanodiamonds were first isolated from carbonaceous chondrites (Lewis *et al.*, 1987), and the isolates were initially thought to be relatively pure. However, it was later recognized they contain significant amounts of amorphous to poorly crystalline carbons that were difficult to quantify by TEM and X-ray diffraction. Acid-dissolution residues *always* contain non-diamond impurities, representing: minerals that survive acid dissolution, transformation products/residues/condensates of acid dissolution, and laboratory contaminants (e.g., Gilmour *et al.*, 1992, 2003; Daulton *et al.*, 1996; Stroud *et al.*, 2011; Israde-Alcántara *et al.,* 2012a; Heck *et al.*, 2014; Kinzie *et al.*, 2014). The amount of impurities is usually large, ~50% to near 100%, and can be dominated by amorphous to poorly crystalline carbons. Israde-Alcántara *et al.* (2012a) and Kinzie *et al.* (2014) subjectively estimated the purity of their acid residues at "about ±50%" and "< 50%", respectively.

Due to the significant levels of non-diamond phases in the acid dissolution isolates, the abundance estimations of nanodiamonds in sediments based on mass balance are subject to large error. For nanodiamond concentrations below ~several ppm, where the recovered nanodiamond masses are very small (<micrograms per gram of processed material) and subject to greater relative contamination, the mass

balance approach has extremely large error. In fact, contamination levels are greater and nanodiamonds are more readily lost when large amounts of matrix (> several tens of grams) are processed, and this is particularly problematic with small nanodiamond concentrations (i.e., less than a ppm). Kinzie *et al.* (2014) processed between 20 to 150 g of dry-sieved material per sediment horizon and state, "The acid extraction process commonly yielded very little residue that was nearly invisible to the naked eye inside the centrifuge tubes and often was detectable only by light microscope." They further state in their supplemental materials that, "We placed all the residue on a single [TEM] grid, whenever possible. If not, we measured the total amounts used or not used to get a percentage per grid."

The combined errors in measurement of the minuscule mass of the recovered residue, and the fraction thereof placed on the TEM grid, is compounded with the error in measuring relative modal (mass) abundance of the different minerals present in the non-pure residue. Accurate measurements of modal abundances are required for determination of the mass of the recovered nanodiamonds from the mass of acid residues or from the mass of crushed carbon spherules. Kinzie *et al.* (2014), Bement *et al.* (2014), and Kurbatov *et al.* (2010) estimated modal abundances by measuring projected areal densities (i.e., projected TEM support film coverage) of nanometer to submicron-sized grains deposited on TEM grids. Projected areal densities are not measurements of the relative mass of nanodiamonds with respect to the mass of non-diamond minerals, and their use will yield large errors in the determination of the nanodiamond abundance in sediments, carbon spherules, and ice cores. For example, to estimate the relative mass of the ubiquitous amorphous to poorly graphitized carbon within which the nanocrystals were observed requires measurement of the thickness and mass density of those carbon forms, in additional to a projected areal density. The thickness – and therefore mass – of the amorphous to poorly graphitized carbon can vary greatly on the TEM grids.

Furthermore, the greatest limitation of the approach of Kinzie *et al.* (2014) and others is that detailed measurements must be performed on each individual grain in order to correctly identify it as diamond (see, Daulton *et al.*, 2010). Kinzie *et al.* (2014) state, "NDs represent <50% of the residue, and the remaining non-ND residue can mask the NDs, thus making them difficult to identify. In addition, there are inherent difficulties and uncertainties in correctly identifying tiny crystals <2 nm in diameter." Kinzie *et al.* (2014) further state, "By themselves, SA[E]D patterns are

insufficient to identify NDs, and so further investigations, such as those using HRTEM, FFT, ED[X]S, and EELS, were performed on these nanoparticles to confirm that they are NDs and not some other mineral." In their conclusions, Kinzie *et al.* (2014) wrote, "The identification of the isolated NDs involves two main methods, electron microscopy imaging and electron spectroscopy, using up to nine imaging, analytical, or quantification procedures: scanning electron microscopy, STEM, TEM, HRTEM, ED[X]S, SA[E]D, FFT, EELS, and EFTEM. The entire procedure is labor-intensive and technically demanding." However, Kinzie *et al.* (2014) perplexingly describe in their supplemental materials, ". . . for the purpose of estimating abundances, *we assumed that all rounded particles were NDs* [emphasis added]. We also observed abundant amorphous carbon nanoparticles, but almost none were rounded, and therefore, we discounted them. This estimation procedure *focused solely on the presence or absence of rounded particles* [emphasis added]." Given the importance of this point, it is troubling that it was stated not in the main paper but only in the supplemental materials. We reiterate that Kinzie *et al.* (2014) measured projected areal densities of "rounded particles," not necessarily nanodiamonds, and they certainly did not measure modal mass abundances. This is a critical flaw, given that the acid-dissolution residues and crushed spherules are not pure diamond.

Israde-Alcántara *et al.* (2012a) report that, "[Lake] Cuitzeo [Mexico] CSp [carbon spherules] contain numerous noncarbon particles including aluminosilicates." We observed a range of non-carbonaceous crystalline minerals in carbon spherules from Arlington Canyon; their mass abundance was of the order of several percent of the spherule mass. We also found the carbon spherules contained amorphous-carbon with rounded nanocrystals embedded with their matrix (Fig. 6) that were strikingly similar to nanodiamond containing spherule fragments reported by Kennett *et al.* (2009b), Bement *et al.* (2014), and Kinzie *et al.* (2014). However, we found the embedded nanocrystals were native Cu in all spherule fragments examined. In no case did we observe diamond, "n-diamond," and "i-carbon," and while our observations cannot prove their absence in the carbon spherules, they clearly demonstrate that native Cu nanocrystals occur at far higher concentrations than "n-diamond." As in the case for the carbon spherules, glass-like carbon from YDB sediments have been shown to contain nanocrystals of Ca-rich, Ti-rich, Ti-rich, and Fe-rich phases which can have rounded morphologies (van Hoesel, 2014). Nanocrystals of native Cu, Cu compounds, and other minerals that are present in

crushed carbon spherules are undoubtedly included in the counting statistics of Kinzie *et al.* (2014) and others that counted "rounded particles."

The method of estimating TEM grid surface coverage of rounded particles by Kinzie *et al.* (2014) is further puzzling given that angular, octahedral, and euhedral nanodiamonds have been reported in YDB-aged sediments. Kennett *et al.* (2009b) claim, ". . . clusters of stable cubic diamonds (≈1,000 in total) were found with carbon elongates . . . These diamonds appear more angular than the associated n-diamonds," and "TEM study revealed conspicuous subrounded, spherical, and octahedral crystalline particles . . . Analysis of the particles by electron diffraction show reflections consistent with . . . metastable 'new-diamond' polymorph or n-diamond." Similar descriptions of the YDB nanodiamonds appear in Kennett *et al.* (2009a). Furthermore, an example of a cubic diamond from black mat sediments of presumed YDB-age at Lommel Belgium, and shown in Fig. 2 of Tian *et al.* (2011), is flake-like with an irregular non-rounded shape. van Hoesel *et al.* (2012) reported submicron cubic diamonds with irregular non-rounded shape (their Fig. 6) in the Usselo horizon at Geldrop-Aalsterhut, The Netherlands. Israde-Alcántara *et al.* (2012a) described the nanodiamonds they reportedly identified as, ". . . nanocrystalline carbon particles ranging in shape from spherical to elongate to euhedral . . . embedded in amorphous carbon, as Tian *et al.* (14) described. We identified three of four previously reported ND variants, of which, n-diamond was the most abundant."

Kinzie *et al.* (2014) prepared TEM specimens by placing dried acid residues or crushed spherules into suspension using NH_4OH, depositing aliquots of suspended grains on the TEM grids, and allowing the aliquots to evaporate. Another limitation of the TEM approach for determining modal abundances is that depositing liquid-suspended grains on a TEM grid results in highly heterogeneous grain dispersions. This is problematic because variation in surface chemistry of different minerals or mineral grains of different sizes can result in different tendencies to cluster and/or adhere to the TEM support film. Consequently, measured modal distributions based only on analysis of the TEM-accessible regions, with nearly monolayer dispersions of spatially well-separated grains, can be greatly skewed from the true modal distribution. Often electron-transparent multilayer deposits form, consisting of overlapping grains that make it difficult to identify individual grains or determine modal abundances. Furthermore, thick grain aggregates are electron-beam opaque and cannot be analyzed by TEM. These regions can have different mineral modal

abundances than the TEM-accessible regions.

Kinzie *et al.* (2014) state in their supplemental materials that they analyzed between 16 and 92 (average of 28) random 350 x 350 nm^2 TEM field of views. Unfortunately, the sampling was not identical for each TEM grid, and it is unclear which sediment horizons received increased scrutiny (e.g., the horizons that were expected to contain nanodiamonds). A larger problem is that their mean sampling corresponds to ≈0.000017% of the viewable area of a TEM grid. Given the highly inhomogeneous grain dispersions on their TEM grids, this represents a statistically inadequate grain sampling that could account for the 0 ppb nanodiamond abundances they measured in sediments that bracketed the reported YDB layer. Of course, TEM can provide no measure of any grains dispersed on the TEM inaccessible grid bars.

The numerous experiment difficulties in using TEM to measure nanodiamond abundances in sediments render this approach infeasible. The only analytical method accepted to reasonably assess ~several to tens of ppm abundances of nanodiamonds within a matrix is a technique applied to meteoritic nanodiamonds that measures the amount of supernova-derived Xe-HL gases (see review by Daulton, 2006) released during stepped combustion of acid-dissolution residues. By measuring a tracer unique to the nanodiamonds, only the nanodiamonds are measured; this contrasts with the mass-balance approach that measures the combined mass all the different materials (including adsorbed moisture) present in the acid residue. Diamonds are thought to be the only carriers of the Xe-HL gases in the non-pure nanodiamond isolates, based on the smooth elemental abundance pattern of extracted noble gases relative to cosmic abundances, suggesting all HL noble gases are a single gas component trapped in a single mineral species (Huss and Lewis, 1994). This assumption is also based on the high release temperatures (1100-1600°C) of the HL gas component (Huss and Lewis, 1994). Furthermore, the release of HL gases is accompanied by release of CO_2 (Lewis, 1994), indicating that the HL component resides only in the most refractory carbonaceous minerals (see also Daulton, 2006). This method has the advantage that it can be used to monitor any decrease in the HL gas component (i.e., loss of the carrier phase) after each step of the acid-dissolution process, or following any post-processing. However, the method has the disadvantage that is does not directly measure nanodiamonds that lack Xe-HL gases.

A number of noble gas measurements have been performed on terrestrial diamonds (for a review, see Basu *et al.*, 2013). For example, Verchovsky *et al.*

(1991) measured one diamond from the Popigai crater and reported unusually high concentrations of radiogenic ^{40}Ar. Subsequent measurements of Popigai diamonds yielded a similar range of ^{40}Ar/^{36}Ar ratios as in kimberlitic diamonds, however with significantly higher ^{40}Ar concentrations (Shelkov *et al.*, 1998). Metamorphic microdiamonds from the Kokchetav Massif have primary ^{40}Ar concentrations that fall between the ranges exhibited by kimberlitic and Popigai impact diamonds (Verchovsky *et al.*, 1993). Secondary processes, such as implantation of U and Th decay products, appear to have severely modified the primary isotopic compositions of the noble gases that were trapped during formation of the microdiamonds. Kokchetav microdiamonds contain ^{4}He concentrations that are among the highest observed in any terrestrial diamonds (Verchovsky *et al.*, 1993). Carbonado diamonds from Africa and Brazil also contain large amounts implanted radiogenic ^{4}He in addition to nucleogenic Xe and Kr (Ozima *et al.*, 1991). Unfortunately, there have been no measurements of trapped noble gases performed on nanodiamonds from the YDB boundary or the underlying/overlaying sediment layers. Therefore it is unclear if they carry any unique trapped gas component useful as a tracer for abundance measurements.

Carbon Isotopic Compositions of Nanodiamonds

Nanodiamonds are a minor component (see Lewis *et al.*, 1987; Rietmeijer and Mackinnon, 1987, Dai *et al.*, 2002) of the ~ 4 x10^{7} kg/yr interplanetary dust flux that is accreted by Earth (Love and Brownlee, 1993), with accretion rates in the last glacial period comparable to the present (Yada *et al.*, 2004). In arguing against the fall of interplanetary dust as an explanation for nanodiamonds in YDB sediments, Israde-Alcántara *et al.* (2012a) incorrectly state that "Tian *et al.* (14) concluded that YDB NDs are not cosmic because they display δ^{13}C abundances (−28.1 to −26.3‰) that are terrestrial." van Hoesel *et al.* (2012) make a similar incorrect statement. Tian *et al.* (2011) actually stated, "carbon isotope measurements and C/N values were determined from the black material of the Lommel YDB layer. The nanodiamond particles in the present material could not be analyzed separately because of their small size." Tian *et al.* (2011) performed these measurements to look for evidence of an impact event through the presence of C in the sediments that originated from the impactor and concluded that, "results obtained on the Lommel material do not

distinguish between terrestrial and extraterrestrial origins for the carbon." Israde-Alcántara *et al.* (2012a) also incorrectly concluded that "Isotopic analyses of the carbon-rich YDB interval at Cuitzeo yielded values ranging from −23 to −19‰ for $\delta^{13}C$ consistent with the formation of Cuitzeo NDs from terrestrial, not cosmic, carbon." Similar to Tian *et al.* (2011), Israde-Alcántara *et al.* (2012a) measured sediment, not nanodiamond isolates. Neither of the bulk sediment $\delta^{13}C$ measurements can provide direct information about the nanodiamonds, which make up only a tiny fraction of the C in the sediments. Kinzie *et al.* (2014) also invoke this erroneous evidence by citing both papers and stating, "($\delta^{13}C$, $\delta^{15}N$, and C/N) in YDB NDs are consistent with a terrestrial origin." They also incorrectly interpret the $\delta^{13}C$ measurements of sediments by Tian *et al.* (2011) as ruling out a mantle origin of the nanodiamonds.

Measurement of the $\delta^{13}C$ compositions of nanodiamonds isolated from sediments or matrix by acid dissolution is experimentally challenging. The non-diamond carbonaceous phases, which can comprise over half the residue, are potentially of different origin as the nanodiamonds and hence can have different C isotopic compositions. While $\delta^{13}C$ values measured from C released at high temperature during stepped combustion of the acid residue will limit C contributions from the most labile (low-temperature released) components, it is not possible to correct for contributions from the non-diamond carbonaceous minerals that combust along with the nanodiamonds. Consequently, bulk C isotopic measurements of acid residues are highly suspect with respect to the true nanodiamond C isotopic composition. Therefore, bulk C isotopic measurements of acid dissolution isolates of terrestrial sediment nanodiamonds (Carlisle, 1992; Gilmour *et al.*, 1992), impact diamonds (Hough *et al.*, 1995; Gilmour *et al.*, 2003), and meteoritic nanodiamonds (c.f., Swart *et al.*, 1983, Russell *et al.*, 1996) cannot provide information about their origins. Indeed, this point has driven recent attempts by two groups to pursue C isotopic measurements of individual meteoritic nanodiamonds using atom probe tomography (Heck *et al.*, 2014).

Synchronous Chronologies and Stratigraphic YDB Markers

An important challenge for the YD Impact Hypothesis is that, in order to attribute the source of nanodiamonds in Late Pleistocene sediments to an impactor/bolide

event, it is necessary that all sediments reported to contain nanodiamonds date synchronous to the YD onset. However, nanodiamonds (and "n-diamond") have been reported in sediments and in carbonaceous forms within sediments that do not date to the YDB (Firestone *et al.*, 2007, 2010a; Yang *et al.*, 2008; van Hoesel *et al.*, 2012, 2013; Bement *et al.*, 2014; Kinzie *et al.*, 2014). Most importantly, and despite widespread claims of synchroneity by YD impact proponents (see, Kennett *et al.*, 2015a,b), age control is poor or nonexistent at nearly all sites where nanodiamonds are reported "at" the YDB layer (e.g., see Blaauw *et al.*, 2012; Ives and Froese, 2013; Wittke *et al.*, 2013c; van Hoesel *et al.*, 2013, 2014; Meltzer *et al.*, 2014; Holliday *et al.*, 2014). There are only two sites where nanodiamonds are reported at a layer that can be confidently dated to the YD onset: Daisy Cave and Sheriden Cave (Meltzer *et al.*, 2014). However, Meltzer *et al.* (2014) cautions that at Sheriden Cave, ". . . the supposed YDB layer has the required age, but its age is inconsistent with the ages of the layers that encompass it."

The YDB sediment layer is often described as being at the base of a dark-colored stratum termed by YD impact proponents as "the black mat" that is used as the primary stratigraphic marker for the YDB (Firestone *et al.*, 2007, 2010a; Firestone 2009, Mahaney *et al.*, 2010; Israde-Alcántara *et al.*, 2012a; Wittke *et al.*, 2013a). Nanodiamonds and other proposed impact markers are reported directly beneath the black mat (Firestone *et al.*, 2007, 2010a). A distinct, dark colored stratum is present at the Murray Springs, Arizona archeological site, with sediments containing Clovis artifacts and megafaunal fossils below the horizon and sediments devoid of these materials above. Haynes (2008) identified 55 localities in the western United States and 2 in the eastern United States with ". . . a black organic-rich layer or 'black mat' in the form of mollic paleosols, aquolls, diatomites, or algal mats with radiocarbon ages suggesting they are stratigraphic manifestations of the Younger Dryas cooling episode." These and other similar deposits have been described as organic-rich, silty sediments (e.g., Brakenridge, 1981; Quade *et al.*, 1998; Baker *et al.,* 2008), however their total organic carbon content varies (most cases < 5 wt. %) and is not correlated with sediment texture and color (see Pinter *et al.*, 2011; Harris-Parks, 2014, 2016). In fact, such deposits vary in color and white-colored diatomites have been described as "black mats" (Haynes, 2008). These deposits form in wet environments ranging from wet meadows to shallow ponds (Quade *et al.*, 1998; Haynes, 2008; Harris-Parks, 2016). "Black mat" formation, at least in southern Nevada, peaked during the YD

from 11,200-10,000 ^{14}C a BP (Quade *et al.*, 1998). However, formation was time-transgressive across, rather than synchronous with, the YDB (Holliday and Meltzer, 2010; Harris-Parks, 2014, 2016). Such dark colored deposits are not unique to the western United States or to the YDB, but in fact are well recognized as paleo-wetland deposits found in similar settings around the world and at numerous time horizons through at least the late Quaternary (e.g., Quade *et al.*, 1998; Rech *et al.*, 2003; Mandel, 2008; Pinter *et al.*, 2011; Pigati *et al.,* 2012).

Black mats and the unreliable reports of spikes in the nanodiamond concentration, as discussed previously, cannot link chronologies at different sites. The reported concentration spikes of the other currently debated mineralogical and geochemical markers at the YDB have all been vigorously challenged. These markers include combustion products (charcoal/soot, glass-like carbon, carbon elongates, and carbon spherules), magnetic minerals (grains, spherules), and Ir (see, Firestone *et al.*, 2007, 2010a; Firestone, 2009; Kennett *et al.*, 2008, 2009b). In addition, Bunch *et al.* (2012) reported a correlation between elevated abundances of siliceous scoria-like objects and Fe/Si-rich microspherules at the YDB layer at three out of 18 sites studied (Abu Hureyra, Syria; Melrose, Pennsylvania; and Blackville, South Carolina). Of these materials, nanodiamonds have been reported within glass-like carbons (Firestone *et al.*, 2007, 2010a; Firestone, 2009; Israde-Alcántara *et al.,* 2012a supplemental materials; Kinzie *et al.*, 2014), carbon elongates (Kennett *et al.*, 2009b), and carbon spherules (Firestone, 2009, Firestone *et al.*, 2010a; Kennett *et al.*, 2009a; Israde-Alcántara *et al.,* 2012a supplemental materials; Kinzie *et al.*, 2014).

One aspect of most versions of the YD Impact Hypothesis is the assertion that intense, impact-ignited wildfire raged across North America and Europe (Kristan-Tollmann and Tollmann, 1992; Firestone *et al.*, 2006). Charcoal/soot, glass-like carbon, carbon elongates, and carbon spherules reported in YDB sediments are interpreted as high-temperature combustion products and evidence of synchronous intercontinental wildfires (Firestone *et al.*, 2007, 2010a; Firestone, 2009; Kennett *et al.*, 2008, 2009a,b; Wittke *et al.*, 2013a). For instance, Firestone *et al.* (2007) propose, ". . . glass-like carbon, carbon spherules, and nanodiamonds were produced in the YDB by high temperatures resulting from the impact and associated biomass burning." Kennett *et al.* (2008) studied the wildfire evidence and wrote, "Intense wildfire evidence is also indicated by the presence of carbon spherules . . . spherules occur widely in the YDB layer in North America and have also been found in surficial

sediments associated with intense coniferous forest crown fires (Firestone *et al.,* 2007)." In apparent contradiction, Israde-Alcántara *et al.* (2012a) state that the, ". . . indication that the YDB proxies [e.g., carbon spherules, nanodiamonds, magnetic spherules] are not wildfire-related is that marker peaks (2.80 to 2.75 m) were deposited earlier than the wildfire charcoal peak (2.70 to 2.65)," suggesting wildfires were not synchronous with (and immediately caused by) the impact event at their study site, Lake Cuitzeo. As for the nanodiamonds in the YDB spherules, Firestone *et al.* (2006) first speculated that they ". . . rode in with an asteroid or comet, or on the supernova debris cloud," but later speculated they were formed during the impact event Firestone *et al.* (2007). Kinzie *et al.* (2014) conclude, ". . . the best explanation is that ND-rich carbon spherules derive from conifers that were incinerated by the impact event", and cite Israde-Alcántara *et al.,* 2012a who cite Kimbel *et al.* (2008), which report the formation of "n-diamonds" in charred coal, coconut shells, and wood; they state, ". . . [our] procedure is identical to the commercial process for producing activated charcoal . . . The process of forming n-diamonds requires conditions unlike any that are normal to the Earth's surface . . . [and] match the extreme conditions that exist during an ET impact or airburst." Kinzie *et al.* (2014) stress that the nanodiamonds and their host carbon spherules must have been formed within the impact fireball itself, and provide several arguments against their formation by wildfire, stating, ". . . there is no evidence for and no known process for production of NDs in natural wildfires." Millimeter-diameter, nanodiamond-containing carbon spherules that formed in an impact fireball should be localized to the immediate area of the impact site(s). However, despite the assertion by impact proponents that the primary YD impact site is in North America, nanodiamond-containing carbon spherules are reported widely distributed over several continents. For example, Kinzie *et al.* (2014) report the abundance of nanodiamonds in carbon spherules from YDB sediments in Ommen, the Netherlands are higher than at 12 out of 14 North American sites studied, and abundances in Lingen, Germany are higher than at 10 of those North American sites.

A study of 35 lake sediment cores across North America could neither confirm a charcoal peak associated with the YDB at any location nor find any indication of continent-wide wildfire (Marlon *et al.*, 2009). Similar conclusions were drawn from subsequent studies (Gill *et al.*, 2009; Daniau *et al.*, 2010; Pinter *et al.*, 2011). In fact, most YD-aged "black mats" in North America contain negligible amounts of charcoal

(Haynes *et al.*, 2010a; Harris-Parks, 2014, 2016). As for as the other proposed impact-derived combustion products, Scott *et al.* (2010) report that glass-like carbon, carbon elongates, and carbon spherules are ubiquitous in sediments and occur throughout Late Pleistocene to Holocene sedimentary sequences. Further, sclerotia are morphologically identical to the reported YDB carbon spherules (Scott *et al.*, 2010), and are commonly reported in sediments (e.g., see McWeeney, 1989; Shay and Kapinga, 1997; Deal, 2005).

The reported spikes in concentration at the YDB of magnetic spherules, siliceous scoria-like objects, and Ir are also strongly contested. These markers are not reported to be directly associated with nanodiamonds and, in fact, nanodiamonds are not reported at the three YDB sites where lechatelierite-containing magnetic spherules and scoria-like objects are reported. Therefore, these markers will not be discussed further, but reviews of the contested studies are found in Pinter *et al.* (2001), van Hosesel (2014), van Hoesel *et al.* (2014), and Holliday *et al.* (2014). The point is that there are no clear and undisputed concentration spikes for any mineral or geochemical signature that can be used identify the YDB and link chronologies at different sites.

Even if the reported concentration spikes in Late Pleistocene sediments are accepted, there are problems in interpreting them as indicators of impact/bolide event(s). Impact/bolide events should result in nearly simultaneous deposition of impact markers with respect to the mean sedimentary rates at a given site. Natural mixing processes (e.g., bioturbation, transport, and redeposition) should thoroughly mix the different mineralogical and geochemical markers within a sediment horizon and widen their distribution vertically in stratigraphic sequences. While some sorting might occur, the peaks in abundance with respect to stratigraphy should approximately overlap for all markers. Multiple abundance peaks for any given marker, and marker peaks that are vertically offset and distinct from one another, would not be expected. At several Carolina Bays (M31 and M33 of Myrtle Beach, South Carolina), two well-separated peaks in magnetic grain abundance are reported, with the peak at the higher stratigraphic level correlated with a peak in charcoal abundance (Firestone *et al.*, 2010a). Firestone *et al.* (2007, 2010a) report at Chobot, Alberta Canada correlated abundance peaks in carbon spherules, glass-like carbon, and charcoal in sediments that lie below sediments with correlated abundance peaks in magnetic grains and magnetic spherules. At Topper, South Carolina, Firestone *et al.* (2007, 2010a) report that the abundance peaks in glass-like carbon and magnetic

grains do not overlap. At the Gainey, Michigan, Firestone *et al.* (2010a) report two peaks in magnetic grain abundance, with the peak at the lower stratigraphic level correlated with a peak in magnetic spherules abundance. At Arlington Canyon, two well separated sets of correlated peaks at ≈ 400 and ≈ 500 cm below surface (cmbs) for charcoal, carbon elongates, carbon spherules, and nanodiamonds are reported that bracket a horizon of gravel to coarse sand (Kennett *et al.*, 2008, 2009b; Kinzie *et al.*, 2014). Note that Kenneth *et al.* (2008, 2009b) report carbon spherules are absent between 95 to 416 cmbs and their abundance peaks near 500 cmbs, while the abundance of carbon elongates has two resolved peaks near 394 cmbs and 500 cmbs. Kinzie *et al.* (2014), with Kennett as a coauthor, provide no abundance measurements for carbon elongates and instead report two peaks in the abundance of carbon spherules at 394 cmbs and 500.5 cmbs at concentrations that are a sum of carbon spherule and carbon elongate concentrations reported by Kenneth *et al.* (2008, 2009b).

Discussion and Conclusions

The YDB nanodiamond data are considered by some as the strongest physical evidence for an YD impact/bolide event. We have analyzed the nanodiamond data used to provide evidence for the YD Impact Hypothesis and have identified critical problems with the collection of those data and/or the data interpretation. In evaluating the evidence we arrived at four main conclusions.

1) The presence of lonsdaleite in sedimentary deposits can suggest – but cannot on its own demonstrate – that an impact event occurred. In YDB sediment, however, there is no credible evidence of the presence of lonsdaleite. In previous studies, graphene/graphane aggregates have been misidentified as lonsdaleite, diffraction patterns have been incorrectly indexed to lonsdaleite, and FFT transforms of single high-resolution lattice images used to identify lonsdaleite are known to yield misleading results.

2) While there is evidence of cubic nanodiamonds in Late Pleistocene sediments, their presence does not provide evidence of an impact because they have not been linked with impact processes. To do so would require correlating the nanodiamonds to an established and recognized impact marker. There are no established reports in YDB sediments of any of the accepted and recognized shock minerals found at known

impact structures (c.f., French and Koeberl, 2010; van Hoesel *et al.*, 2014). Carbon spherules, carbon elongates, and glass-like carbon reported associated with the nanodiamonds are not recognized as impact markers. Furthermore, these associations are reported to occur in sediments that are not limited to the YDB and therefore cannot provide evidence of processes unique to the YD onset.

3) The use of the controversial "n-diamond" as an impact marker, which constitutes the majority of the nanodiamond evidence for the YD Impact Hypothesis, is problematic due to the presence of native Cu nanocrystals in sediments that can be easily confused for "n-diamond". Further, "n-diamond" is reported in sediments that do not date to the YD onset, and more importantly, formation of these nanocrystals have not been linked exclusively to shock formation processes.

4) The presence of a single spike in nanodiamond concentration within Pleistocene to Holocene sediments at the YDB layer would strongly suggest that a unique event – but not necessarily an impact – occurred at the YD onset. Nanodiamond abundances from bulk sediments processed by acid dissolution, for crushed carbon spherules, and for ice by Kinzie *et al.* (2014) and those previously published by several of its coauthors in other studies (e.g., Kennett *et al.*, 2009a,b; Kurbatov *et al.*, 2010; Israde-Alcántara *et al.*, 2012a), as well as by a coauthor of Kennett *et al.* (2009a) (Bement *et al.*, 2014) are all based on TEM studies. However, the TEM measurements by Kinzie *et al.* (2014) and others using similar methodologies are not of nanodiamonds, but are of "rounded particles." More importantly, the many experiment difficulties inherent in using TEM to measure nanodiamond abundances lead to large unconstrained error, rendering this approach infeasible. We find there is no evidence to suggest a unique spike in the nanodiamond concentration at the YDB layer. The distribution of nanodiamonds in Pleistocene to Holocene sediments (and in ice, if present, which has yet to be confirmed by independent groups, see Boslough, 2013b) remains unclear. Therefore, considering conclusions 1-4, the reports of nanodiamonds in Late Pleistocene sediments cannot provide evidence for an YD impact.

Various criticisms have been raised on both sides of the debate regarding the identification, analysis, and interpretation of proposed YD impact markers. To advance this field, it would be advantageous for working groups to develop and standardize techniques for collection, splitting/distribution, and analysis of specimens

from key YDB sites, in order to try to reconcile conflicting results and prevent the use of inappropriate approaches that lead to erroneous results. To perform the highly challenging measurement of nanodiamond abundance in sediments/ice, methods other than TEM will need to be explored and developed. Any method must be tested/calibrated against control specimens (sediments/ice initially devoid of nanodiamonds, that are spiked with measured ppb amounts of nanodiamonds). Furthermore, unlike previous abundance measurements, future measurements must be conducted as blind studies to preclude unconscious bias.

Acknowledgements. This research was partially supported by the McDonnell Center for the Space Sciences and Institute for Material Science and Engineering (TLD) as well as grants from the National Geographic Society (8321-07) to NP and from the National Science Foundation (EAR-0746015) to NP and RSA. ACS undertook the completion of this research while in receipt of a Leverhulme Emeritus Fellowship (EM-2012-054), which is gratefully acknowledged. We thank Ph. Claeys (Vrije Universiteit Brussel) for providing YDB sediment specimens from Lommel Belgium. We thank M. Watanabe (Tokyo Metropolitan University, Graduate School of Urban Environmental Sciences) for valuable discussions. We thank the numerous staff at the Channel Islands. ACS thanks Sharon Gibbons and Neil Holloway for technical support. We thank reviewers C. Koeberl and B. Alloway for valuable comments.

Abbreviations: DF, dark field; BF, bright field; EDXS, energy dispersive X-ray spectroscopy; EELS, electron energy loss spectroscopy; FFT, fast Fourier transformation; GIF, Gatan imaging filter; NMR, nuclear magnetic resonance; ppb, parts per billion; ppm, parts per million; SDD, silicon drifted detector; HR-TEM, high-resolution transmission electron microscopy; STEM, scanning transmission electron microscopy; TEM, transmission electron microscopy; YD, Younger Dryas; YDB, Younger Dryas Boundary

References

Algra RE, Hocevar M, Verheijen MA, Zardo I, Immink GGW, van Enckevort WJP, Abstreiter G, Kouwenhoven LP, Vlieg E, Bakkers EPAM. 2011. Crystal structure transfer in core/shell nanowires. *Nano Letters* **11**: 1690-1694.

Allan DS, Delair JB. 1994. When the Earth nearly died: Compelling evidence of a catastrophic world change 9500 BC. Gill & Macmillan Ltd, Dublin, Ireland.

Allan DS, Delair JB. 1997. Cataclysm: Compelling evidence of a cosmic catastrophe in 9500 B.C., Bear & Company, Rochester, VT.

Amasya A, Narisawa K, Watanabe M. 2015. Analysis of sclerotia-associated fungal communities in cool-temperate forest soils in North Japan. *Microbes Environ* **30**: 113-116.

Andronikov AV, Subetto DA, Lauretta DS, Andronikova IE, Drosenko DA, Kuznetsov DD, Sapelko TV, Syrykh LS. 2014. In search for fingerprints of an extraterrestrial event: Trace element characteristics of sediments from the Lake Medvedevskoye (Karelian Isthmus, Russia). *Doklady Earth Sciences* **457**: 819-823.

Baker DW, Miranda PJ, Gibbs KE. 2008. Montana evidence for extra-terrestrial impact event that caused ice-age mammal die-off. *EOS Trans. Am. Geophys. Union* **89**: P41A-05.

Barnosky AD, Koch PL, Feranec RS, Wing SL, Shabel AB. 2004. Assessing the causes of the Late Pleistocene extinctions on the continents. *Science* **306**: 70-75.

Basu S, Jones AP, Verchovsky AB, Kelley SP, Stuart FM. 2013. An overview of noble gas (He, Ne, Ar, Xe) contents and isotope signals in terrestrial diamond. *Earth-Science Reviews* **126**: 235-249.

Bement LC, Madden AS, Carter BJ, Simms AR, Swindle AL, Alexander HM, Fine S, Benamara M. 2014. Quantifying the distribution of nanodiamonds in pre-Younger Dryas to recent age deposits along Bull Creek, Oklahoma Panhandle, USA. *Proc. Natl. Acad. Sci. USA* **111**: 1726-1731.

Benedict JB. 2011. Sclerotia as indicators of mid-Holocene tree-limit altitude, Colorado Front Range, USA. *The Holocene* **21**: 1021-1023.

Benhamou N, Chet I. 1996. Parasitism of sclerotia of *Sclerotium rolfsii* by *Trichoderma harzianum*: Ultrastructural and cytochemical aspects of the interaction. *Biochemistry and Cell Biology* **86**: 405-416.

Berger WH. 1990. The Younger Dryas cold spell – a quest for causes. *Palaeogeography, Palaeoclimatology, Palaeoecology* **89**: 219-237.

Bertnatowicz TJ, Cowsik R, Gibbons PC, Lodders K, Fegley Jr. B, Amari S, Lewis RS. 1996. Constraints on stellar grain formation from presolar graphite in the

Murchison meteorite. *The Astrophys. J.* **472**: 760-782.

Bhargava S, Bist HD, Sahli S, Aslam M, Tripathi HB. 1995. Diamond polytypes in the chemical vapor deposited diamond films. *Appl. Phys. Lett.* **67**: 1706-1708.

Billinge SJL, Levin I. 2007. The problem with determining atomic structure at the nanoscale. *Science* **316**: 561-565.

Blaauw M, Holliday VT, Gill JL, Nicoll K. 2012. Age models and the Younger Dryas Impact Hypothesis. *Proc. Natl. Acad. Sci. USA* **109**: E2240.

Boslough M. 2012. Inconsistent impact hypotheses for the Younger Dryas. *Proc. Natl. Acad. Sci. USA* **109**: E2241.

Boslough M, Nicoll K, Holliday V, Daulton TL, Meltzer D, Pinter N, Scott AC, Surovell T, Claeys P, Gill J, Paquay F, Marlon J, Bartlein P, Whitlock C, Grayson D, Jull AJT. 2012. Arguments and evidence against a Younger Dryas impact event. *Climates, Landscapes, and Civilizations*. *Geophysical Monograph Series* **198**: American Geophysical Union; 13-26.

Boslough M. 2013a. Greenland Pt anomaly may point to noncataclysmic Cape York meteorite entry. *Proc. Natl. Acad. Sci. USA* **110**: E5035.

Boslough M. 2013b. Faulty protocols yield contaminated samples, unconfirmed results. *Proc. Natl. Acad. Sci. USA* **110**: E1651.

Boslough M, Harris AW, Chapman C, Morrison D. 2013. Younger Dryas impact model confuses comet facts, defies airburst physics. *Proc. Natl. Acad. Sci. USA* **110**: E4170.

Boslough M, Nicoll K, Daulton TL, Scott AC, Claeys P, Gill JL, Marlon JR, Bartlein P J. 2015. Incomplete Bayesian model rejects contradictory radiocarbon data for being contradictory. *Proc. Natl. Acad. Sci. USA* **112**: E6722.

Bostick BC, Jones RE, Ernst WG, Chen C, Leech ML, Beane RJ. 2003. Low-temperature microdiamond aggregates in the Maksyutov Metamorphic Complex, South Ural Mountains, Russia. *Am. Mineral.* **88**: 1709-1717.

Brakenridge GR. 1981. Terrestrial paleoenvironmental effects of a Late Quaternary-age supernova. *Icarus* **46**: 81-93.

Brakenridge GR. 2011. Core-collapse supernovae and the Younger Dryas/terminal Rancholabrean extinctions. *Icarus* **215**: 101-106.

Brooks MJ, Taylor BE, Ivester AH. 2010. Carolina Bays: Time capsules of culture and climate change. *Southeastern Archaeology* **29**: 146-163.

Bunch TE, West A, Firestone RB, Kennett JP, Wittke JH, Kinzie CR, Wolbach WS. 2010. Geochemical data reported by Paquay et al. do not refute Younger Dryas impact event. *Proc. Natl. Acad. Sci. USA* **107**: E58.

Bunch TE, Hermes RE, Moore AMT, Kennett DJ, Weaver JC, Wittke JH, DeCarli PS, Bischoff JL, Hillman GC, Howard GA, Kimbel DR, Kletetschka G, Lipo CP, Sakai S, Revay Z, West A, Firestone RB, Kennett JP. 2012. Very high-temperature impact melt products as evidence for cosmic airbursts and impacts 12,900 years ago. *Proc. Natl. Acad. Sci. USA* **109**: E1903-E1912.

Bundy FP, Kasper JS. 1967. Hexagonal diamond—A new form of carbon. *J. Chem. Phys.* **46**: 3437-3446.

Burkhard G, Dan K, Tanabe Y, Sawaoka AB, Yamada K. 1994. Formation of cubic carbon by dynamic shock compression of a diamond/amorphous carbon powder mixture. *Jpn. J. Appl. Phys.* **33**: 5875-5885.

Carlisle DB, Braman DR. 1991. Nanometre-size diamonds in the Cretaceous/Tertiary boundary clay of Alberta. *Nature* **352**: 708-709.

Carlisle DB. 1992. Diamonds at the K/T boundary. *Nature* **357**: 119-120.

Carlson AE. 2013. The Younger Dryas Climate Event. Encyclopedia of Quaternary Science, editors S. A. Elias and C. J. Mock (Elsevier, Amsterdam, The Netherlands), vol. 3, pp. 126-134.

Cartigny P, Chinn I, Viljoen KS, Robinson D. 2004. Early proterozoic ultrahigh pressure metamorphism: Evidence from microdiamonds. *Science* **304**: 853-855.

Cartigny P. 2010. Mantle-related carbonados? Geochemical insights from diamonds from the Dachine komatiite (French Guiana). *Earth and Planetary Science Letters* **296**: 329-339.

Cayron C, Hertog MD, Latu-Romain L, Mouchet C, Secouard C, Rouviere J-L, Rouviere E, Simonato J-P. 2008. Odd electron diffraction patterns in silicon nanowires and silicon thin films explained by microtwins and nanotwins. *Journal of Applied Crystallography* **42**: 242-252.

Cerva H. 1991. High-resolution electron microscopy of diamond hexagonal silicon in low pressure chemical vapor deposited polycrystalline silicon. *J. Mater. Res.* **6**: 2324-2336.

Chaverri P, Samuels GJ. 2002. *Hypocrea lixii*, the teleomorph of *Trichoderma harzianum*. *Mycological Process* **1**: 283-286.

Chen CJ, Chang L, Lin TS, Chen FR. 1996. Direct observations of heteroepitaxial diamond on silicon(110) substrate by microwave plasma chemical vapor deposition. *J. Mat. Res.* **11**: 1002-1010.

Chopin C, Sobolev NV. 1995. Principal mineralogic indicators of UHP in crustal rocks. (Chapter 3) in *"Ultrahigh Pressure Metamorphism"* editors R. G. Coleman and X. Wan (Cambridge University Press, New York, New York, 1995), pp. 96-131.

Clarke Jr. RS, Appleman DE, Ross DR. 1981. An Antarctic iron meteorite contains preterrestrial impact-produced diamond and lonsdaleite. *Nature* **291**: 396-398.

Collard M, Buchanan B, Hamilton MJ, O'Brien MJ. 2010. Spatiotemporal dynamics of the Clovis-Folsom transition. *J. Arch. Sci.* **37**: 2513-2519.

Cooper A, Turney C, Hughen KA, Brook BW, McDonald HG, Bradshaw CJA. 2015. Abrupt warming events drove Late Pleistocene Holarctic megafaunal turnover. *Science* **349**: 602-606.

Dahmen U, Hetherington CJ, Pirouz P, Westmacott KH. 1989. The formation of hexagonal silicon at twin intersections. *Scripta Metallurgica* **23**: 269-272.

Dai ZR, Bradley JP, Joswiak DJ, Brownlee DE, Hill HGM, Genge MJ. 2002. Possible in situ formation of meteoritic nanodiamonds in the early Solar System. *Nature* **418**: 157-159.

Daniau A-L, Harrison SP, Bartlein PJ. 2010. Fire regimes during the Last Glacial. *Quaternary Science Reviews* **29**: 2918-2930.

Darrah TH, Poreda RJ, Kennett JP, Becker L, West A, Kennett DJ, Elrandson JM. 2007. Mineralogical and noble gas evidence for an ET impact at the Younger Dryas. *Eos Trans. AGU* **88**: (23) PP41A-04.

Daulton TL, Eisenhour DD, Bernatowicz TJ, Lewis RS, Buseck PR. 1996. Genesis of presolar diamonds: Comparative high-resolution transmission electron microscopy study of meteoritic and terrestrial nano-diamonds. *Geochimica et Cosmochimica Acta* **60**: 4853-4872.

Daulton TL, Bernatowicz TJ, Lewis RS, Messenger S, Stadermann FJ, Amari S. 2003. Polytype distribution of circumstellar silicon carbide: Microstructural characterization by transmission electron microscopy. *Geochimica et Cosmochimica Acta* **67**: 4743-4767.

Daulton TL. 2006. Extraterrestrial nanodiamonds in the cosmos, (Chapter II) in "*Ultrananocrystalline Diamond: Synthesis, Properties, and Applications"* editors O. Shenderova and D. Gruen, (William Andrew Publishers, Norwich, New York, 2006), pp. 23-78.

Daulton TL, Pinter N, Scott AC. 2010. No evidence of nanodiamonds in Younger-Dryas sediments to support an impact event. *Proc. Natl. Acad. Sci. USA* **107**: 16043-16047.

Daulton TL. 2012. Suspect cubic diamond "impact" proxy and a suspect lonsdaleite identification. *Proc. Natl. Acad. Sci. USA* **109**: E2242.

Deal M. 2005. Palaeoethnobotanical research at Port au Choix. *Newfoundland and Labrador Studies* **20**: 131-156.

den Hertog MI, Cayron C, Gentile P, Dhalluin F, Oehler F, Baron T, Rouviere JL. 2012. Hidden defects in silicon nanowires. *Nanotechnology* **23**: 1-10.

Dennis RL. 1976. *Palaeosclerotium*, a Pennsylvanian age fungus combining features of modern ascomycetes and basidiomycetes. *Science* **192**: 66-68.

Deutsch A, Koeberl C, Blum JD, French BM, Glass BP, Grieve R, Horn P, Jessberger EK, Kurat G, Reimold WU, Smit J, Stöffler D, Taylor SR. 1994. The impact-flood connection: Does it exist? *Terra Nova* **6**: 644-650.

de Wit MCJ. 2004. The diamondiferous sediments on the farm Nooitgedacht (66), Kimberley South Africa. *South African Journal of Geology* **107**: 477-488.

Dobosi G, Kurat G. 2010. On the origin of silicate-bearing diamondites. *Miner. Petrol.* **99**: 29-42.

Dobrzhinetskaya LF, Eide EA, Larsen RB, Sturt BA, Trønnes RG, Smith DC, Taylor WR, Posukhova TV. 1995. Microdiamond in high-grade metamorphic rocks of the Western Gneiss region, Norway. *Geology* **23**: 597-600.

Dobrzhinetskaya LF, Wirth R, Green II HW. 2007. A look inside of diamond-forming media in deep subduction zones. *Proc. Natl. Acad. Sci. USA* **104**: 9128-9132.

Dobrzhinetskaya LF. 2012. Microdiamonds - Frontier of ultrahigh-pressure metamorphism: A review. *Gondwana Research* **21**: 207-223.

Dobrzhinetskaya LF, Wirth R, Green HW, Schreiber A, Obannon E. 2013. First find of polycrystalline diamond in ultrahigh-pressure metamorphic terrane of Erzgebirge, Germany. *Journal of Metamorphic Geology* **31**: 5-18.

Dubinchuk VT, Simakov SK, Pechnikov VA. 2010. Lonsdaleite in diamond-bearing metamorphic rocks of the Kokchetav Massif. *Doklady Earth Sciences* **430**: 40-42.

Elad Y, Barak R, Chet I. 1984. Parasitism of sclerotia of *Sclerotium rolfsii* by *Trichoderma harzianum*. *Soil Biol. Biochem.* **16**: 381-386.

Elias DC, Nair RR, Mohiuddin TMG, Morozov SV, Blake P, Halsall MP, Ferrari AC, Boukhvalov DW, Katsnelson MI, Geim AK, Novoselov KS. 2009. Control of graphene's properties by reversible hydrogenation: Evidence for graphane. *Science* **323**: 610-613.

Faith JT, Surovell TA. 2009. Synchronous extinction of North America's Pleistocene mammals. *Proc. Natl. Acad. Sci. USA* **106**: 20641-20645.

Fallon PJ, Brown LM. 1993. Analysis of chemical-vapour-deposited diamond grain boundaries using transmission electron microscopy and parallel electron energy loss spectroscopy in a scanning transmission electron microscope. *Diamond and Related Materials* **2**: 1004-1011.

Fayek M, Anovitz LM, Allard LF, Hull S. 2012. Framboidal iron oxide: Chondrite-

like material from the black mat, Murray Springs, Arizona. *Earth and Planetary Science Letters* **319-320**: 251-258.

Fedoseev DV, Bukhovets VL, Varshavskaya IG, Lavrent'ev AV, Derjaguin BV. 1983. Transition of graphite into diamond in a solid phase under the atmospheric pressure. *Carbon* **21**: 237-241.

Ferdinandsen C, Winge Ö. 1925. *Cenococcum Fr.*: A monographic study. Den Kongelige Veterinaer-og Landbohøjskole Aarsskrift, 332-382 (in Danish).

Fiedel SJ. 2011. The mysterious onset of the Younger Dryas. *Quaternary International* **242**: 262-266.

Firestone RB, Topping W. 2001. Terrestrial Evidence of a nuclear catastrophe in Paleoindian times. *Mammoth Trumpet* **16**: 9-16.

Firestone RB, Topping W. 2002. Response to the comments by J. R. Southon and R. E. Taylor. *Mammoth Trumpet* **17**: 14-17.

Firestone R, West A, Warwick-Smith S. 2006. The Cycle of Cosmic Catastrophes: Flood, Fire, and Famine in the History of Civilization. Bear & Company, Rochester, VT.

Firestone RB, West A, Kennett JP, Becker L, Bunch TE, Revay ZS, Schultz PH, Belgya T, Kennett DJ, Erlandson JM, Dickenson OJ, Goodyear AC, Harris RS, Howard GA, Kloosterman JB, Lechler P, Mayewski PA, Montogomery J, Poreda R, Darrah T, Que Hee SS, Smith AR, Stich A, Topping W, Wittke JH, Wolbach WS. 2007. Evidence for an extraterrestrial impact 12,900 years ago that contributed to the megafaunal extinctions and the Younger Dryas cooling. *Proc. Natl. Acad. Sci. USA* **104**: 16016-16021.

Firestone RB. 2009. The case for the Younger Dryas extraterrestrial impact event: Mammoth, megafauna, and Clovis extinction, 12,900 years ago. *Journal of Cosmology* **2**: 256-285.

Firestone RB, West A, Revay Z, Hagstrum JT, Belgya T, Que Hee SS, Smith AR. 2010a. Analysis of the Younger Dryas impact layer. *Journal of Siberian Federal University Engineering & Technologies* **3**: 30-62.

Firestone RB, West A, Bunch TE. 2010b. Confirmation of the Younger Dryas boundary (YDB) data at Murray Springs, AZ. *Proc. Natl. Acad. Sci. USA* **107**: E105.

Fleischer R. 1998. A rift model for the sedimentary diamond deposits of Brazil. *Mineralium Deposita* **33**: 238-254.

French BM, Koeberl C. 2010. The convincing identification of terrestrial meteorite impact structures: What works, what doesn't, and why. *Earth-Science Reviews* **98**: 123-170.

Frezzotti M-L, Peccerillo A. 2007. Diamond-bearing COHS fluids in the mantle beneath Hawaii. *Earth and Planetary Science Letters* **262**: 273-283.

Frezzotti M-L, Huizenga J-M, Compagnoni R, Selverstone J. 2014. Diamond formation by carbon saturation in C-O-H fluids during cold subduction of oceanic lithosphere. *Geochimica et Cosmochimica Acta* **143**: 68-86.

Frondel C, Marvin UB. 1967. Lonsdaleite, a hexagonal polymorph of diamond. *Nature* **214**: 587-589.

Geim AK, Novoselov KS. 2007. The rise of graphene. *Nature Materials* **6**: 183-191.

Gill JL, Williams JW, Jackson ST, Lininger KB, Robinson GS. 2009. Pleistocene megafaunal collapse, novel plant communities, and enhanced fire regimes in North America. *Science* **326**: 1100-1103.

Gilmour I, Russell SS, Arden JW, Lee MR, Franchi IA, Pillinger CT. 1992. Terrestrial carbon and nitrogen isotopic ratios from cretaceous-tertiary boundary nanodiamonds. *Science* **258**: 1624-1626.

Gilmour I, French BM, Franchi IA, Abbott JI, Hough RM, Newton J, and Koeberl C. 2003. Geochemistry of carbonaceous impactites from the Gardnos impact structure, Norway. *Geochimica et Cosmochimica Acta* **67**: 3889-3903.

Golovnya SV, Khvostova VP, Makarov ES. 1977. Hexagonal modification of diamond (lonsdaleite) in the eclogites of metamorphic complexes. *Geochem. Int.* **14**: 82-84 (translated from: Geokhimiya, 1977(5), 790-793).

Gorshkov AI, Vinokurov SF, Solodov DI, Bershov LV, Mokhov AV, Solodova YP, Sivtsov AV. 1999. Polycrystalline diamond from the Udachnaya Pipe, Yakutia: Mineralogical, geochemical, and genetic characteristics. *Lithology and Mineral Resources* **34**: 397-410.

Goryainov SV, Likhacheva AY, Rashchenko SV, Shubin AS, Afanas'ev VP, Pokhilenko NP. 2014. Raman identification of lonsdaleite in Popigai impactites. *J. Raman Spectros.* **45**: 305-313.

Grant JA, Brooks MJ, Taylor BE. 1998. New constraints on the evolution of the Carolina Bays from ground-penetrating radar. *Geomorphology* **22**: 325-345.

Grayson DK. 2007. Deciphering North American Pleistocene extinctions. *J. Anthropol. Res.* **63**: 185-213.

Gurov E, Gurova E, Chernenko Y, Yamnichenko A. 2009. The Obolon impact structure, Ukraine, and its ejecta deposits. *Meteoritics & Planetary Science* **44**: 389-404.

Haggerty SE. 1999. A diamond triology: Superplumes, supercontinents, and supernovae. *Science* **285**: 851-860.

Haggerty SE. 2014. Carbonado: Physical and chemical properties, a critical evaluation of proposed origins, and a revised genetic model. *Earth Science Reviews* **130**: 49-72.

Hanneman RE, Strong HM, Bundy FP. 1967. Hexagonal diamonds in meteorites: Implications. *Science* **155**: 995-997.

Hardiman M, Scott AC, Collinson ME, Anderson RS. 2012. Inconsistent redefining of the carbon spherule "impact" proxy. *Proc. Natl. Acad. Sci. USA* **109**: E2244.

Harris-Parks E. 2014. The micromorphology of Younger Dryas-aged black mats from Nevada, Arizona, Texas and New Mexico. M.S. thesis, The University of Arizona.

Harris-Parks E. 2016. The micromorphology of Younger Dryas-aged black mats from Nevada, Arizona, Texas and New Mexico. Quaternary Research, http://dx.doi.org/10.1016/j.yqres.2015.11.005.

Hauge HIT, Verheijen MA, Conesa-Boj S, Etzelstorfer T, Watzinger M, Kriegner D, Zardo I, Fasolato C, Capitani F, Postorino P, Kölling S, Li A, Assali S, Stangl J, Bakkers EPAM. 2015. Hexagonal silicon realized. *Nano Lett.* **15**: 5855-5860.

Haynes Jr. C. 2008. Younger Dryas "black mats" and the Rancholabrean termination in North America. *Proc. Natl. Acad. Sci. USA* **105**: 6520-6525.

Haynes Jr. CV, Boerner J, Domanik K, Lauretta D, Ballenger J, and Goreva J. 2010a. The Murray Springs Clovis site, Pleistocene extinction, and the question of extraterrestrial impact. *Proc. Natl. Acad. Sci. USA* **107**: 9, 4010-4015.

Haynes Jr. CV, Lauretta DS, Ballenger JAM. 2010b. Reply to Firestone *et al.*: No confirmation of impact at the lower Younger Dryas boundary at Murray Springs, AZ. *Proc. Natl. Acad. Sci. USA* **107**: E106.

Heaney PJ, Vicenzi EP, De S. 2005. Strange diamonds: The mysterious origins of carbonado and framesite. *Elements* **1**: 85-89.

Heck PR, Stadermann FJ, Isheim D, Auciello O, Daulton TL, Davis AM, Elam JW, Floss C, Hiller J, Larson DJ, Lewis JB, Mane A, Pellin MJ, Savina MR, Seidman DN, Stephan T. 2014. Atom-probe analysis of nanodiamonds from Allende. *Meteoritics & Planetary Science* **49**: 453-467.

Higgins MD, Lajeunesse P, St-Onge G, Locat J, Duchesne M, Ortiz J, Sanfaçon R. 2011. Bathymetric and petrological evidence for a young (Pleistocene?) 4-km diameter impact crater in the Gulf of Saint Lawrence, Canada. *Lunar & Planetary Science Conference* **XLII**: 1504.

Hirai H, Kondo K-I. 1991. Modified phases of diamond formed under shock compression and rapid quenching. *Science* **253**: 772-774.

Holliday VT, Meltzer DJ. 2010. The 12.9-ka ET impact hypothesis and North

American Paleoindians. *Current Anthropology* **51**: 575-607.

Holliday VT, Surovell T, Meltzer DJ, Grayson DK, Boslough M. 2014. The Younger Dryas impact hypothesis: A cosmic catastrophe. *Journal of Quaternary Science* **29**: 515-530.

Holliday VT. 2015. Problematic dating of claimed Younger Dryas boundary proxies. *Proc. Natl. Acad. Sci. USA* **112**: E6721.

Hormes A, Karlén W, Possnert G. 2004. Radiocarbon dating of palaeosol components in moraines in Lapland, northern Sweden. *Quaternary Science Reviews* **23**: 2031-2043.

Hosseini MR, Schaffie M, Pazouki M, Darezereshki E, Ranjbar M. 2012. Biologically synthesized copper sulfide nanoparticles: Production and characterization. *Materials Science in Semiconductor Processing* **15**: 222-225.

Hough RM, Gilmour I, Pillinger CT, Arden JW, Gilkes KWR, Yuan J, Milledge HJ. 1995. Diamond and silicon carbide in impact melt rock from the Ries impact crater. *Nature* **378**: 41-44.

Hough RM, Gilmour I, Pillinger CT, Langenhorst F, Montanari A. 1997. Diamonds from the iridium-rich K-T boundary layer at Arroyo el Mimbral, Tamaulipas, Mexico. *Geology* **25**: 1019-1022.

Huss GR, Lewis RS. 1994. Noble gases in presolar diamonds I: Three distinct components and their implications for diamond origins. *Meteoritics* **29**: 791-810.

Israde-Alcántara I, Bischoff JL, Domínguez-Vázquez G, Li H-C, DeCarli PS, Bunch TE, Wittke JH, Weaver JC, Firestone RB, West A, Kennett JP, Mercer C, Xie S, Richman EK, Kinzie CR, Wolbach WS. 2012a. Evidence from central Mexico supporting the Younger Dryas extraterrestrial impact hypothesis. *Proc. Natl. Acad. Sci. USA* **109**: E738-E747.

Israde-Alcántara I, Bischoff JL, DeCarli PS, Domínguez-Vázquez G, Bunch TE, Firestone RB, Kennett JP, West A. 2012b. Reply to Blaauw et al., Boslough, Daulton, Gill et al., and Hardiman et al.: Younger Dryas impact proxies in Lake Cuitzeo, Mexico. *Proc. Natl. Acad. Sci. USA* **109**: E2245-E2247.

Itoh N, Sakagami N, Torimura M, Watanabe M. 2012. Perylene in Lake Biwa sediments originating from *Cenococcum geophilum* in its catchment area. *Geochim. et Cosmochim. Acta* **95**, 241-251.

Itoh N, Hashimoto B, Sakagami N, Watanabe M. 2013. The structure of a perylene-containing fossilized sclerotium is maintained by original silica. *Organic Geochemistry* **63**: 37-39.

Ives JW, Froese D. 2013. The Chobot site (Alberta, Canada) cannot provide evidence of a cosmic impact 12,800 y ago. *Proc. Natl. Acad. Sci. USA* **110**: E3899.

Kaminsky FV, Blinova GK, Galimov EM, Gurkina GA, Kliuev YA, Kooptil VI, Krivonos VF, Frolova LN, Khrenov AY. 1985. Polycrystalline aggregates of diamond with lonsdaleite from placers in Yakutiya. *Mineralogical Journal* **7**: 27-36 (in Russian).

Kaminsky FV. 1994. Carbonado and yakutite: Properties and possible genesis. in Proceedings of the Fifth International Kimberlite Conference, vol. 2, Diamonds: Characterization, Genesis, and Exploration, edited by H. O. A. Meyer and O. H. Leonardos, pp. 136-143, Companhia de Pesquisa de Reeursos Minerais, Rio de Janeiro, Brazil.

Kennett DJ, Kennett JP, West GJ, Erlandson JM, Johnson JR, Hendy IL, West A, Culleton BJ, Jones TL, Stafford Jr. TW. 2008. Wildfire and abrupt ecosystem disruption on California's Northern Channel Islands at the Ållerød-Younger Dryas boundary (13.0-12.9 ka). *Quaternary Science Reviews* **27**: 2530-2545.

Kennett DJ, Kennett JP, West A, Mercer C, Que Hee SS, Bement L, Bunch TE, Sellers M, Wolbach WS. 2009a. Nanodiamonds in the Younger Dryas boundary sediment layer. *Science* **323**: 94.

Kennett DJ, Kennett JP, West A, West J, Bunch TE, Culleton BJ, Erlandson JM, Que Hee SS, Johnson JR, Mercer C, Shen F, Sellers M, Stafford Jr. TW, Stich A, Weaver JC, Wittke JH, Wolbach WS. 2009b. Shock-synthesized hexagonal diamonds in Younger Dryas boundary sediments. *Proc. Natl. Acad. Sci. USA* **106**: 12623-12628.

Kennett JP, Kennett DJ, Culleton BJ, Tortosa JEA, Bischoff JL, Bunch TE, Daniel Jr., IR, Erlandson JM, Ferraro D, Firestone RB, Goodyear AC, Israde-Alcántara I, Johnson JR, Pardo JFJ, Kimbel DR, LeCompte MA, Lopinot NH, Mahaney WC, Moore AMT, Moore CR, Ray JH, Staford Jr. TW, Tankersley KB, Wittke JH, Wolbach WS, West A. 2015a. Bayesian chronological analyses consistent with synchronous age of 12,835-12,735 Cal B.P. for Younger Dryas boundary on four continents. *Proc. Natl. Acad. Sci. USA* **112**: E4344-E4353.

Kennett JP, Kennett DJ, Culleton BJ, Tortosa JEA, Bunch TE, Erlandson JM, Johnson JR, Pardo JFJ, LeCompte MA, Mahaney WC, Tankersley KB, Wittke JH, Wolbach WS, West A. 2015a. Reply to Holliday and Boslough et al.: Synchroneity of widespread Bayesian-modeled ages supports Younger Dryas impact hypothesis. *Proc. Natl. Acad. Sci. USA* **112**: E6723-E6724.

Kerr RD. 2008. Experts find no evidence for a mammoth-killer impact. *Science* **319**: 1331-1332.

Ketcham RA, Koeberl C. 2013. New textural evidence on the origin of carbonado diamond: An example of 3-D petrography using X-ray computed tomography. *Geosphere* **9**: 1-12.

Kimbel D, West A, Kennett JP. 2008. A new method for producing nanodiamonds based on research into the Younger Dryas extraterrestrial impact. *AGU Fall Meeting*, abstract #PP13C-1470.

Kincaid BM, Meixner AE, Platzman PM. 1978. Carbon *K* edge in graphite measured using electron-energy-loss spectroscopy. *Phys. Rev. Lett.* **40**: 1296-1299.

Kinzie CR, Que Hee SS, Stich A, Tague KA, Mercer C, Razink JJ, Kennett DJ, DeCarli PS, Bunch TE, Wittke JH, Israde-Alcántara I, Bischoff JL, Goodyear AC, Tankerseley KB, Kimbel DR, Culleton BJ, Erlandson JM, Stafford TW, Kloosterman JB, Moore AMT, Firestone RB, Aura Tortosa JE, Jordá Pardo JF, West A, Kennett JP, Wolbach WS. 2014. Nanodiamond-rich layer across three continents consistent with major cosmic impact at 12,800 Cal BP. *Journal of Geology* **122**: 475-505.

Koeberl C, Masaitis VL, Shafranovsky GI, Gilmour I, Langenhorst F, Schrauder M. 1997. Diamonds from the Popigai impact structure, Russia. *Geology* **25**: 967-970.

Kohno H, Ozaki N, Yoshida H, Tanaka K, Takeda S. 2003. Misleading fringes in TEM images and diffraction patterns of Si nanocrystallites. *Cryst. Res. Technol.* **38**: 1082-1086.

Konyashin I, Zern A, Mayer J, Aldinger F, Babaev V, Khvosov V, Guseva M. 2001. A new carbon modification: "n-diamond" or face-centred cubic carbon? *Diam. and Related Mat.* **10**: 99-102.

Kristan-Tollmann E., Tollmann A. 1992. Der Sintflut-Impakt (The flood impact). *Mitteilungen Der Österreichischen Geographischen Gesellschaft* **84**: 1-63 (in German).

Kristan-Tollmann E., Tollmann A. 1994. The youngest big impact on Earth deduced from geological and historical evidence. *Terra Nova* **6**: 209-217.

Ksanda CJ, Henderson EP. 1939. Identification of diamond in the Canyon Diablo Iron. *American Mineralogist* **24**: 677-680.

Kulnitskiy B, Perezhogin I, Dubitsky G, Blank V. 2013. Polytypes and twins in the diamond-lonsdaleite system formed by high-pressure and high-temperature treatment of graphite. *Acta Crystal. Section B* **B69**: 474-479.

Kurat G, Dobosi G. 2000. Garnet and diopside-bearing diamondites (framesites). *Mineralogy and Petrology* **69**: 143-159.

Kurbatov AV, Mayewski PA, Steffensen JP, West A, Kennett DJ, Kennett JP, Bunch TE, Handley M, Introne DS, Que Hee SS, Mercer C, Sellers M, Shen F, Sneed SB, Weaver JC, Wittke JH, Stafford Jr. TW, Donovan JJ, Xie S, Razink JJ, Stich A, Kinzie CR, Wolbach WS. 2010. Discovery of a nanodiamond-rich layer in the Greenland ice sheet. *J. Glaciol.* **56**: 749-759.

Kvasnitsa VN, Sobotovich EV, Kovalyukh NN, Litvin AL, Rybalko SI, Sharkin OP, Egorova LN. 1979. High-pressure carbon polymorphs in the peats of Tunguska catastrophe region. *Doklady Akademii Nauk USSR* **B12**: 999-1004 (in Russian).

Kvasnytsya V, Wirth R, Dobrzhinetskaya L, Matzel J, Jacobsen B, Hutcheon I, Tappero R, Kovalyukh M. 2013. New evidence of meteoritic origin of the Tunguska cosmic body. *Planetary and Space Science* **84**: 131-140.

Lajeunesse P, St-Onge G, Locat J, Duchesne MJ, Higgins MD, Sanfaçon R, Ortiz J. 2013. The Corossol structure: A possible impact crater on the seafloor of the northwestern Gulf of St. Lawrence, Eastern Canada. *Meteoritics & Planetary Science* **48**: 2542-2558.

Largent F. 2008. The Clovis Comet Part I: Evidence for a cosmic collision 12,900 years ago. *Mammoth Trumpet* **23**: 1-3,19-20.

LaViolette PA. 1987. Cosmic-ray volleys from the galactic center and their recent impact on the Earth environment. *Earth, Moon, and Planets* **37**: 241-286.

LaViolette PA. 2005. Earth Under Fire: Humanity's Survival of the Ice Age. Bear & Company, Rochester, VT.

LaViolette PA. 2011. Evidence for a solar flare cause of the Pleistocene mass extinction. *Radiocarbon* **53**: 303-323.

Lewis RS. 1994. Precision noble gas measurements on presolar diamonds from the Murchison meteorite. *Lunar and Planetary Science Conference* **XXV**: 793.

Lewis RS, Tang M, Wacker JF, Anders E, Steel E. 1987. Interstellar diamonds in meteorites. *Nature* **326**: 160-162.

Lewis RS, Anders E, Draine BT. 1989. Properties, detectability and origin of interstellar diamonds in meteorites. *Nature* **339**: 117-121.

Lifshitz Y, Duan XF, Shang NG, Li Q, Wan L, Bello I, Lee ST. 2001. Epitaxial diamond polytypes on silicon. *Nature* **412**: 404.

Love SG, Brownlee DE. 1993. A direct measurement of terrestrial mass accretion rate of cosmic dust. *Science* **262**: 550-553.

Luyten W, van Tendeloo G, Amelinckx S, Collins JL. 1992. Electron microscopy study of defects in synthetic diamond layers. *Philosophical Magazine A* **66**: 899-915.

Madden A, Swindle A, Bement L, Carter B, Simms A, Benamara M. 2012. Nanodiamonds and carbonaceous grains in Bull Creek Valley, Oklahoma. *Mineral. Mag.* **76**: 2051.

Mahaney WC, Kalm V, Krinsley DH, Tricart P, Schwartz S, Dohm J, Kim KJ, Kapran B, Miner MW, Beukens R, Boccia S, Hancock RGV, Hart KM, Kelleher B. 2010. Evidence from the northwestern Venezuelan Andes for extraterrestrial impact: The black mat enigma. *Geomorphology* **116**: 48-57.

Manceau A, Nagy KL, Marcus MA, Lanson M, Geoffroy N, Jacquet T,

Kirpichtchikova T. 2008. Formation of metallic copper nanoparticles at the soil-root interface. *Environ. Sci. Technol.* **42**: 1766-1772.

Mandel RD. 2008. Buried paleoindian-age landscapes in stream valleys of the Central Plains, USA. *Geomorphology* **101**: 342-361.

Marlon JR, Bartlein PJ, Walsh MK, Harrison SP, Brown KJ, Edwards ME, Higuera PE, Power MJ, Anderson RS, Briles C, Brunelle A, Carcaillet C, Daniels M, Hu FS, Lavoie M, Long C, Minckley T, Richard PJH, Scott AC, Shafer DS, Tinner W, Umbanhowar Jr. CE, Whitlock C. 2009. Wildfire responses to abrupt climate change in North America. *Proc. Natl. Acad. Sci. USA* **106**: 8, 2519-2524.

Masaitis VL, Shafranovsky GI, Grieve RAF, Langenhorst F, Peredery WV, Therriault AM, Balmasov EL, Fedorova IG. 1999. Impact diamonds in the suevitic breccias of the Black member of the Onaping formation, Sudbury structure, Ontario, Canada. in *"Large meteorite impacts and planetary evolution II"* editors B. O. Dressler and V. L. Sharpton, (Geological Society of America, Boulder, Colorado, 2000), pp. 317-321.

Matyushenko NN, Strel'nitskiĭ VE, Gusev VA. 1979. A dense new version of crystalline carbon C_8. *JETP Lett.* **30**: 199-202.

McCall GJH. 2009. The carbonado diamond conundrum. *Earth-Science Reviews* **93**: 85-91.

McLaren D, Fedje D, Hay MB, Mackie Q, Walker IJ, Shugar DH, Eamer JBR, Lian OB, Neudorf C. 2014. A post-glacial sea level hinge on the central Pacific coast of Canada. *Quaternary Science Reviews* **97**: 148-169.

McWeeney L. 1989. What lies lurking below the soil: Beyond the archaeobotanical view of flotation samples. *North Amer. Arch.* **10**: 227-230.

Melosh HJ. 2009. Airburst in the sky with diamonds? Shock limits to a Younger Dryas impact. *American Geophysical Union, Fall Meeting*, PP33B-03.

Melton FA, Schriever W. 1933. The Carolina "Bays" – Are they Meteorite Scars? *The Journal of Geology* **41**: 52-66.

Meltzer DJ, Holliday VT. 2010. Would North American Paleoindians have noticed Younger Dryas age climate changes? *J. World Prehist.* **23**: 1-41.

Meltzer DJ, Holliday VT, Cannon MD, Miller DS. 2014. Chronological evidence fails to support claim of an isochronous widespread layer of cosmic impact indicators dated to 12,800 years ago. *Proc. Natl. Acad. Sci. USA* **111**: E2162-E2171.

Münzenberger B, Bubner B, Wöllecke J, Sieber TN, Bauer R, Fladung M, Hüttl RF. 2009. The ectomycorrhizal morphotype *Pinirhiza sclerotia* is formed by *Acephala macrosclerotiorum* sp. nov., a close relative of *Phialocephala fortinii*. *Mycorrhiza* **19**: 481-492.

Myasnikov I, Chernysheva M, Badun G, Korobkov V, Kulikova N. 2014. Humic substances alter uptake of nanodiamonds by wheat plants. *Third International Conference of CIS IHSS on Humic Innovative Technologies Tenth International Conference daRostim Humic Substances and Other Biologically Active Compounds in Agriculture HIT-daRostim-2014,* Nov. 19-23, 2014 Lomonosov Moscow State University, Moscow Russia, 59.

Nakamuta Y, Aoki Y. 2000. Mineralogical evidence for the origin of diamond in ureilites. *Meteoritics & Planetary Science* **35**: 487-493.

Napier WM, Bunch TE, Kennett JP, Wittke JH, Tankersley KB, Kletetschka G, Howard GA, West A. 2013. Reply to Boslough et al.: Decades of comet research counter their claims. *Proc. Natl. Acad. Sci. USA* **110**: E4171.

Németh P, Garvie LAJ, Aoki T, Dubrovinskaia N, Dubrovinsky L, Buseck PR. 2014. Lonsdaleite is faulted and twinned cubic diamond and does not exist as a discrete material. *Nature Communications* **5**: 5447 doi:10.1038/ncomms6447.

Netherlands Patent Release. 1965. No. 6506395, November 22, 1965, E. I. du Pont de Nemours and Company.

Nowicki TE, Moore RO, Gurney JJ, Baumgartner MC. 2007. Chapter 46 Diamonds and associated heavy minerals in kimberlite: A review of key concepts and applications. *Developments in Sedimentology* **58**: 1235-1267.

Ogasawara Y. 2005. Microdiamonds in ultrahigh-pressure metamorphic rocks. *Elements* **1**: 91-96.

Ona S, Nakamoto Y, Kagayama T, Shimizu K, Nishikawa Y, Murakami M, Kusakabe K, Watanuki T, Ohishi Y. 2008. Stability of hexagonal diamond under pressure. *Journal of Physics: Conference Series* **121**: 1-3.

Ozima M, Zashu S, Tomura K, Matsuhisa Y. 1991. Constraints from noble-gas contents on the origin of carbonado diamonds. *Nature* **6**: 472-474.

Pantidos N, Horsfall LE. 2014. Biological synthesis of metallic nanoparticles by bacteria, fungi and plants. *J. Nanomed. Nanotechnol.* **5**: 233. doi: 10.4172/2157-7439.1000233.

Paquay FS, Goderis S, Ravizza G, Vanhaeck F, Boyd M, Surovell TA, Holliday VT, Haynes Jr. CV, Claeys P. 2009. Absence of geochemical evidence for an impact event at the Bølling-Allerød/Younger Dryas transition. *Proc. Natl. Acad. Sci. USA* **106**: (51), 21505-21510.

Paquay FS, Goderis S, Ravizza G, Claeys P. 2010. Reply to Bunch et al.: Younger Dryas impact proponents challenge new platinum group elements and osmium data unsupportive of their hypothesis. *Proc. Natl. Acad. Sci. USA* **107**: E59-E60.

Pechnikov VA, Kaminsky FV. 2008. Diamond potential of metamorphic rocks in the Kokchetav Massif, northern Kazakhstan. *Eur. J. Mineral.* **20**: 395-413.

Perevedentseva E, Hong S-F, Huang K-J, Chiang L-T, Lee C-Y, Tseng Y-T, Cheng C-L. 2013. Nanodiamond internalization in cells and the cell uptake mechanism. *J. Nanopart. Res.* **15**: 1834, 1-12.

Perraki M, Proyer A, Mposkos E, Kaindl R, Hoinkes G. 2006. Raman micro-spectroscopy on diamond, graphite, and other carbon polymorphs from the ultrahigh-pressure metamorphic Kimi Complex of the Rhodope Metamorphic Province, NE Greece. *Earth and Planetary Science Letters* **241**: 672-685.

Petaev MI, Huang S, Jacobsen SB, Zindler A. 2013a. Large Pt anomaly in the Greenland ice core points to a cataclysm at the onset of Younger Dryas. *Proc. Natl. Acad. Sci. USA* **110**: 12917-12920.

Petaev MI, Huang S, Jacobsen SB, Zindler A. 2013b. Reply to Boslough: Is Greenland Pt anomaly global or local? *Proc. Natl. Acad. Sci. USA* **110**: E5036.

Petrovsky VA, Filonenko VP, Silaev VI, Zibrov IP, Sukharev AE, Zemnukhov AL, Pomazansky BS. 2013. Yakutit X-ray analysis and evaluation of content of lonsdaleite impurities. *Bulletin of the University of Perm. Geology* **3(20)**: 43-60 (in Russian).

Pigati JS, Latorre C, Rech JA, Betancourt JL, Martïnez KE, Budahn JR. 2012. Accumulation of impact markers in desert wetlands and implications for the Younger Dryas impact hypothesis. *Proc. Natl. Acad. Sci. USA* **109**: (19), 7208-7212.

Pinter N, Ishman SE. 2008. Impacts, mega-tsunami, and other extraordinary claims. *GSA Today* **18**: 37-38.

Pinter N, Scott AC, Daulton TL, Podoll A, Koeberl C, Anderson RS, Ishman SE. 2011. The Younger Dryas impact hypothesis: A requiem. *Earth-Science Reviews* **106**: 247-264.

Quade J, Forester RM, Pratt WL, Carter C. 1998. Black mats, spring-fed streams, and Late-Glacial-age recharge in the Southern Great Basin. *Quaternary Research* **49**: 129-148.

Rech JA, Pigati JS, Quade J, Betancourt JL. 2003. Re-evaluation of mid-Holocene deposits at Quebrada Puripica, northern Chile. *Paleogeograhy, Paleoclimatology, Paleoecology* **194**: 207-222.

Redmond BG, Tankersley KB. 2011. Species response to the theorized Clovis comet impact at Sheriden Cave, Ohio. *Curr. Res. Pleistocene* **28**: 141-143.

Reichle RE, Alexander JV. 1965. Multiperforate septations, Woronin bodies, and septal plugs in *Fusarium*. *J. Cell Biol.* **24**: 489-496

Reimold WU, Ferrière L, Deutsch A, Koeberl C. 2014. Impact controversies: Impact recognition criteria and related issues. *Met. & Planet. Sci.* **49**: 723-731.

Rietmeijer FJM, Mackinnon IDR. 1987. Metastable carbon in two chondritic porous interplanetary dust particles. *Nature* **326**: 162-165.

Rodriguez AB, Waters MN, Piehler MF. 2012. Burning peat and reworking loess contribute to the formation and evolution of a large Carolina-bay basin. *Quaternary Research* **77**: 171-181.

Rozen OM, Zorin YM, Zayachkovsky AA. 1972. A find of diamonds linked with eclogites of the Precambrian Kokchetav massif. *Akademiya Nauk SSR Doklady* **203**: 674-676 (in Russian).

Rothwell GW. 1972. *Palaeosclerotium pusillium* gen. et sp. nov., a fossil eumycete from the Pennsylvanian of Illinois. *Can. J. Bot.* **50**: 2353-2356.

Russell SS, Arden JW, Pillinger CT. 1996. A carbon and nitrogen isotope study of diamond from primitive chondrites. *Meteoritics & Planetary Science* **31**: 343-355.

Salvadori MR, Lepre LF, Ando RA, Oller do Nascimento CA, Corrêa B. 2013. Biosynthesis and uptake of copper nanoparticles by dead biomass of *Hypocrea lixii* isolated from the metal mine in the Brazilian Amazon Region. *PLOSone* **8**: eB0519.

Salvadori MR, Ando RA, Oller do Nascimento CA, Corrêa B. 2014. Bioremediation from wastewater and extracellular synthesis of copper nanoparticles by the fungus *Trichoderma koningiopsis*. *Journal of Environmental Science and Health* **49**: 1286-1295.

Sass HR. 1944. When the Comet Struck. *Saturday Evening Post* **217**: 12-13,105-107.

Schmidt S, Nagel TJ, Froitzheim N. 2010. A new occurrence of microdiamond-bearing metamorphic rocks, SW Rhodopes, Greece. *Eur. J. Mineral.* **22**: 189-198.

Scott AC, Pinter N, Collinson ME, Hardiman M, Anderson RS, Brain APR, Smith SY, Marone F, Stampanoni M. 2010. Fungus, not comet or catastrophe, accounts for carbonaceous spherules in the Younger Dryas "impact layer". *Geophys. Res. Lett.* **37**: L14302, 1-5.

Scott AC, Hardiman M, Daulton TL, Pinter N, Anderson RS, Ejarque A, Higham T, Finch P, Carter-Champion A. 2016. Late Quaternary fluvial sequences, Santa Rosa Island, California: Recording, sampling, intepretation, and implications for the Younger Dryas Impact Hypothesis. submitted to *Journal of Quaternary Science*.

Shay CT, Kapinga MRM. 1997. *Cenococcum geophilum* sclerotia from an archaeological site in western Canada. *North American Archaeologist* **18**: 363-370.

Shelkov DA, Verchovsky AB, Milledge HJ, Kaminsky FV, Pillinger CT. 1998. Carbon, nitrogen, argon and helium study of impact diamonds from Ebeliakh

alluvial deposits and Popigai crater. *Meteoritics & Planetary Science* **33**: 985-992.

Shirey SB, Cartigny P, Frost DJ, Keshav S, Nestola F, Nimis P, Pearson DG, Sobolev NV, Walter MJ. 2013. Diamonds and the geology of mantle carbon. *Reviews in Mineralogy & Geochemistry* **75**: 355-421.

Shumilova TG, Mayer E, Isaenko SI. 2011. Natural monocrystalline lonsdaleite. *Dokl. Earth Sci.* **441**: 1552-1554.

Shumilova T, Kis VK, Masaitis V, Isaenko S, Makeev B. 2014. Onion-like carbon in impact diamonds from the Popigai astrobleme. *Eur. J. Mineral.* **26**: 267-277.

Smith JV, Dawson JB. 1985. Carbonado: Diamond aggregates from early impacts of crustal rocks? *Geology* **13**: 342-343.

Smith ME, Henkel TW, Rollins JA. 2015. How many fungi make sclerotia? *Fungal Ecology* **13**: 211-220.

Sobolev NV, Shatsky VS. 1990. Diamond inclusions in garnets from metamorphic rocks: A new environment for diamond formation. *Nature* **343**: 742-746.

Sokhor MI, Polkanov YA, Yeremenko GK. 1973. A find of the hexagonal diamond (lonsdaleite) in placers, USSR. *Doklady Academy of Science USSR* **209**: 118-121 (in Russian).

Southon JR, Taylor RE. 2002. Brief comments on "Terrestrial evidence of a nuclear catastrophe in paleoindian times," by Richard B. Firestone and William Topping. *Mammoth Trumpet* **17**: 14-17.

Stöckhert B, Duyster J, Trepmann C, Massonne H-J. 2001. Microdiamond daughter crystals precipitated from supercritical COH + silicate fluids included in garnet, Erzgebirge, Germany. *Geology* **29**: 391-394.

Stroud RM, Chisholm MF, Heck PR, Alexander CMO'D, Nittler LR. 2011. Supernova shock-wave-induced co-formation of glassy carbon and nanodiamond. *The Astrophysical Journal Letters* **738**: L27.

Surovell TA, Holliday VT, Gingerich JAM, Ketron C, Haynes Jr. CV, Hilman I, Wagner DP, Johnson E, Claeys P. 2009. An independent evaluation of the Younger Dryas extraterrestrial impact hypothesis. *Proc. Natl. Acad. Sci. USA* **106**: 43, 18155-18158.

Swart PK, Grady MM, Pillinger CT, Lewis RS, Anders E. 1983. Interstellar carbon in meteorites. *Science* **220**: 406-410.

Taylor RE, Bar-Yosef O. 2014. Radiocarbon Dating: An Archaeological Perspective. Left Coast Press, Inc: Walnut Creek, CA.

Taylor TN, Krings M, Taylor EL. 2015. Fossil Fungi. Elsevier Academic Press, London UK.

Thy P, Willcox G, Barfod GH, Fuller DQ. 2015. Anthropogenic origin of siliceous scoria droplets from Pleistocene and Holocene archaeological sites in northern Syria. *J. Arch. Sci.* **54**: 193-209.

Tian H, Schryvers D, Claeys P. 2011. Nanodiamonds do not provide unique evidence for a Younger Dryas impact. *Proc. Natl. Acad. Sci. USA* **108**: 40-44.

Titkov SV, Gorshkov AI, Vinokurov SF, Bershov LV, Solodov DI, Sivtsov AV. 2001. Geochemistry and genesis of carbonado for Yakutian diamond deposits. *Geochemistry International* **39**: 228–236.

Tollmann A. 2001. Kosmische gross-impakte der Jung- und Nacheiszeit (Cosmic mega-impacts during the Late- and Post-Pleistocene). *Sitzungsberichte Abt. I - Ostenreichische Akademie der Wissenschaften* **208**: 3-13 (in German).

Trappe JM. 1931. *Cenococcum graniforme* - Its distribution, ecology, mycorchiza formation and inherent variation. Ph.D. thesis, University of Washington.

Trappe JM. 1969. Studies on *Cenococcum graniforme.* I. An efficient method for isolation from sclerotia. *Can. J. Bot.* **47**: 1389-1390.

van Hoesel A, Hoek WZ, Braadbaart F, van der Plicht J, Pennock GM, Drury MR. 2012. Nanodiamonds and wildfire evidence in the Usselo horizon postdate the Allerød–Younger Dryas boundary. *Proc. Natl. Acad. Sci. USA* **109**: 7648-7653.

van Hoesel A, Hoek WZ, van der Plicht J, Pennock GM, Drury MR. 2013. Cosmic impact or natural fires at the Allerød-Younger Dryas boundary: A matter of dating and calibration. *Proc. Natl. Acad. Sci. USA* **110**: 41, E3896.

van Hoesel A. 2014. The Younger Dryas climate change was it caused by an extraterrestrial impact? Ph.D. thesis, Universiteit Utrecht.

van Hoesel A, Hoek WZ, Pennock GM, Drury MR. 2014. The Younger Dryas impact hypothesis: a critical review. *Quaternary Science Reviews* **83**: 95-114.

van Hoesel A, Hoek WZ, Pennock GM, Kaiser K, Plümper O, Jankowski M, Hamers MF, Schlaak N, Küster M, Andronikov AV, Drury MR. 2015. A search for shocked quartz grains in the Allerød-Younger Dryas boundary layer. *Meteor. & Planet. Sci.* **50**: 483-498.

van Peer AF, Müller WH, Boekhout T, Lugones LG, Wösten HAB. 2009. Cytoplasmic continuity revisited: Closure of septa of the filamentous fungus *Schizophyllum commune* in response to environmental conditions. *PLoS One* **4** (e5977): 1-4

Verchovsky AB, Valter AA, Shukolyukov YA. 1991. Noble gases in shock-produced diamond from Popigai meteorite crater. *Europ. Geophys. Soc.* C57.

Verchovsky AB, Ott U, Begemann F. 1993. Implanted radiogenic and other noble

gases in crustal diamonds from Northern Kazakhstan. *Earth and Planetary Science Letters* **120**: 87-102.

Vincent L, Patriarche G, Hallais G, Renard C, Gardès C, Troadec D, Bouchier D. 2014. Novel heterostructured Ge nanowires based on polytype transformation. *Nano Lett.* **14**: 4828-4836.

Watanabe M, Fujitake N, Ohta H, Yokoyama T. 2001. Aluminum concentrations in sclerotia from a buried humic horizon of volcanic ash soils in Mt. Myoko, Central Japan. *Soil Sci. Plant Nutr.* **47**: 411-418.

Watanabe M, Ohishi S, Pott A, Hardenbicker U, Aoki K, Sakagami N, Ohta H, Fujitake N. 2004a. Soil chemical properties and distribution of sclerotium grains in forest soils, Harz Mts., Germany. *Soil Sci. Plant Nutr.* **50**: 863-870.

Watanabe M, Genseki A, Sakagami N, Inoue Y, Ohta H, Fujitake N. 2004b. Aluminum oxyhydroxide polymorphs and some micromorphological characteristics in sclerotium grains. *Soil Sci. Plant Nutr.* **50**: 1205-1210.

Wen B, Zhao JJ, Li TJ. 2007. Synthesis and crystal structure of n-diamond. *International Materials Reviews* **3**: 131-151.

West A, Firestone RB, Kennett JP, Becker L. 2007. Extraterrestrial markers found at Clovis sites across North America. *Eos Trans. AGU* **88**: (23) PP41A-02.

Wirth R, Rocholl A. 2003. Nanocrystalline diamond from the Earth's mantle underneath Hawaii. *Earth and Planetary Science Letters* **211**: 357-369.

Wittke JH, Weaver JC, Bunch TE, Kennett JP, Kennett DJ, Moore AMT, Hillman GC, Tankersley KB, Goodyear AC, Moore CR, Daniel IR, Ray JH, Lopinot NH, Ferraro D, Israde-Alcántara I, Bischoff JL, DeCarli PS, Hermes RE, Kloosterman JB, Revay Z, Howard GA, Kimbel DR, Kletetschka G, Nabelek L, Lipo CP, Sakai S, West A, Firestone RB. 2013a. Evidence for deposition of 10 million tonnes of impact spherules across four continents 12,800 y ago. *Proc. Natl. Acad. Sci. USA* **110**: (23), E2088-E2097.

Wittke JH, Bunch TE, Kennett JP, Kennett DJ, Culleton BJ, Tankersley KB, Daniel Jr. IR, Kloosterman JB, Kletetschka G, West A, Firestone RB. 2013b. Reply to van Hoesel et al.: Impact-related Younger Dryas boundary nanodiamonds from The Netherlands. *Proc. Natl. Acad. Sci. USA* **110**: E3897-3898.

Wittke JH, Bunch TE, Tankersley KB, Daniel Jr. IR, Kloosterman JB, Kletetschka G, West A, Firestone RB. 2013c. Reply to Ives and Froese: Regarding the impact-related Younger Dryas boundary layer at Chobot site, Alberta, Canada. *Proc. Natl. Acad. Sci. USA* **110**: E3900.

Woodman N, Athfield NB. 2009. Post-Clovis survival of American Mastodon in the southern Great Lakes region of North America. *Quaternary Research* **72**: 359-363.

Xiao S-Q, Pirouz P. 1992. On diamond-hexagonal germanium. *J. Mater. Res.* **7**: 1406-1412.

Xu S, Okay AI, Ji S, Sengör AMC, Su W, Liu Y, Jiang L. 1992. Diamond from the Dabie Shan metamorphic rocks and its implication for tectonic setting. *Science* **256**: 80-82.

Xu S, Liu Y, Chen G, Ji S, Ni P, Xiao W. 2005. Microdiamonds, their classification and tectonic implications for the host eclogites from the Dabie and Su-Lu regions in central eastern China. *Mineralogical Magazine* **69**: 509-520.

Xu Z, Gleason ML, Mueller DS, Esker PD, Bradley CA, Buck JW, Benson DM, Dixon PM, Monteiro JEBA. 2008. Overwintering of *Sclerotium rolfsii* and *S. rolfsii* var. *delphinii* in different latitudes of the United States. *Plant Disease* **92**: 719-724.

Yada T, Nakamura T, Takaoka N, Noguchi T, Terada K, Yano H, Nakazawa T, Kojima H. 2004. The global accretion rate of extraterrestrial materials in the last glacial period estimated from the abundance of micrometeorites in Antarctic glacier ice. *Earth Planets Space* **56**: 67-79.

Yang J, Xu Z, Dobrzhinetskaya LF, Green HW, Pei X, Shi R, Wu C, Wooden JL, Zhang J, Wan Y, Li H. 2003. Discovery of metamorphic diamonds in central China: an indication of a >4000-km-long zone of deep subduction resulting from multiple continental collisions. *Terra Nova* **15**: 370–379.

Yang ZQ, Verbeeck J, Schryvers D, Tarcea N, Popp J, Rösler W. 2008. TEM and Raman characterisation of diamond micro- and nanostructures in carbon spherules from upper soils. *Diamond and Related Materials* **17**: 937-943.

Yoshiasa A, Murai Y, Ohtaka O, Katsura T. 2003. Detailed structures of hexagonal diamond (lonsdaleite) and wurtzite-type BN. *Jpn. J. Appl. Phys.* **42**: 1694-1704.

Zhang X, Hu W, Li J, Tao L, Wei Y. 2012. A comparative study of cellular uptake and cytotoxicity of multi-walled carbon nanotubes, graphene oxide, and nanodiamond. *Toxicol. Res.* **1**: 62-68.

Figure Captions

Figure 1: (a) A HR-TEM lattice image of a nanocrystal from the Allende meteorite acid-dissolution residue. The nanocrystal exhibits a homoepitaxial interface between two crystal lattices that is consistent with the (b) 3C cubic diamond and 2H lonsdaleite atomic structure (figure adapted from Daulton *et al.*, 1996). The grain displays one domain with close packed tetrahedral planes stacked in the $(A^b)(B^c)(C^a)$... sequence defining the 3C structure and a second domain stacked in the $(A^b)(B^a)$... sequence defining the 2H structure. Through-focus HR-TEM imaging (not shown) is consistent with these atomic structures. Furthermore, since this grain exhibits a homoeptiaxial interface of two crystal structures, the possible pairs of candidate phases that comprise the grain are significantly limited. (c) Atomic models of the six unique (fundamental) bilayer planes (A^b, A^c, B^a, B^c, C^a, and C^b) in diamond (top), that comprise stacked tetrahedral planes (depicted normal to stacking direction shown at bottom). The two basic stacking arrangements, $(X^y)(Y^x)$ and $(X^y)(Y^z)$ where X, Y, and Z are all different, form planes of vertex-sharing antiparallel and parallel tetrahedra, respectively.

Figure 2: HR-TEM images of well-ordered (a) $[01\bar{1}]$ zone of cubic diamond and (b) [010] zone of lonsdaleite from products of thermobaric high-pressure, high-temperature treatment of graphite. (c) Calculated HR-TEM image of lonsdaleite for [010] zone axis (figure adapted from Kulnitskiy *et al.*, 2013). (d) HR-TEM image of diamond grown on (100)-oriented Si held at 600 or 700° C by bombardment with 80 or 200 eV ions from a (CH_4 or C_2H_2)/Ar/H_2-fed Kaufmann source (figure adapted from Lifshitz *et al.*, 2001). (e) Schematic atomic model of lonsdaleite projected along the [010] zone axis.

Figure 3: Shown in top row Fig. 6 part b and part d of Kurbatov *et al.* (2010); its figure caption states, "Lonsdaleite analyses. (b) HR-TEM image showing characteristic lonsdaleite lattice spacings. (d) Fast Fourier transform (FFT) of lonsdaleite ND crystal. All values (Miller indices) are consistent with each other and with the published lattice spacings for lonsdaleite as shown in Table 3. Sample numbers, as referenced in Table 2, are shown in the lower left of

each image." Shown at bottom is a schematic of the atomic structure of lonsdaleite. In diamond, C atoms covalently bond to four other C atoms in a tetrahedral geometry. The {002} planes in the lonsdaleite structure contain the base of the C tetrahedra that are stacked in the structure. The set of {002} planes are oriented edge-on only in [*hk*0] zone axes projections, and high-resolution lattice images of [*hk*0] zone axes display only one set of {002} planes, contrary to the nanocrystal shown by Kurbatov *et al.* (2010).

Figure 4: Shown in top row is Fig. S2 (part B) of Kennett *et al.* (2009b); its figure caption states, "(*B*) cluster of lonsdaleite crystals and associated diffraction pattern from 4.59-4.64m(AC#348)." We modified the diffraction pattern from the original published by Kennett *et al.* (2009b) by inverting its contrast to aid in visual clarity and by superimposing additional annotations on the pattern. In right of top row, ovals were superimposed to demonstrate the azimuthal asymmetry of the diffraction pattern and the presence of additional partial diffraction rings. Half circles were superimposed to illustrate the predicted reflections for lonsdaleite. The scale of the diffraction pattern was calibrated assuming that the ring labeled (110) by Kennett *et al.* (2009b) corresponds to the (110) reflection of lonsdaleite. Notice, there are many missing lonsdaleite reflections. Left of bottom row is Fig. 15 (part B) of Kinzie *et al.* (2014); its figure caption states, "Younger Dryas Boundary lonsdaleite-like crystal". This is the same grain shown in Kennett *et al.* (2009b). Shown at right of the bottom row is the diffraction pattern of Kennett *et al.* (2009b) with half circles superimposed to illustrate the predicted reflections for a homogeneous mixture of graphene and graphane where the <100> *d*-spacing in graphane is contracted by a factor of 1.054 from that of graphene (Daulton *et al.*, 2010). The scale of the diffraction pattern was calibrated assuming the ring labeled (110) by Kennett *et al.* (2009b) corresponds to the (100) reflection of graphene. Consistent with this diffraction pattern, disordered graphite could be present and predominantly oriented with its [001] crystallographic axis in the electron beam direction. As such, the high-resolution lattice image published for this grain (see Fig. 16, Kinzie *et al.*, 2014) is consistent with a [001] zone axis of graphitic/graphene structure. Similarly, the diffraction pattern identified as lonsdaleite by Redmond and Tankersley (2011) is

consistent with [001] graphite.

Figure 5: Typical electron diffraction pattern from aggregates of polycrystalline graphene/graphane recovered from sediments exhibits a) azimuthally asymmetric electron diffraction rings indicative of texturing of two phases (Daulton *et al.*, 2010). Different regions within the *same* aggregate exhibit diffraction rings from b) only graphene (solid triangles), c) both graphene and graphane, or d) only graphane (open triangles). To aid in visual clarity, the diffraction patterns are displayed in reverse contrast.

Figure 6: SEM images of carbon spherules from Arlington Canyon YDB sediments (AC-003): a) Fig. 1 (part A), b) Fig. S6 (part E), and c) Fig. S6 (part F) of Kennett *et al.* (2009b). Their figure captions state, "SEM images represent carbon spherules (A)" and "(*E*) [relabeled B here] Bisected carbon spherule showing typical internal reticulate (honeycomb) structure and thin, nonreticulate crust. (*F*) [relabeled C here] Close-up of carbon spherule interior shown in *E* [relabeled B here] with well-organized reticulate (honeycomb) structure and thin, nonreticulate crust." d) Light microscope image of fungal sclerotia charred at 350°C for 5 mins. e) SEM image of broken fungal sclerotia from charcoal residue of a low-temperature surface fire, Thursley, Common, Surrey, England. f) SEM image of broken fungal sclerotia charred at 350°C for 5 mins showing mesh-like internal structure comprising fused fungal hyphae.

Figure 7: Left column is Fig. 5 of the supplemental materials of Israde-Alcántara *et al.* (2012a). Their figure caption states, "CARBON SPHERULES from the 2.8-m layer. A) The upper inset show a whole CSp in reflected light. B) SEM image of a crushed CSp; C) Photomicrograph of the same crushed CSp. D) Closeup of bottom of crushed CSp, illustrating the lack of filamentous texture, as typical of fungal sclerotia, and indicating that these objects are not sclerotia, as speculated by Scott *et al.* (2010)." Right column or panel e) SEM image of the interior of cross-sectioned *C. geophilum* sclerotia displaying a hollow center with smooth interior walls (image courtesy of M. Watanabe).

Figure 8: a) SEM image of the interior of cross-sectioned *C. geophilum* sclerotia displaying micron-sized holes (septal pores), which are morphological features characteristic of sclerotia (image courtesy of M. Watanabe). b) SEM image of the interior of a carbon spherule from Arlington Canyon YDB sediments (AC-003) from Fig. S6 (part F) of Kennett *et al.* (2009b). The originally published image (shown in Fig. 6c of this paper with a modified panel label) has been cropped with circles overlaid to denote several of the submicron-sized holes present in the cell-like walls. Their figure caption states, "(F) Close-up of carbon spherule interior shown in E with well-organized reticulate (honeycomb) structure and thin, nonreticulate crust." The presence of the holes provides a conclusive identification of the spherule as a sclerotium (private communication M. Watanabe). Both images are reproduced at the same spatial scale.

Figure 9: High-resolution TEM lattice images (top row) and bright-field (BF) TEM image of nanocrystals embedded within amorphous fragments (middle row) obtained from finely crushed carbon spherules collected from Arlington Canyon YDB sediments (AC-003). Many of the nanocrystals exhibit twining, particularly Σ=3 twin boundaries or occasionally Σ=9 twin boundaries when successive Σ=3 twin domains impinge on one another (e.g., see Luyten *et al.*, 1992; Daulton *et al.*, 2003), characteristic of face centered cubic structures. Shown in the bottom row are Figure 13 (part A) and Figure 6 (part C) from Kinzie *et al.* (2014); their respective figure captions states, "carbon spherules from Gainey, Michigan (Younger Dryas Boundary [YDB]: 3933 ppb at 30 cm below surface [cmbs]" and "nanodiamonds (NDs) in carbon spherules (CS) . . . n-Diamond from Topper, South Carolina (YDB: 108 ppb at 60 cmbs)."

Figure 10: Representative diffraction pattern from amorphous grains obtained from finely crushed carbon spherules collected from Arlington Canyon YDB sediments (AC-003) that contain nanocrystals (see, Fig. 6, middle row). The diffraction pattern is displayed in reversed contrast and three different electron exposures are superimposed to cover the large dynamic range of the Bragg

intensities. The diffraction lines of cubic diamond (along with the kinematically forbidden diamond reflections denoted by *) are shown.

Figure 11: Top: Bright-field (BF) and Dark-field (DF) STEM images of nanocrystals embedded within an amorphous grain from finely crushed carbon spherules collected from Arlington Canyon YDB sediments (AC-003). Below are STEM Energy Dispersive X-ray Spectroscopy (EDXS) and Electron Energy Loss Spectroscopy (EELS) maps (in dashed rectangle) of relative elemental composition normalized to the sum of all measured elements. Areas in the maps that exhibit a deficit of C and Fe correlate to areas that show an excess of Cu. For nanocrystals on the surface of the amorphous C-rich and Fe-containing grain, this is a result of the normalization of the compositions. For nanocrystals within the grain, this results from the nanoparticles displacing the amorphous C-rich and Fe-containing matrix. The 256 grey scale look-up table (LUT) is linearly mapped between the minimum and maximum element composition for each map. (The elemental maps are published online in false color with a dynamic range of 1786 colors.) As described in the text, the amorphous matrix had an elemental composition, as determined by EDXS, of 82.49 at.% (70.56 wt.%) C, 13.40 at.% (15.27 wt.%) O, 2.87 at.% (11.41 wt.%) Fe, 0.39 at.% (0.89 wt.%) S, 0.35 at.% (0.70 wt.%) Si, 0.17 at.% (0.47 wt.%) K, 0.12 at.% (0.21 wt.%) Mg, 0.10 at.% (0.29 wt.%) Ca, 0.05 at.% (0.11 wt.%) P, 0.05 at.% (0.10 wt.%) Al.

Figure 12: Top: Bright-field (BF) image of nanocrystals from finely crushed carbon spherules collected from Arlington Canyon YDB sediments (AC-003). Below are STEM Energy Dispersive X-ray Spectroscopy (EDXS) maps of relative elemental composition normalized to the sum of C, O, Cu, and S contributions. Carbon and O is associated with the support film and deficits in those elements occur in the maps where the nanocrystals are located due to the normalization of the elemental compositions to the sum of C, O, Cu, and S contributions. If the nanocrystals contained C, excesses in C would be observed at the locations of the nanocrystals. The 256 grey scale look-up table (LUT) is linearly mapped between the minimum and maximum element composition for each map. (The elemental maps are published online in false

color with a dynamic range of 1786 colors.)

Table 1: Lonsdaleite Bragg Reflections

	Predicted†	Bundy and Kasper (1967)	Frondel and Marvin (1967)	Fedoseev *et al.* (1983)	Bhargava *et al.* (1995)	Ona *et al.* (2008)
(*hkl)*				d-spacing (Å)		
(100)	2.182	2.19	2.18	2.20-2.18	2.181	2.165
(002)	2.060	2.06	2.061	2.06-2.07	2.045	2.089
(101)	1.928	1.92	1.933	1.92	1.949	1.933
(102)	1.498	1.50	1.50	1.50-1.53		1.504
(110)	1.260	1.26	1.257	1.26-1.27	1.257	1.251
(103)	1.162	1.17	1.17	1.18	1.167	1.172
(200)	1.091					
(112)	1.075	1.075	1.075	1.06-1.07	1.073	1.076
(201)	1.055	1.055			1.067	
(202)	0.964			0.970-0.985		
(203)	0.854			0.870		
(210)	0.825			0.820		
(211)	0.809	0.855				
(105)	0.771	0.820				
(212)	0.766					
(300)	0.727					
(213)	0.707					
(006)	0.687					
(302)	0.686					

† lattice parameters: a = 2.52 Å and c = 4.12 Å.

Table 2: Comparison of Cu and Cu_2O Bragg Reflections to those of "n-diamond" and "i-carbon".

Cu		"n-diamond"	Cu_2O			"i-carbon" / "C_8"		
	Predicted†	Konyashin *et al.* (2001)			Predicted‡	Matyushenko *et al.* (1979)	Hirai and Kono (1991)	Burkhard *et al.* (1994)
(*hkl*)	d-spacing (Å)		(*hkl*)	Int.	d-spacing (Å)			
(111)	2.087	2.067	(110)	w	3.019	3.02	3.04	3.03
(200)	1.807	1.791	(111)	vs	2.465		2.42	2.49
(220)	1.278	1.261	(200)	m	2.135	2.13	2.08	2.13
(311)	1.090	1.078	(211)	w	1.743	1.74	1.70	1.78
(222)	1.044	1.032	(220)	m	1.510	1.52	1.49	1.59
(400)	0.904	0.892	(221)	vw	1.423			
(331)	0.829	0.817	(310)	w	1.350	1.352		
(420)	0.808	0.796	(311)	w	1.287		1.26	1.29
(422)	0.738	0.727	(222)	w	1.233	1.234	1.19	
(333)	0.696	0.686	(321)	vw	1.141		1.09	1.09
(440)	0.639	0.630	(400)	w	1.067			1.05

† lattice parameter: $a = 3.6149$ Å

‡ lattice parameter: $a = 4.2696$ Å

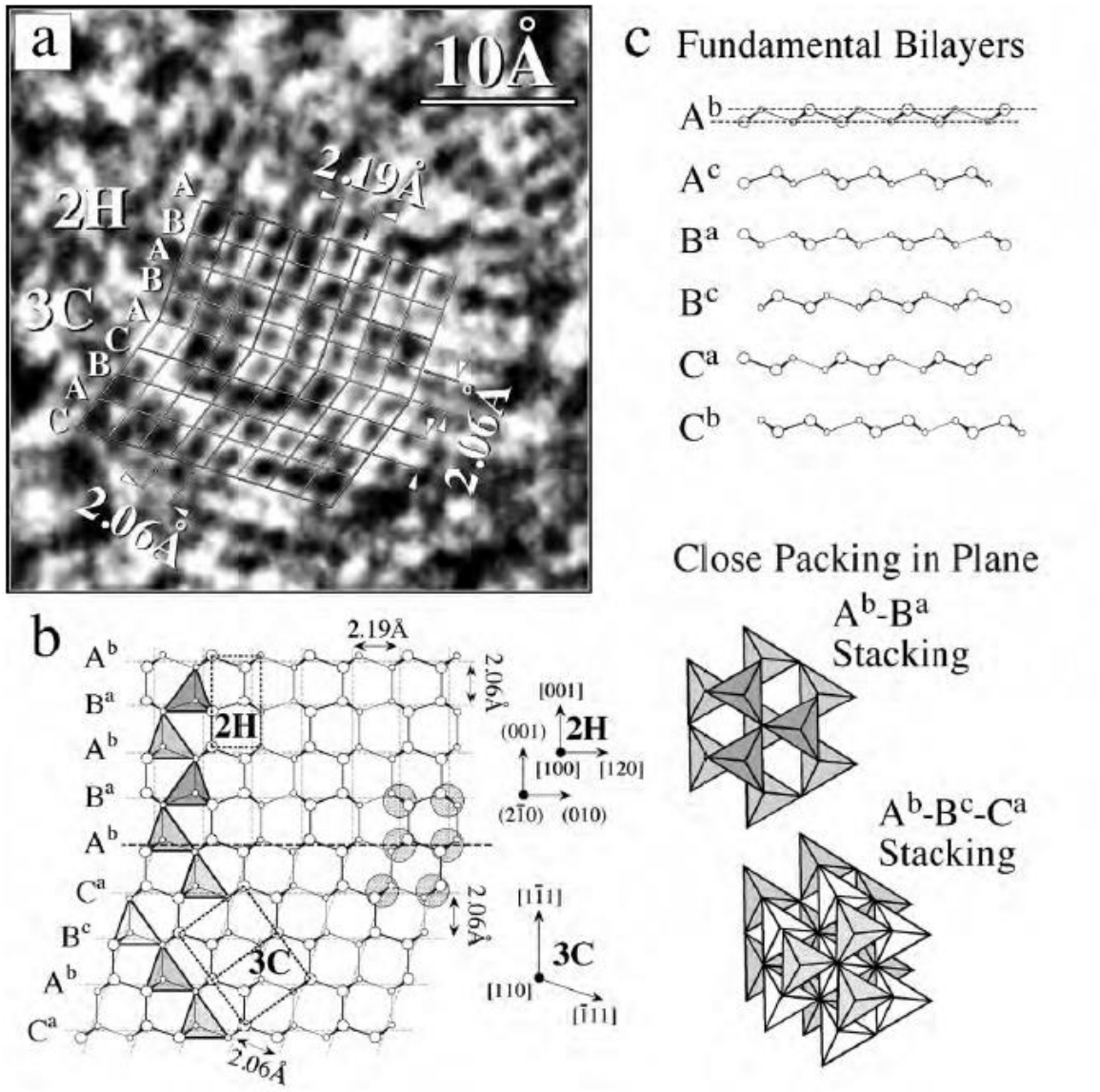
a
10Å
2.19Å
2H
3C
2.06Å
2.06Å
b
2.19Å
2.06Å
2H
3C
2.06Å
[001]
(001)
[100]
[120]
(2$\bar{1}$0)
(010)
[1$\bar{1}$1]
[110]
[$\bar{1}$11]
c Fundamental Bilayers
Close Packing in Plane
A^b-B^a Stacking
A^b-B^c-C^a Stacking

Figure 1

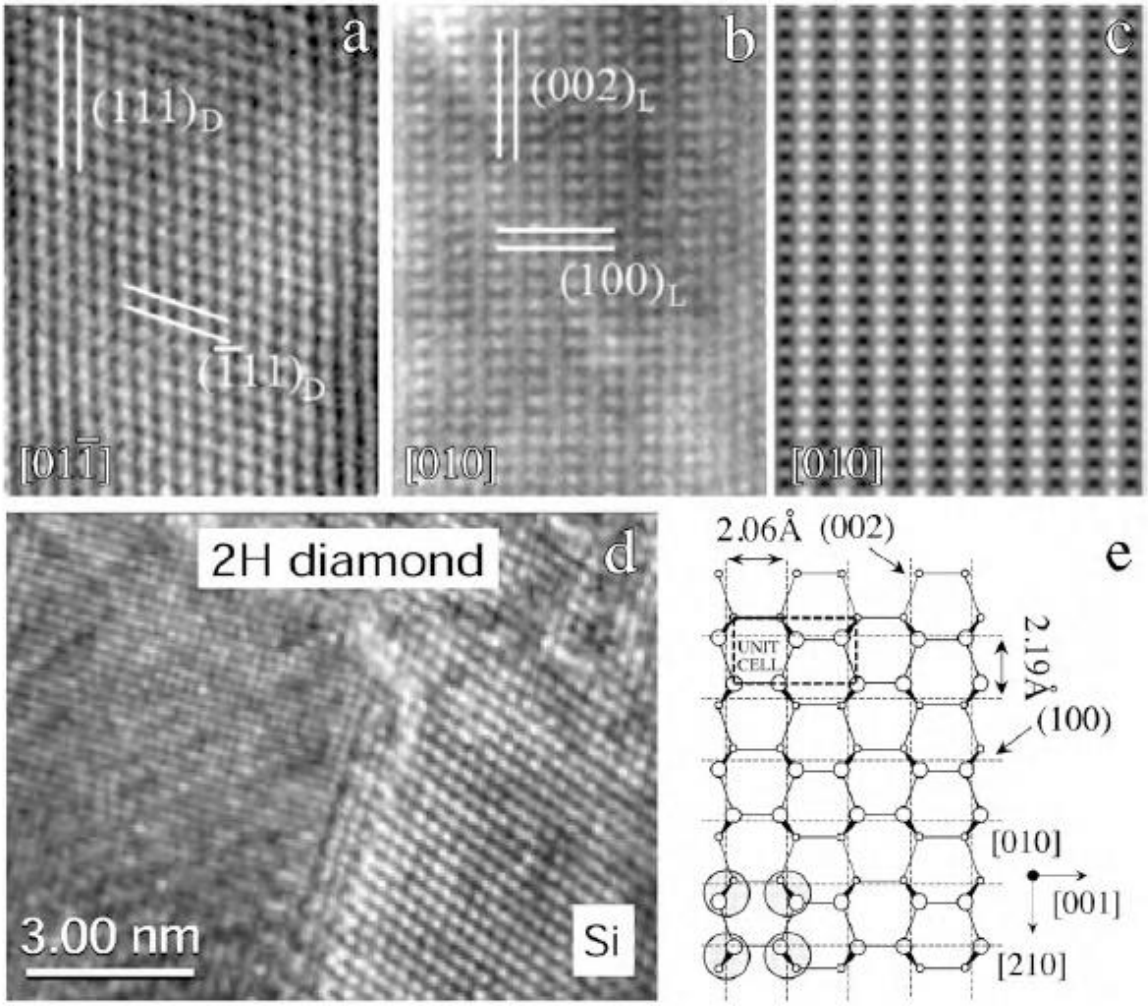
a
$(111)_D$
$(\bar{1}11)_D$
[01$\bar{1}$]
b
$(002)_L$
$(100)_L$
[010]
c
[010]
2H diamond
d
3.00 nm
Si
2.06Å (002)
e
UNIT CELL
2.19Å
(100)
[010]
[001]
[210]

Figure 2

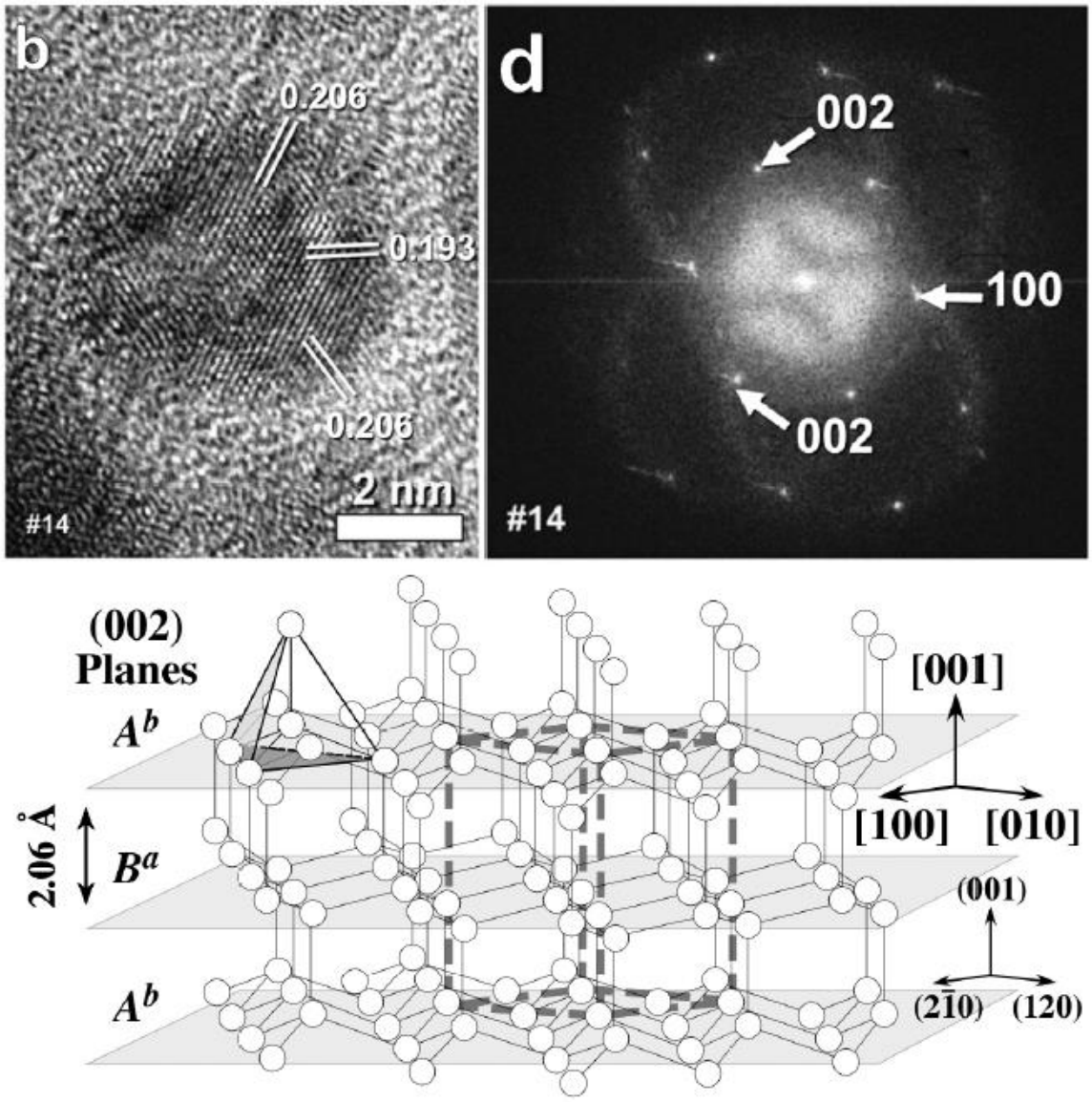
b
0.206
0.193
0.206
2 nm
#14
d
002
100
002
#14
(002)
Planes
A^b
B^a
A^b
2.06 Å
[001]
[100]
[010]
(001)
(2$\bar{1}$0)
(120)

Figure 3

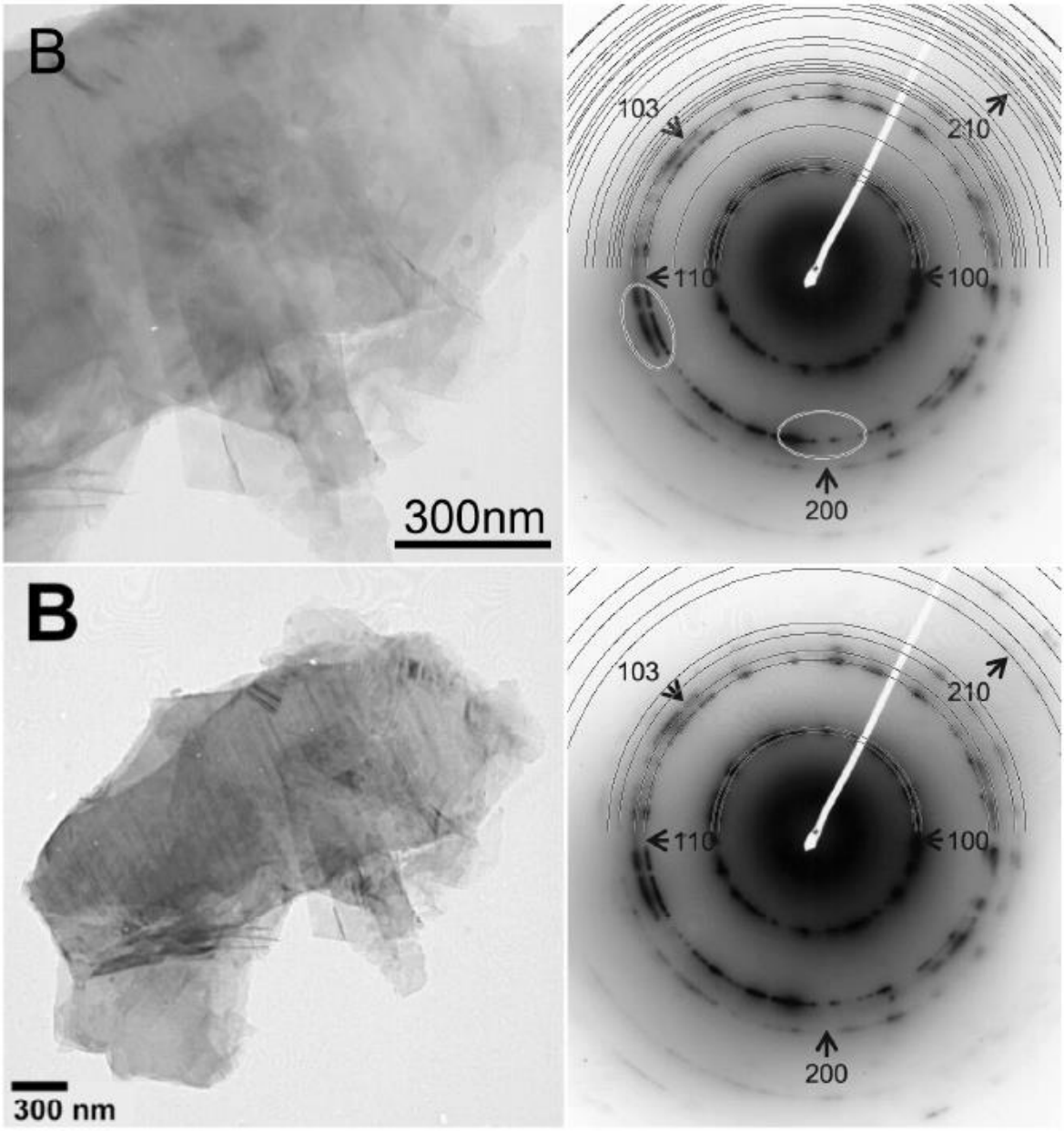

Figure 4

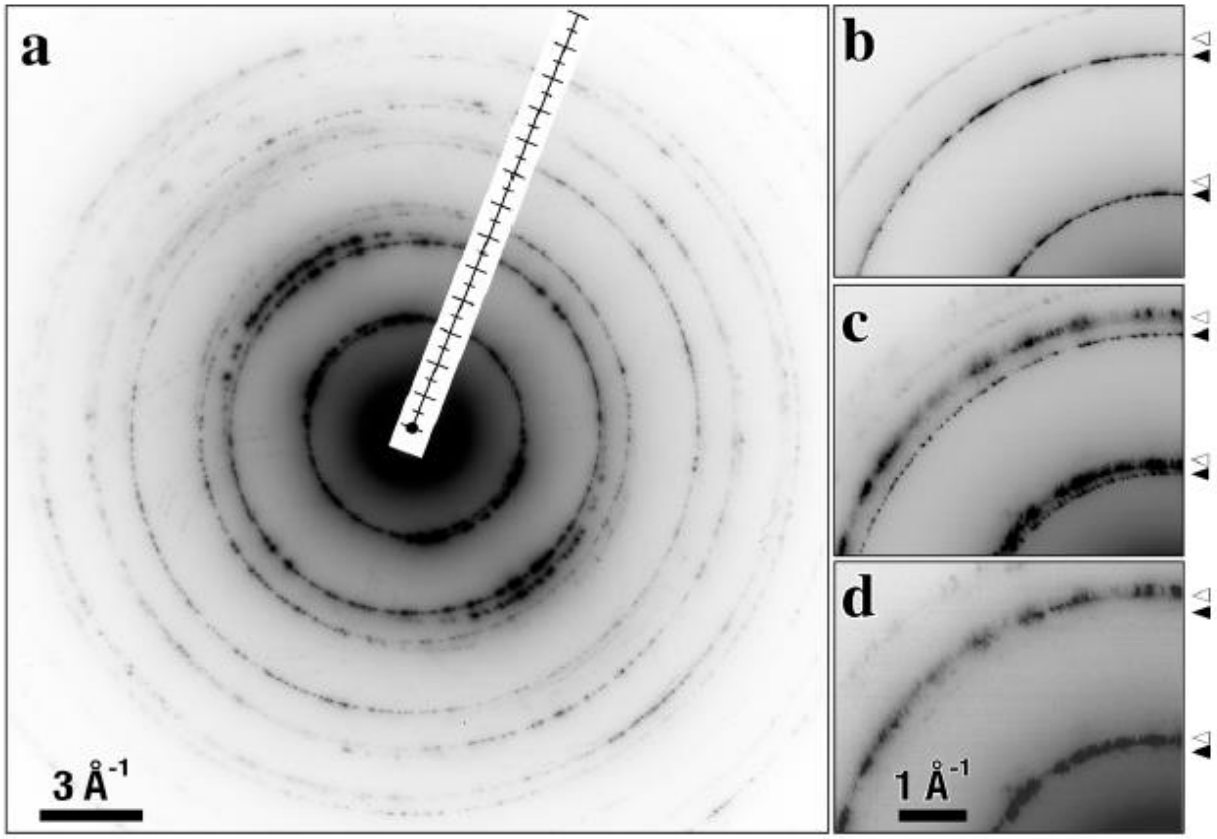

Figure 5

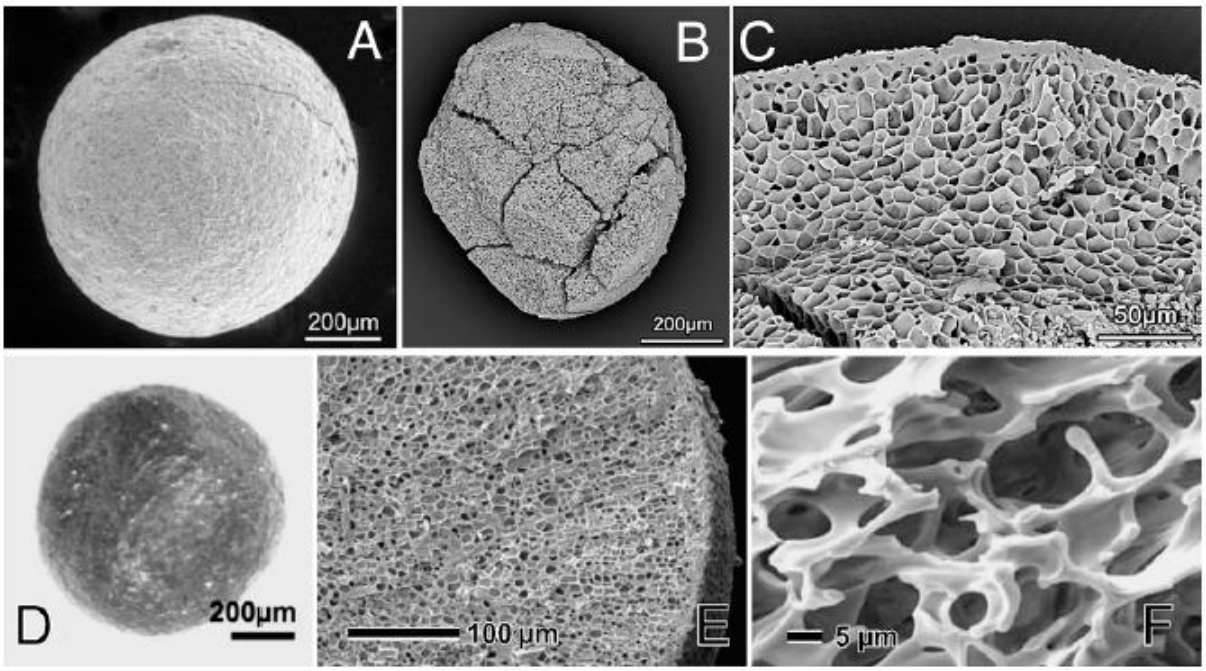

Figure 6

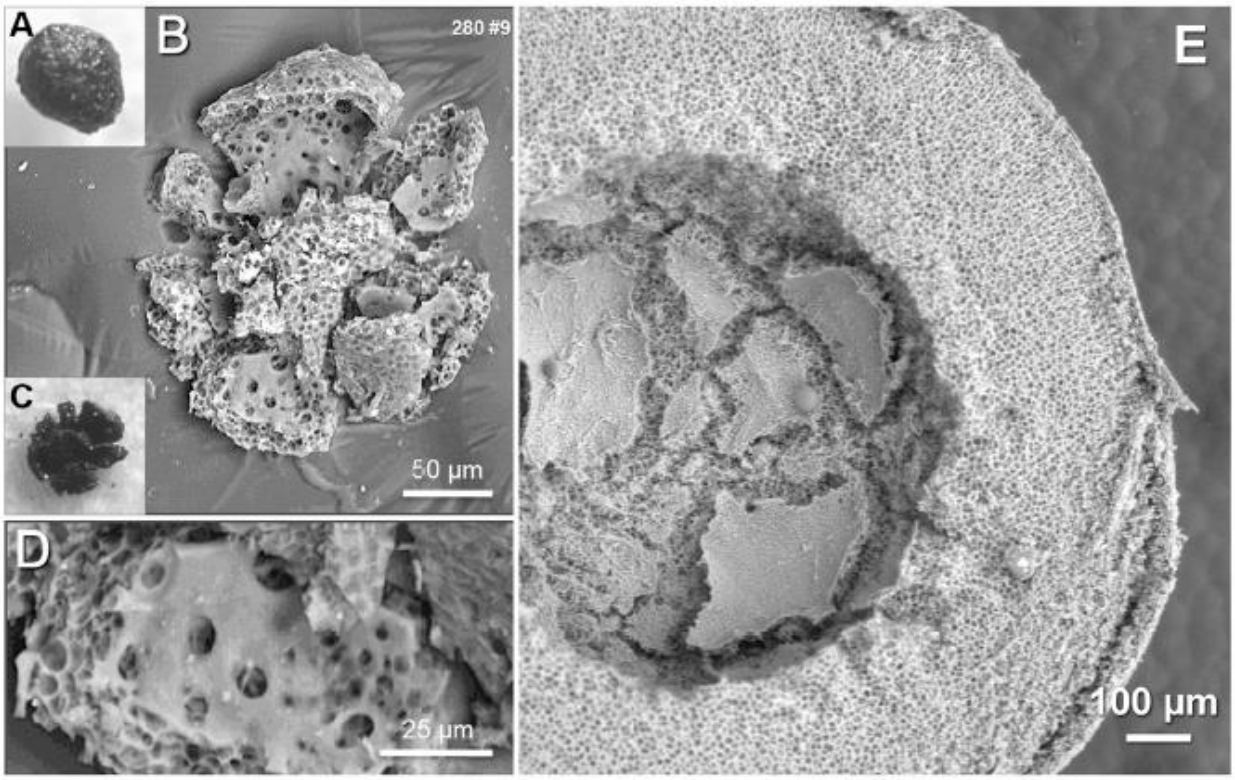

Figure 7

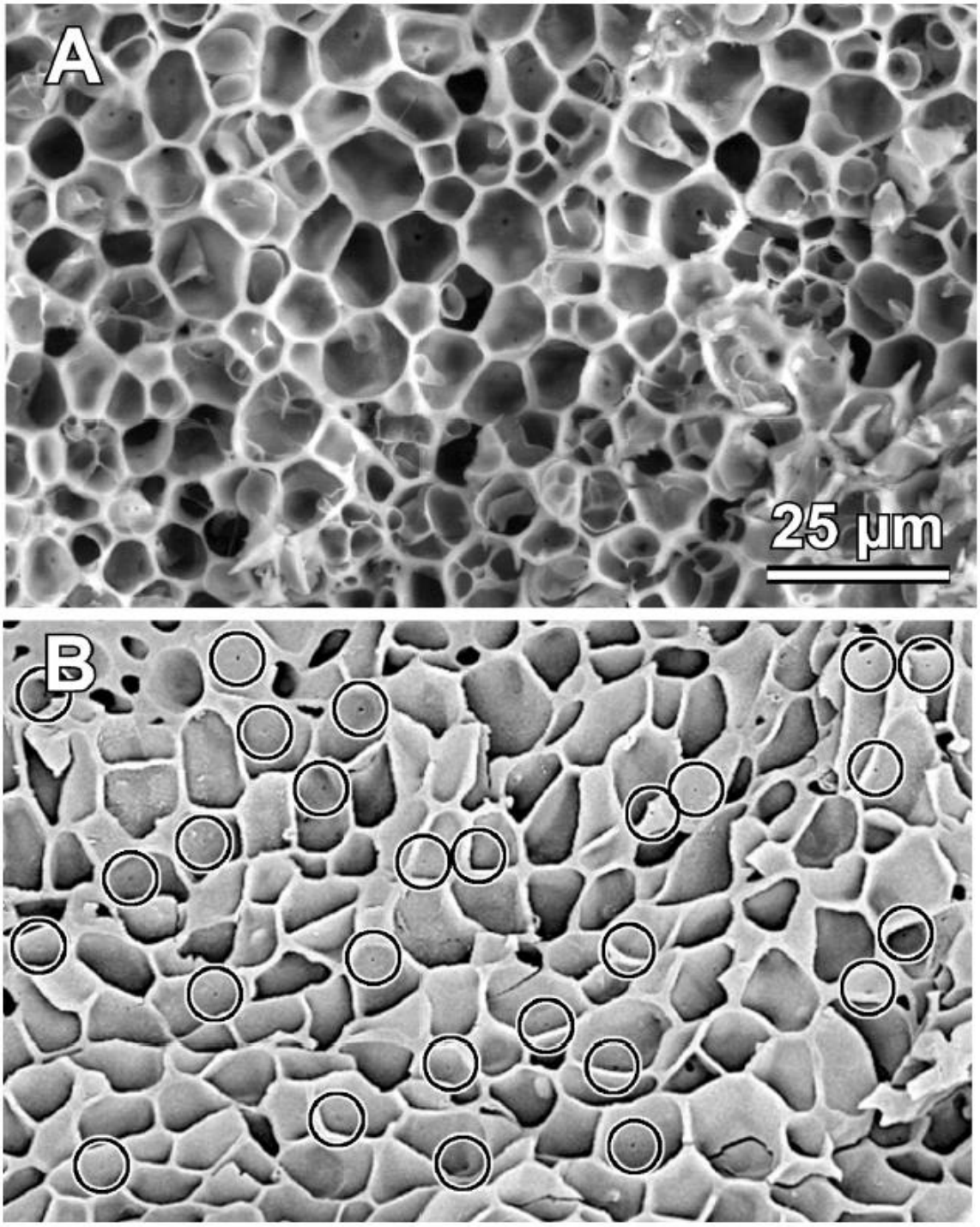

Figure 8

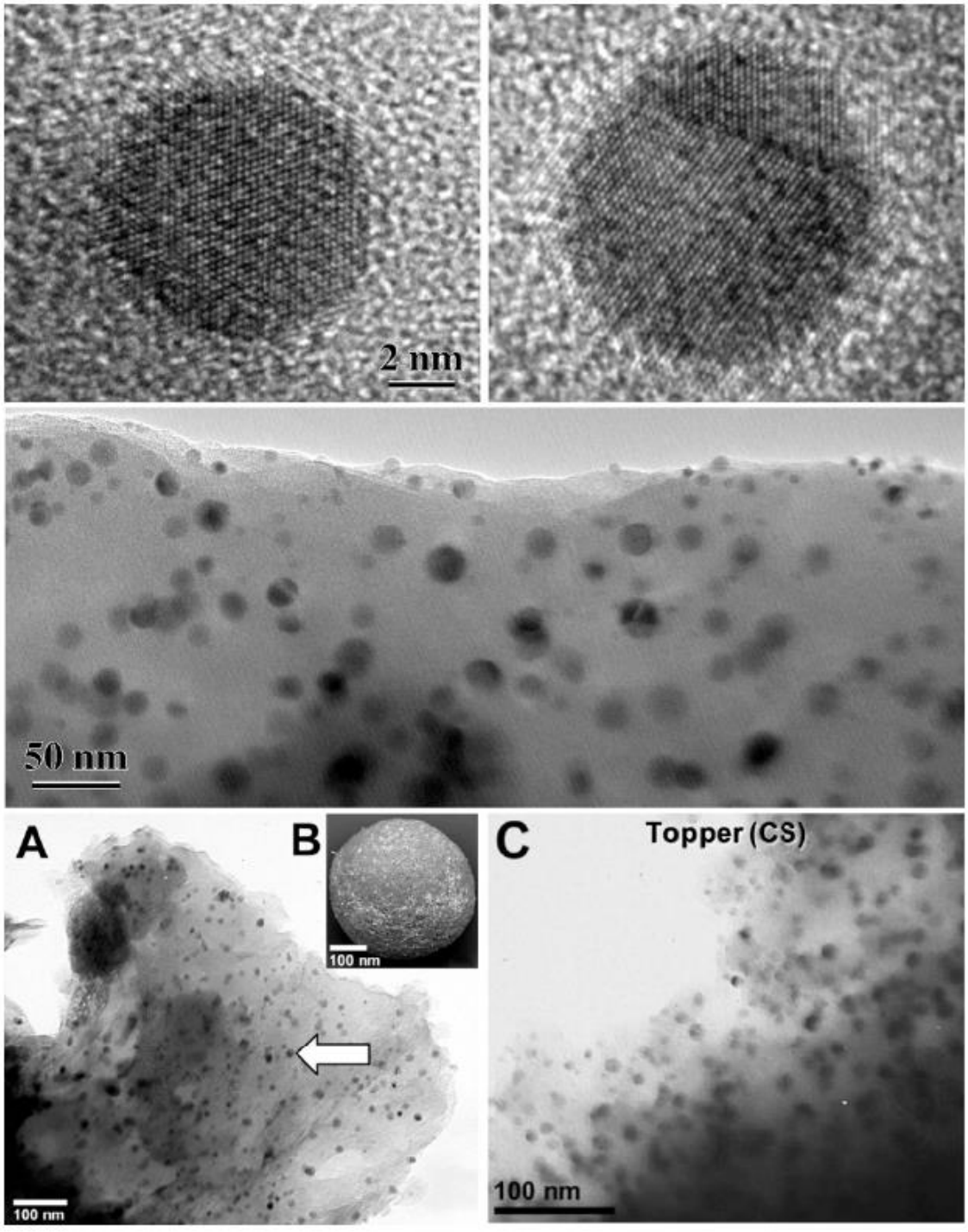

Figure 9

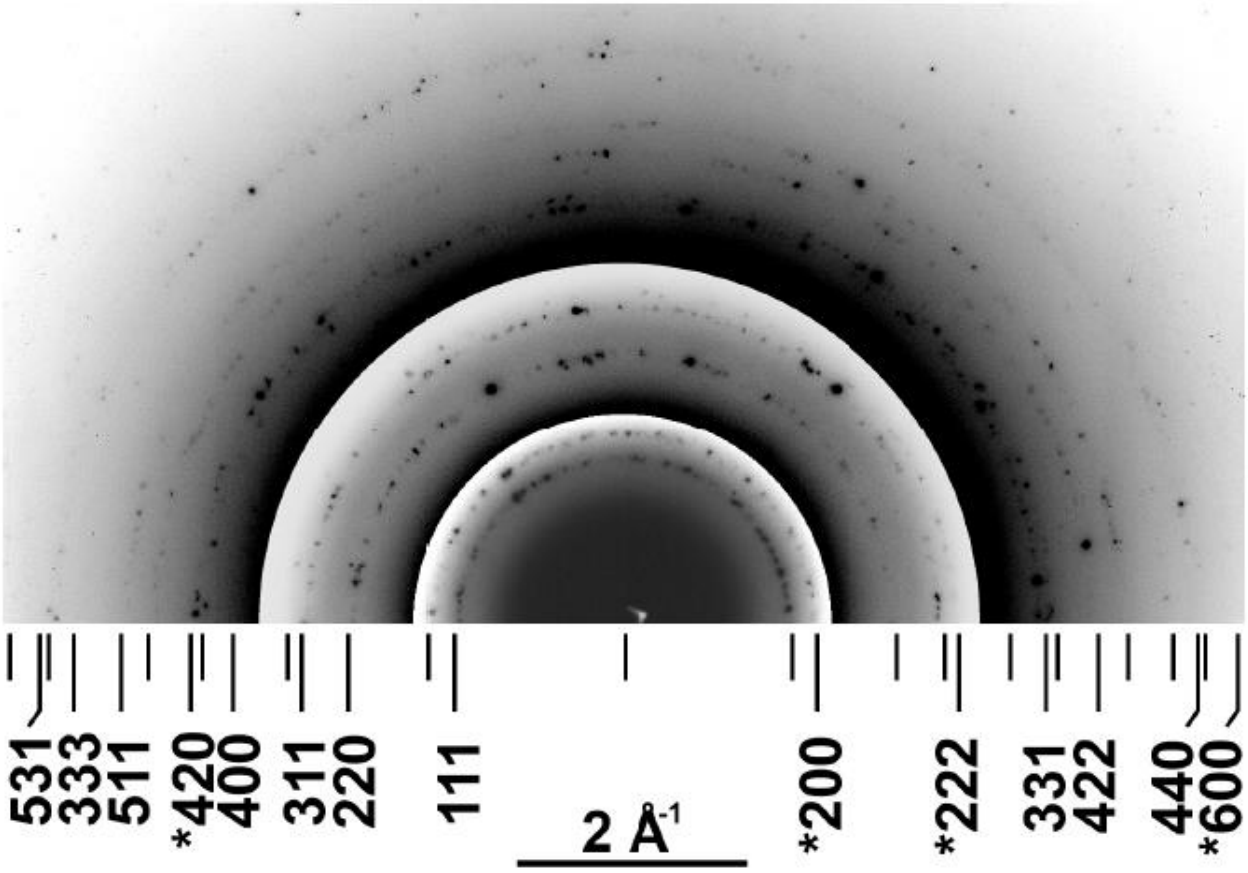

Figure 10

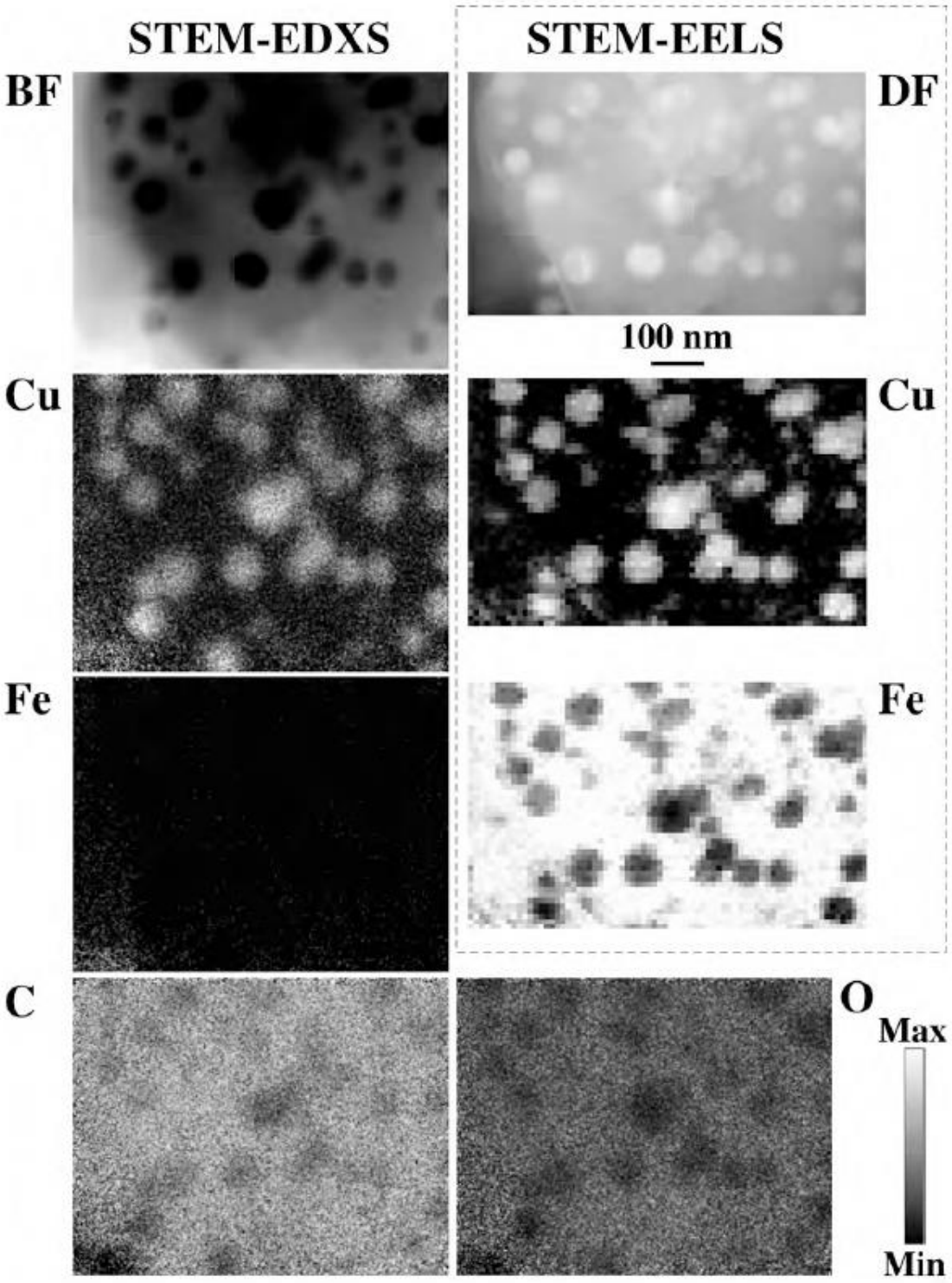

Figure 11

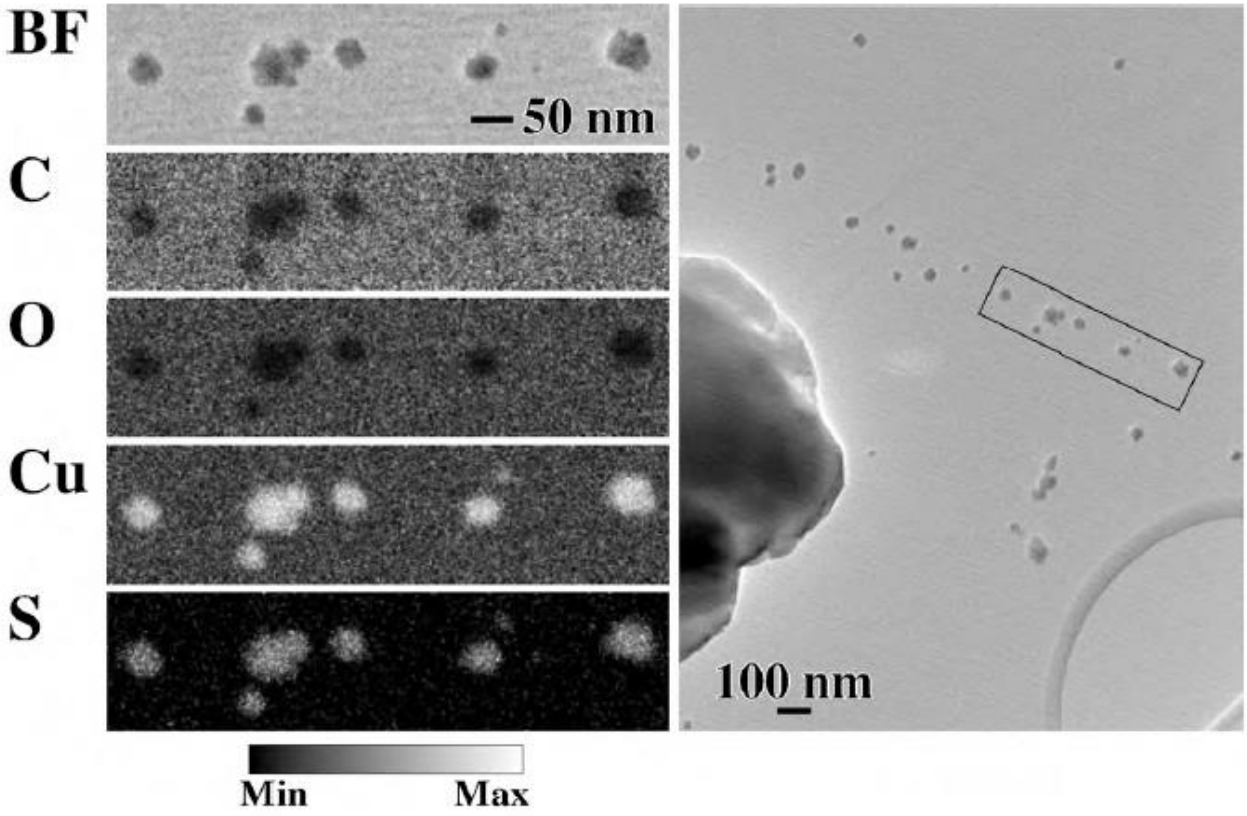

Figure 12